TAMPEREEN TEKNILLINEN YLIOPISTO
TAMPERE UNIVERSITY OF TECHNOLOGY

Antti Rostedt

Diffusion Charging-Based Aerosol Instrumentation: Design, Response Characterisation and Performance

Julkaisu 1527 • Publication 1527

Tampere 2018

Tampereen teknillinen yliopisto. Julkaisu 1527
Tampere University of Technology. Publication 1527

Antti Rostedt

Diffusion Charging-Based Aerosol Instrumentation: Design, Response Characterisation and Performance

Thesis for the degree of Doctor of Science in Technology to be presented with due permission for public examination and criticism in Rakennustalo Building, Auditorium RG202, at Tampere University of Technology, on the 23rd of February 2018, at 12 noon.

Tampereen teknillinen yliopisto - Tampere University of Technology
Tampere 2018

Doctoral candidate:	Antti Rostedt, M.Sc. Laboratory of Physics Tampere University of Technology Tampere, Finland
Supervisor:	Jorma Keskinen, Prof. Laboratory of Physics Tampere University of Technology Tampere, Finland
Instructor:	Leonidas Ntziachristos, Assoc. Prof. Laboratory of Physics Tampere University of Technology Tampere, Finland
	Laboratory of Heat Transfer and Environmental Engineering Aristotle University of Thessaloniki Thessaloniki, Greece
Pre-examiners:	Heikki Junninen, Ph.D. Institute of Physics University of Tartu Tartu, Estonia
	Department of Physics University of Helsinki Helsinki, Finland
	Pramod Kulkarni, D.Sc. Centers for Disease Control and Prevention National Institute for Occupational Safety and Health Cincinnati, USA
Opponent:	Thomas A.J. Kuhlbusch, Prof. Hazardous Substances Management Federal Institute of Occupational Safety and Health Dortmund, Germany

ISBN 978-952-15-4084-4 (printed)
ISBN 978-952-15-4116-2 (PDF)
ISSN 1459-2045

Abstract

The growing concern for the air quality in urban areas and the subsequent development of measurement networks has increased the need for lightweight and cost-effective air quality instrumentation. In urban areas, traffic-related emissions are one of the major contributors to the worsened air quality, which in turn has led to the stringed emission regulations set for vehicles. These regulations necessitate both on-board monitoring of the operation of the exhaust after-treatment devices and measurement of the real-word driving emissions with portable emission measurement systems. Both of these aspects increase the demand for sensor-type instrumentation for emission measurement.

This thesis focusses on the development of diffusion charging–based aerosol instrumentation towards more compact and sensor-type instruments. The work was started by developing an add-on module for the electrical low-pressure impactor. This extended the instrument measurement capabilities by enabling the measurement of the effective density of particles in real-time. Focussing more on the sensor-type instrumentation, three different sensors were presented for measuring particle emission directly from the exhaust line: Two of them targeting the engine laboratory work or for the portable emission measurement and one designed for on-board diagnostics. The instrument developed for the on-board emission measurement provided a very good temporal performance owing to the miniaturisation of the instrument design. Lastly, a new sensor design approach was presented in which the flow rate dependence of the instruments response is minimised. This, together with the minimised pressure drop in the design, helps in lowering the instrument cost by promoting the use of a low-cost fan for generating the sample flow.

Instrument response characterisation and response modelling made a central part of the study. Results from the characterisation measurements were presented for all instruments, and comprehensive response models were built for the sensor-type instruments. Depending on the instrument, both simplified approximations and theoretical responses of the instrument components were used as the starting point for the response models. Additionally, the instrument performance was demonstrated in practical measurements related to the application of each instrument. The obtained response models provide necessary information for the instrument performance evaluation and the measurement data processing.

Preface

This work was carried out in the Aerosol Physics Laboratory at the Tampere University of Technology. I am deeply grateful for my supervisor Prof. Jorma Keskinen for all the support and guidance I have had. My instructor, Assoc. Prof. Leonidas Ntziachristos, I would like to thank for the valuable comments on this thesis and for the help in preparing Paper IV. I would also like to thank Prof. Jyrki Mäkelä, for making the work in the laboratory easy from the administrative side.

During these years, I have had the privilege to work with many talented people. I would like to acknowledge all the co-authors in the publications for their contribution. Especially Dr. Marko Marjamäki, Dr. Jaakko Yli-Ojanperä and Dr. Anssi Arffman deserve a major credit for all the valuable discussions we have had in and outside of the office. Doc. Topi Rönkkö is acknowledged for providing the possibilities to test the instrument prototypes in different measurement campaigns. I would also like to thank Mr. Miska Olin for sharing the office for several years. The work with instrument prototypes would have been impossible without the support from the skilled people of the former Physics workshop. I am especially thankful for the contribution of Mr. Antti Lepistö and Mr. Veli-Pekka Plym. For funding, I wish to acknowledge MMEA research program of the Cluster for Energy and Environment (CLEEN Ltd.), funded by the Finnish Funding Agency for Technology and Innovation (TEKES). Additionally, I wish to thank Dekati Oy and Pegasor Oy and the personnel of these companies for the support and funding in different research projects.

All this would have been impossible without the support of the family. I am grateful to my parents and my brother and sister for laying out such a solid foundation in life. Unfortunately, my father is no longer with us, but his memory never fades away. I wish to thank my wife Mia and our sunshine Mari for being there for me and keeping my thoughts (mostly) away from work at home.

Tampere, January 2018

Antti Rostedt

Symbols and Abbreviations

ε	Permittivity of particle
ε_0	Permittivity of vacuum
η_c	Particle collection efficiency of the particle-collecting component
η_g	Gas viscosity
ηi	Particle collection efficiency of an impactor
η_{ma}	Particle collection efficiency of the mobility analyser
ρ_{eff}	Effective density of particles
ρ_0	Unit density 1 g/cm^3
ξ	Dimensionless term characterising the diffusion losses
τ	Time constant
a	Fitting parameter in charging efficiency approximation
b	Fitting parameter in charging efficiency approximation
B	Particle mechanical mobility
C_c	Slip correction factor
c_i	Mean thermal velocity of ions
$d_{50\%}$	Cut point diameter corresponding to 50% collection efficiency
$d_{50\%,n}$	Cut point diameter of impactor stage n
d_a	Aerodynamic particle diameter
d_b	Mobility equivalent particle diameter
d_{duct}	Diameter of flow duct
d_{ia}	Aerodynamic median size of particles
d_{im}	Mobility median size of particles
e	Elementary charge
d_p	Particle diameter
E_{ave}	Average electric field strength
E_c	Electric field strength in the particle-charging region
E_{ch}	Charger efficiency
E_t	Electric field strength in the ion trap
F_d	Drag force
I_c	Charger ion source supply current
I_c’	Return current from the charger ion source to power supply
I_{ch}	Current component related to generated ions in a charger
I	Current size distribution of particles
I’	Modified current size distribution of particles
I_i	Current component related to ions collected in an ion trap
I_{ic}	Current component related to particle initial charge
I_{il}	Current component related to ions escaping the charger
I_m	Measured current component related
I_{out}	Current component flowing out from the charger
I_{pc}	Current component related to particle charge
I_{pl}	Current component related to charged particle losses
k	Boltzmann constant
L_{eff}	Effective length of charging region
l_{ma}	Length of the mobility analyser
n_{ave}	Average number of charges per particle
n_d	Average number of charges per particle from diffusion charging
n_f	Average number of charges per particle from field charging

N_i	Concentration of ions
P_{ch}	Charger penetration
P_d	Particle diffusion losses expressed as penetration
P_i	Particle penetration through the instrument
P_{il}	Particle inertial losses expressed as penetration
P_{ma}	Mobility analyser particle penetration
Q_p	Volumetric pump flow rate of an ejector
Q_s	Volumetric sample flow rate
R	Flow velocity factor
R_{ch}	Response of the diffusion charger
R_{ETaPS}	Response of the Electrical Tail Pipe Sensor
R_f	Response of an instrument combining diffusion charger and filter collection
R_i	Overall response of the instrument
R_{ma}	Response of an instrument combining diffusion charger and mobility analyser
$R_{PPS\text{-}M}$	Response of the PPS-M
s	Fitting parameter in the impactor collection efficiency approximation
s_i	Inner diameter of an annular flow channel
s_o	Outer diameter of an annular flow channel
T	Gas temperature
t	Residence time
t_r	Rise time
u_0	Fitting parameter related to diffusion losses
V_{flow}	Flow velocity
V_{ma}	Mobility analyser collection voltage
V_{min}	Minimum flow velocity
v_p	Particle velocity
Z_0	Limiting electrical mobility of a mobility analyser
Z_i	Ion electrical mobility
Z_p	Particle electrical mobility

CO	Carbon monoxide
CO_2	Carbon dioxide
CPC	Condensation particle counter
DMA	Differential mobility analyser
DOS	di-octyl sebacate
ECT	Escaping charge technique
ETaPS	Electrical Tail Pipe Sensor
FCE	Faraday Cup Electrometer
FIAS	Flow Independent Aerosol Sensor
GSD	Geometric standard deviation of a lognormal particle size distribution
LDSA	Lung deposited surface area
MOS	Metal oxide semiconductor
NO	Nitrogen monoxide
NO_2	Nitrogen dioxide
NO_x	Nitrogen oxides in general
O_3	Ozone
OBD	On-board diagnostics
OPC	Optical particle counter

PM2.5	Total mass of particles smaller than 2.5 µm
PM10	Total mass of particles smaller than 10 µm
PEMS	Portable emission measurement system
RPM	Revolutions per minute
SCAR	Single charged aerosol reference
SMPS	Scanning mobility particle sizer
SO_2	Sulfur dioxide
TEOM	Tapered element oscillating microbalance

List of Publications

Paper I Rostedt, A., Marjamäki, M., and Keskinen, J., 2009. *Modification of the ELPI to Measure Mean Particle Effective Density in Real-Time.* J. Aerosol Sci., 40:823–831, doi: 10.1016/j.jaerosci.2009.05.002.

Paper II Rostedt, A., Marjamäki, M., Yli-Ojanperä, J., Keskinen, J., Janka, K., Niemelä, V. and Ukkonen, A., 2009. *Non-Collecting Electrical Sensor for Particle Concentration Measurement.* AAQR, 9:470–477, doi: 10.4209/aaqr.2009.03.0023

Paper III Rostedt, A., Arffman, A., Janka, K., Yli-Ojanperä, J. and Keskinen, J., 2014. *Characterization and Response Model of the PPS-M Aerosol Sensor.* Aerosol Sci. Technol., 48:10, 1022-1030, doi: 10.1080/02786826.2014.951023

Paper IV Rostedt, A., Ntziachristos, L., Simonen, P., Rönkkö T., Samaras, Z., Hillamo, R., Janka, K., and Keskinen, J., 2017. *A new miniaturized sensor for ultra fast on-board soot concentration measurements*. SAE Int. J. Engines 10(4):2017, doi: 10.4271/2017-01-1008.

Paper V Rostedt, A. and Keskinen, J., 2017, *Flow rate independent electrical aerosol sensor*. Submitted to Aerosol Sci. Technol.

Author's contribution

The work presented in this thesis has been carried out in research projects, and the publications included in this thesis are a result of a collaborative work. The author has had a specific role in each publication, as summarised below:

Paper I A new modification to the electrical low-pressure impactor (ELPI), allowing the measurement of particle effective density, was introduced in this publication. The author designed the integrated mobility analyser and carried out calibration and laboratory test measurements. The author also produced the required response functions and the data processing routines with the help of co-authors and wrote the first draft of the manuscript.

Paper II In this publication, a new electrical sensor for vehicle particle emission measurement was introduced. The author took part in the early stages of instrument design, and the tested prototype instrument was designed by Dr. Janka, Mr. Niemelä and Mr. Ukkonen. Mr. Ukkonen and Dr. Yli-Ojanperä carried out the characterisation measurements, and the author performed the data processing and the field test measurements. The author also formulated the instrument response model with the help of other co-authors and wrote the first version of the manuscript.

Paper III This publication presented a laboratory characterisation and a response model for the PPS-M electrical aerosol sensor. The author designed the response measurement setup and carried out the laboratory response measurements together with Dr. Yli-Ojanperä. Dr. Arffman carried out the CFD modelling presented in the publication. The author was responsible for the data processing and the response model. The author also wrote most parts of the manuscript.

Paper IV A new and miniaturised electrical aerosol sensor, based on the previous PPS-M sensor, was introduced in this publication. The author carried out both laboratory and engine test measurements, produced the response model and wrote most parts of the manuscript.

Paper V This publication is based on the author's idea for a new simplified aerosol sensor. The author designed the instrument prototype by modifying existing instrument parts, designed the laboratory measurements and carried out the data processing. The response model was formulated, and the manuscript was written together with Prof. Keskinen.

Contents

1 Introduction

As awareness of the adverse health effects caused by different anthropogenic emissions has increased, the concern on the air quality of urban areas has become a major issue. There are many different components affecting the air quality. For outdoor air quality, concentrations of gaseous substances such as sulphur dioxide (SO_2), nitrogen oxides (NO_x) and ozone (O_3) are measured and reported. For the particulate matter, values commonly related to air quality are PM2.5 and PM10, which correspond to the mass concentration of all particles smaller than 2.5 µm and 10 µm, respectively. Regulatory authorities have set limits for the key components affecting the air quality. In European Union, the limiting values and related measurement methods are set by EU Directive 2008/50/EC (EU, 2008). Apart from the official air quality measurement sites, fulfilling the regulatory requirements, there is a growing interest towards more lightweight and more widely dispersed air quality measurement (Snyder et al., 2013, Kumar et al., 2015). Simplified instruments targeted for personal exposure measurement or for large area sensor networks are becoming more popular.

Traffic-related emissions are one of the major contributors to the air quality related problems in urban areas (Künzli et al., 2000). Increased concentrations of ultrafine particles, hydrocarbons and nitrogen oxides are reported from traffic congestions (see, e.g., Hu et al., 2009). For this reason, the vehicle emissions are controlled by emission regulations, which currently necessitate the use of exhaust after-treatment devices. Further, the regulations require both real-word emission measurement and continuous monitoring of the operation of the emission control devices (ICCT, 2016). This has led to development of portable emission measurement systems (PEMS), capable of being mounted on board the vehicle, whereas the continuous monitoring is carried out by the on-board diagnostics (OBD) systems of the vehicles. Sensor-type air quality instruments are needed for both of these applications.

For gaseous compounds related to the air quality and emissions, there are several measurement technologies available, as reviewed by Liu et al. (2012). Commonly used technologies in sensor-type applications are based either on the light absorption or on the chemical interaction between the measured gas component and the sensor electrode (Lee and Lee 2001). Through the application of the semiconductor manufacturing techniques, such as micro-electromechanical structures and thick film techniques, it has been possible to introduce miniaturised component-like gas sensors to the market (see, e.g., Park et al., 2009). With the current sensor technologies, it is possible to have low-cost detectors for gaseous compounds, such as, for example, CO, CO_2 and NO_x for ambient concentrations (Piedrahita et al., 2014).

Compared to the gaseous compounds, the aerosol measurement is somewhat more challenging. The complexity starts from the concentration definition, as there are several different ways for quantifying the amount of particles suspended in the air. While the concentration is often the most important property, other properties of the aerosol, such as for instance particle size and morphology, need to be considered. On top of all this, the properties are in a constant change due to various ongoing processes. Concentration decrease due to the particle losses and particle mean size growth due to the condensation are examples of such processes. For this reason, fast online measurement and real-time instruments are preferable in aerosol measurement. From the air quality perspective, the particle size range below 1 µm is important, as most of the emission sources affecting the air quality produces particles in this size range. This sets another challenge for the aerosol instrumentation, as the particle detection gets more challenging with the decreased particle size. Indirect measurement techniques are required, which often lead to increased data processing and decreased accuracy in the measurement. Because of these challenges, the simplified and lightweight aerosol instruments have not been available until quite recently.

In terms of air quality, the aerosol concentration is usually expressed as mass concentration. While the quantity has a strong historical background (Chow 1995), there are only few real-time instruments that can be used for direct measurement of ambient particle mass concentration. From those, the tapered element oscillating microbalance (TEOM, Patashnick and Rupprecht, 1991) is perhaps the most well-known. The TEOM detects the changing mass of the particle-collecting filter by measuring the resonance frequency of the vibrating filter holder. More commonly, the aerosol concentration is measured utilising light scattering, either from single particles or from particle clouds. Optical particle counters (OPCs) count the individual particles to measure the number concentration of particles (Kulkarni et al., 2011). By simultaneously recording the heights of individual scattering peaks, information on the particle size distribution is acquired. While there are high-end instruments with operational particle size ranges reaching down

to 0.05 µm, the use of the OPC for the air quality measurement is limited because the affordable instruments are not sensitive for detecting small particles much below 0.5 µm. In order to extend the particle size range for the optical particle detection, condensation particle counters (CPC's) have been developed. They also rely on measurement of the single-particle scattering pulses, but, apart from the OPCs, the particles are first grown by condensation before the optical measurement. Through this, the lower size limit has been extended down to a few nanometres. The first commercial continuous-flow CPC entered the market in the early eighties (McMurry, 2000, Agarwal and Sem, 1980). The condensing material used in the CPC to grow the particle is usually either n-butanol (Bricard et al., 1976) or water (Hering et al., 2005). By using di-ethylene glycol as the working liquid, it is even possible to extend the lower size limit below 2 nm (Iida et al., 2009). The CPC is a good instrument for the number concentration measurement, but continuous operation requires periodic filling of the condensing liquid. Recent development in the optical particle detection has brought to the market several small and affordable optical particle sensors. These sensors operate without particle growing and are thus only sensitive for the large particles. The output of such sensors is usually calibrated against a mass concentration measurement. Sousana et al. (2017) and Kelly et al. (2017) evaluated the use of these sensors for air quality measurement.

The electrical aerosol concentration measurement relies on particle-charging and subsequent charge measurement. The charge on the particles is typically produced by a diffusion charger, where the aerosol particles are brought into contact with gas phase ions. The ion cloud can be bipolar — containing negative and positive ions — or unipolar, containing only one polarity. For the ion production, different methods such as ionising radiation from radioactive sources, direct x-ray radiation, electric discharge or even thermal emission from flames can be used (Flagan, 1998). Although particle charging was first utilised for particle mobility measurements, the development in the low-level current measurement has made it possible to measure aerosol concentration with instruments based on electrical detection of the charged particles. Currently, there are several different instrument designs, which are based on the diffusion charging of the aerosol particles. Those instruments range from small and lightweight concentration monitors (Marra et al., 2009, Fierz et al., 2011, Fierz et al., 2014) to the more sophisticated instruments measuring the particle size distribution (Keskinen et al., 1992, Tammet et al., 2002 and Biskos et al., 2005a). While the electrical instruments are generally very reliable and produce repeatable results, the measured raw data do not directly correspond to the traditionally used concentration metrics. For converting the output to mass or number concentration, data processing is required, which in turn requires thorough understanding on the instrument operation.

Since the instruments based on the diffusion charging and electrical particle detection are sensitive in detecting the ultrafine particles, this approach has been applied to measure the concentration of the small particles. The instrument designs presented by Liu and Lee (1976) and Lehtimäki (1983) are early versions of such instruments in the literature. It was later determined by Wilson et al. (2007) that the charge measured from the particles after the diffusion charger correlates well with the lung deposited surface area (LDSA) concentration. The LDSA represents the total surface area of the particles depositing in the lung, and it has been linked to the adverse health effects of fine particles by Brown et al. (2001) and Oberdörster et al. (2005). This close correlation promotes the use of diffusion charging-based instrumentation for air quality monitoring. Based on this approach, Fissan et al. (2007) presented one of the first instruments that targeted the measurement of the LDSA concentration. Since then there have been several studies utilising the diffusion charging-based instrumentation for LDSA concentration measurement. For example, Ntziachristos et al. (2007), Järvinen et al. (2015), Viana et al. (2015) and Kuuluvainen et al. (2016) utilised the LDSA concentration measurement for outdoor air quality, whereas Buonanno et al. (2011) and Geiss (2016) concentrated on the air quality of a working environment. More recently, since these instruments are relatively small and affordable, they are being utilised in air quality measurement networks, as demonstrated by Marjovi et al. (2015). Such networks serve an important role in providing supporting information on the air quality in order to complement information obtained from other sources, as suggested, e.g., by Kuhlbusch et al. (2014).

Besides the concentration and the particle size, shape and density of the particles are also important properties of the aerosol. These properties affect to the particle transport and interaction with the surrounding and are of importance for instance in the health effect assessment and in various industrial applications. In the ultrafine particle size range, the particle shape and density are often combined as the effective density of the particles. This is because it is difficult to have a direct measurement on either of these properties separately. Information on the particle effective density can be obtained by combining different particle size measurement techniques, as reviewed by Schmid et al. (2007). The conventional methods used for measuring the particle effective density require the use of multiple instruments (see, e.g., Kelly and McMurry, 1992 and Ristimäki et al., 2002). This leads to complex and expensive measurement set-ups and hence limits the use of these methods in practical applications.

1.1 Aim and scope

This thesis focusses on introducing new real-time aerosol instrument designs based on the diffusion charging and on the characterisation of these instruments. The instrument response, describing the relation between the input aerosol sample and the measured output, plays a key role in this work. For obtaining the response, laboratory characterisation measurements are needed. By combining the laboratory measurement results with the theoretical response functions of the instrument components, a comprehensive model for the instrument response can be built.

In the scope of this thesis, the instrument design and development fall under the four main topics:

- Development of real-time effective density measurement through modification of the electrical low-pressure impactor (ELPI)
- Instrument development and characterisation for measuring the particle concentration directly from exhaust emission
- Development and characterisation of particle concentration sensor for on-board diagnostics of vehicles
- Minimising the instrument response sample flow rate dependence

The first topic was discussed in **Paper I**, where a new add-on module for the ELPI in order to measure the particle effective density was introduced. **Papers II, III** and **IV** focussed on the measurement of the particle concentration directly from the exhaust line of an engine or a vehicle. A new instrument design was introduced in **Paper II**, which consisted of a sensor probe installed directly to the exhaust flow. On the other hand, **Paper III** focussed more on the instrument response characterisation and the response model of a different instrument design. Both of these instruments are targeted for an engine laboratory work or PEMS measurement. In **Paper IV**, a new instrument prototype for the OBD application was presented. Unique to this design, an exceptionally good time resolution was achieved for the instrument, which was characterised and also demonstrated in engine laboratory measurements. The fourth topic was discussed in **Paper V** by introducing a new approach for the electrical aerosol sensor design, where the instrument response is relatively independent on the sample flow rate.

2 Instrument components and theoretical background of the response

The aerosol instruments based on the diffusion charging and the charge detection require only few components for the operation. The main component is the particle charger, where ions are mixed with the aerosol sample. After particle charging, excess ions are removed from interfering the particle detection by an ion trap. The particle concentration is then measured by detecting the charge carried by the particles with a high-sensitivity electrometer. For charge detection, the particles can be collected into an isolated filter or an electrode from which the electric current is measured. Size selective collection methods can be used to measure particle size or to modify the instrument response. It is also possible to use non-collective charge detection techniques.

The instrument response is the link between the instrument output and the input. In the case of the electrical aerosol instruments, the response links the measured current from the charged particles to the particle size and concentration of the aerosol sample. For the aerosol instruments, the response is usually referenced to the particle number concentration, and it is a function of the particle size. In the following, the theoretical background of the instrument response and the main aspects of the instrument design affecting the achievable performance are discussed. The main contributor to the instrument response is the charging efficiency of the charger E_{ch}, which, for the response, can be expressed as the product of the particle penetration through the charger P_{ch} and the average number of charges the particles acquire during the charging n_{ave}, as shown in equation 1 (for reference see, e.g., Marjamäki et al., 2000).

$$E_{ch} = P_{ch} n_{ave} \tag{1}$$

While the notation is omitted in the equation, the charging efficiency is a function of the particle diameter. After the charging, the charge on the particles is distributed; hence, an average number of charges per particle are required. If required, the particle charge distribution can be approximated by a lognormal distribution, as demonstrated by Kaminski et al. (2012). The response of the charger, written in equation 2, is the relation between the current measured from the particles after the charging and the particle concentration. It is the product of the charging efficiency and the charge of the elementary charge e and the volumetric sample flow rate Q_s.

$$R_{ch} = E_{ch} e Q_s \tag{2}$$

Particle deposition also contributes to the instrument response by introducing unwanted particle losses or if utilised for the charge detection. The effect of the particle losses is introduced to the overall instrument response R_i by the particle penetration P_i, whereas the effect of the particle-collecting component is introduced by the collection efficiency η_c. The resulting simplified instrument response equation can be written as equation 3:

$$R_i = P_i h_c E_{ch} e Q_s \tag{3}$$

2.1 Fundamental particle properties related to the response

Particle size is the most important property of the particles that governs the behaviour of the aerosol particles. The particle size can be defined in several ways. Most often the diameter of an equivalent sphere is used to describe the particle size. For instance, surface area and volume equivalent particle diameters correspond to the diameters of the sphere having the same surface area and volume as the possibly irregularly shaped particle. The mobility equivalent particle size, or the Stokes diameter, corresponds to the diameter of the sphere having the same density and settling velocity as the original particle. The aerodynamic particle size corresponds to the diameter of a unit density sphere having an equal aerodynamic drag. The mobility equivalent particle size d_b is related to the aerodynamic particle size d_a by the particle effective density ρ_{eff}, as written in equation 4, where the term ρ_0 is the unit density 1 g/cm^3.

$$\frac{d_a^2}{d_b^2} = \frac{r_{eff}}{r_0} \tag{4}$$

When the particles are in the influence of a force, the particle movement is affected by the interaction between the particle and the surrounding gas. The drag force F_d caused by the gas to the particle migrating at the velocity of v_p is described by the Stokes drag force written in equation 5:

$$F_d = \frac{3\pi h_g v_p d_b}{C_c} \tag{5}$$

The term C_c in the equation above is the slip correction factor, which extends the operational range of the equation form the continuum regime to smaller particle sizes. The factor was introduced by Cunningham (1910), and it is used in the form presented by

Allen and Raabe (1982). The surrounding gas properties are introduced by the gas viscosity η_g. The particle mechanical mobility B is defined as the relation between the migration velocity and the drag force, and it can be written as equation 6:

$$B = \frac{C_c}{3ph_g d_b} \tag{6}$$

As the gas molecules move randomly at thermal velocity around the particles, they collide frequently with the particles. This constant bombardment of gas molecules causes a net particle flux in the direction against the concentration gradient, which is a phenomenon called diffusion. The diffusion is characterised by the diffusion coefficient D_p given by the Stokes-Einstein equation (7), where the new terms are Boltzmann constant k and gas temperature T.

$$D_p = kTB \tag{7}$$

If the particles are charged, the electric field affects particle movement. This effect is characterised by the particle electrical mobility Z_p, which links the drift velocity caused by the electric field to the field strength. The electrical mobility is the product of the number of charges per particle, the charge of the elementary charge and the mechanical mobility:

$$Z_p = neB \tag{8}$$

2.2 Particle charging

Although there are different ways for producing charge on the aerosol particles, the majority of the instrument designs based on electrical aerosol detection rely on chargers utilising corona discharge. Inside the charger, the aerosol particles are charged by the unipolar ions generated in the corona discharge region. Although both positive and negative polarities can be used for the discharge, positive polarity is favourable due to the lower ozone production rate. A comparison of the ozone production rates of the different discharge polarities can be found, for example, in Boelter and Davidson (1997).

The particle-charging properties of both bipolar and unipolar chargers have been widely studied in the literature. The reported performance parameters are often divided to intrinsic and extrinsic charging efficiencies, as introduced by Büscher et al. (1994). The intrinsic charging efficiency relates to the fraction of particles acquiring charge inside the charger, but it does not take into account the electrical particle losses after the charging

takes place. The extrinsic charging efficiency describes the ratio of the charged particle number in the charger output to the total particle number in the charger inlet. While these performance parameters are often reported for the charger designs (see, e.g., Biskos et al., 2005b and Alonso et al., 2006), from the aerosol instrumentation perspective, the most convenient definition for the charging efficiency is the $P_{ch}n_{ave}$ product written in equation 1. The $P_{ch}n_{ave}$ product value can be defined for all particles or only for the charged particle fraction. The product values are equal in both cases, but the ratio between the P_{ch} and n_{ave} may be different, as noted in Virtanen et al. (2001). In the following, the approximations used in the modelling of the charger response are presented. For those interested, the charger performance evaluation is discussed in more detail, for instance, in Marquard et al. (2005).

A schematic view of a simplified unipolar corona charger is shown in figure 2.1, showing the main processes related to the charger operation. The ions are produced by the corona discharge in the volume near the discharge electrode, marked as the ion production zone. The generated ions are dispersed in the aerosol sample by diffusion and the electric field E_c in the sample volume, and the ion dispersion is enhanced by the coulomb repulsion. The ions mix with the aerosol particles in the charging region, and, after that, the excess ions are removed from the sample by the applied electric field E_t.

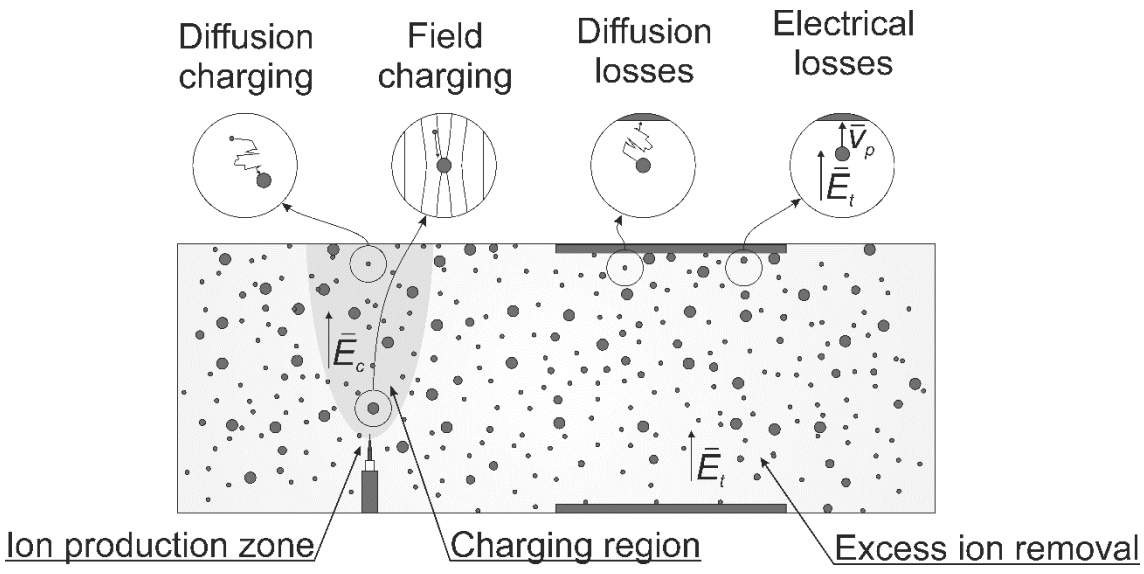

Figure 2.1. Schematic view of a simplified corona discharge-based aerosol charger, showing the main processes related to the charger operation

Inside the charging region, the particles acquire charge by two different charging processes: diffusion and field charging. The diffusion charging, more effective for the small particles, covers the charging process induced by the thermal diffusion of the ions. When the ions move randomly around the particles by Brownian motion, they have a certain probability to collide with the particle. After the time *t*, the particles reach a mean charge level n_d approximated by equation 9 (see, e.g., Hinds, 1999).

$$n_d = \frac{2\pi\varepsilon_0 d_p kT}{e^2} \ln\left(1 + \frac{d_p c_i e^2 N_i t}{8\varepsilon_0 kT}\right), \tag{9}$$

where the term ε_0 is the permittivity of the vacuum, d_p is the particle diameter, k is the Boltzmann constant, T is the temperature, e is the charge of the elementary charge, c_i is the mean thermal velocity of the ions and N_i is the concentration of ions. Although theoretical charging equations, such as the above, are usually valid for spherical particles only, the particle diameter is often substituted by mobility equivalent diameter (d_b). This may not correctly describe the charging of irregularly shaped particles (for more details see e.g. Shin et al. 2010). The effect of the shape is however relatively small and considered insignificant in the scope of this thesis. It is also assumed that the measured aerosol itself does not significantly affect the concentration and properties of the charging ions.

As particle size increases, field charging becomes a more effective process. In the charging region, the particles are always in an electric field: either an external field or that caused by the charged ions. The particles influence this field near the particle surface, which affects the ion movement near the particle. This effect is called field charging and the charge n_f, the particles acquire by field charging is approximated by equation 10 (see, e.g., Hinds, 1999).

$$n_f = \left(\frac{3\varepsilon}{\varepsilon + 2}\right)\left(\frac{E_c \pi \varepsilon_0 d_p^{\,2}}{e}\right)\left(\frac{\pi e Z_i N_i t}{4\pi\varepsilon_0 + \pi e Z_i N_i t}\right) \tag{10}$$

The new terms in the field charging equation are the permittivity of the particle ε, the electrical field strength E_c and the ion electrical mobility Z_i. The combined effect of the charging processes is the sum of the components n_d and n_f. Although equations 9 and 10 provide means to approximate the particle charge after the charger, it is difficult to predict the performance of the practical charger design. This is because it is difficult to obtain accurate values for the average electric field and the ion concentration in the particle-charging region. Furthermore, the charger performance is also affected by the particle penetration through the charger. The penetration, in turn, is affected by the diffusion

losses and the charged particle losses caused by the electric fields present in the charger. Instead of the theoretical approximation, the charging efficiency is, in practice, determined experimentally. A power function of equation 11 is usually used as a fit to the experimental data, for which the best fitting parameter *a* and *b* values are to be found, for instance, by the least squares sum method.

$$E_{ch} = ad_p^b \tag{11}$$

In some cases, a single power function does not provide adequate fit and a partially defined power function fit is required, as, for instance, in Marjamäki et al. (2002). According to equations 9 and 10, diffusion charging is approximately proportional to the particle diameter, whereas field charging is proportional to diameter squared. Based on this, the obtainable power in the charger efficiency fit would be in the range from one to two. The power is, however, also affected by particle losses, which often increases the power in the small particle size range. The charging efficiencies as a function of particle diameter for the instruments studied in **Papers I**–**V** are collected into figure 2.2. The functional forms of power values one and two are also plotted in the figure for comparison. These correspond to the limiting power values, based on the charging theories.

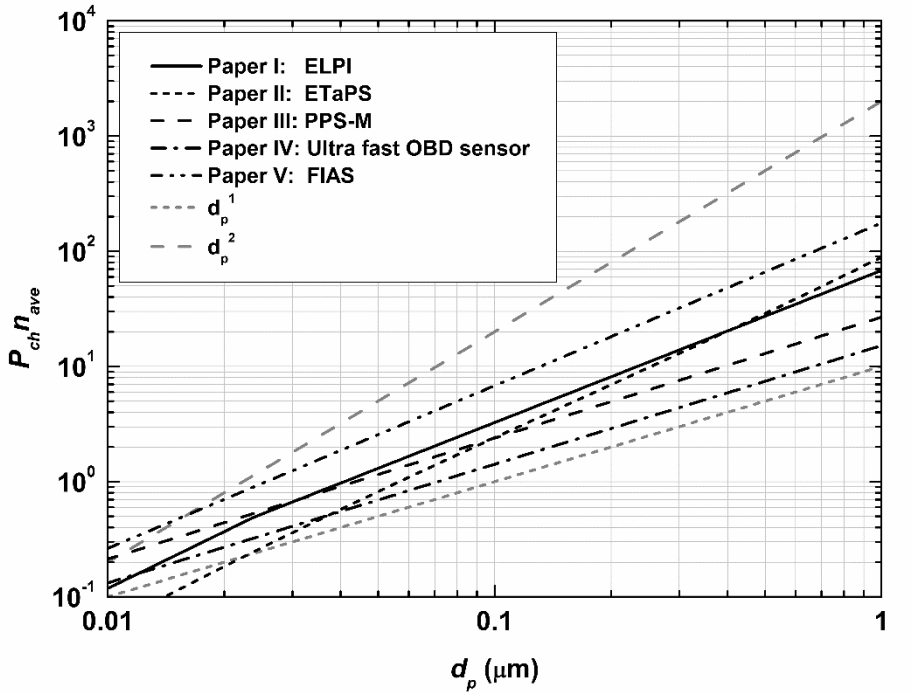

Figure 2.2. Charging efficiencies as a function of the particle diameter for the instruments studied in this thesis. The charging efficiency for the ELPI used in **Paper I** is presented according to Marjamäki et al. (2002). For the other instruments, the charging efficiency is adapted from **Papers II**–**V**. Limiting power values of one and two, based on the charging theory, shown for reference.

2.3 Charger design concepts

The $N_i t$ –product is the key parameter in the charger design that affects charger performance. Davison et al. (1985) studied the effect of the $N_i t$ –product value on different charger performance values, such as the obtained average charge number and particle losses. The results clearly indicate that particle losses increase with increasing $N_i t$ –product, while the rate of increase in the obtained charge number begins to decline with values above 10^7 s/cm^3. Intra and Tippayawong (2009) presented a thorough review on the charger designs used in many studies and commercial instruments. The majority of the $N_i t$ values listed for charger designs in the review are in the order of 10^7 s/cm^3.

Following the classification presented in Kulkarni et al. (2011), the designs fall into two main categories: designs where the measured aerosol sample travels through the corona discharge region and designs where the discharge region is separated from the aerosol sample. The main difference in these two design approaches is the electric field strength involved in the charging process. Three main design approaches for a corona discharge charger are presented in figure 2.3, which shows the ion production zone (1), particle-charging zone (2) and the ion removal area (3). The design of figure 2.3a represents a charger where the corona discharge takes place in the sample volume, whereas in designs b) and c) the discharge region is separated from the sample volume.

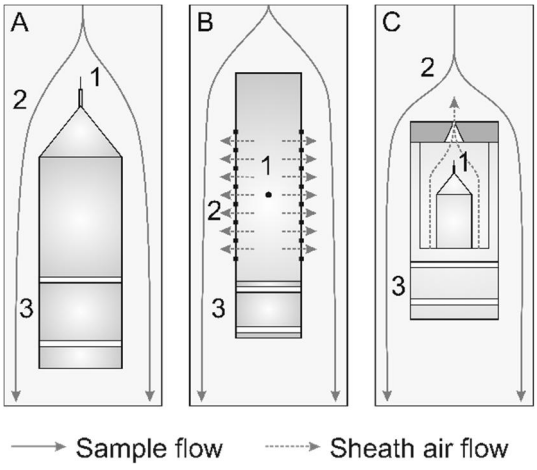

Figure 2.3. Schematic view of three different design approaches for a corona discharge aerosol charger: a) a diode-type charger, b) a triode-type charger and c) a sheath air assisted charger. The ion production zone, the particle-charging region and the ion removal zone are marked with numbers 1, 2 and 3, respectively. The sample flow and sheath air flows are marked with a solid and dashed lines respectively.

The most straightforward design (figure 2.3a) consists of a corona discharge electrode, a needle or a wire placed in an aerosol flow channel. The metal surroundings of the flow channel act as the ground electrode for the discharge. A high voltage, in the order of a few kilovolts, is connected to the discharge electrode to maintain the discharge. The high voltage is typically controlled so that the discharge current is kept constant in the range from a few nanoamperes to a few microamperes. This design represents a charger where the electric field of the corona discharge affects the charging process. Such design is used, for instance, in the Electrical Low Pressure Impactor (ELPI; Keskinen et al., 1992) and in this study in **Paper II** and **Paper V**. While the high electric field strength in the particle-charging region may lead to increased particle losses, the main advantage of this approach is the simplicity of the design. As this design has only two electrodes, it is sometimes referred to as a “diode-type” charger.

Many charger designs aim for higher charger output by addressing the charged particle losses caused by the strong electric field of the corona discharge. Sheath air flows can be used for separating the aerosol sample from the discharge electrodes or the charger walls, as in the design presented by Cheng et al. (1997). Several designs use a grid electrode between the discharge electrode and the ground to separate the discharge region from the aerosol sample flowing in the charging region (see design in figure 2.3b). Hewitt (1957) presented one of the earliest designs based on this operation principle. A perforated grid electrode separates the two regions and the discharge takes place between the needle or wire electrode connected to the high voltage and the grid electrode. A much lower electric field between the grid electrode and the ground is used to guide some of the generated ions into the charging region, where the aerosol sample flows. As the charger design has three electrodes and operation resembles the vacuum tube triode from early electronics, this design is often called a “triode-type” charger. The lower electric field in the charging region decreases the electrical particle losses, which increases the charging efficiency for the small particles. For larger particles, for which the electric field enhances the charging, the charging efficiency is, however, decreased by lack of electric field. Although the field is always much weaker than in the diode-type charger, it is possible to control the field strength to some extent in the triode charger. This provides the possibility to tailor the charging efficiency. On the downside, the ion transport efficiency from the discharge region to the charging region is significantly lower than in the diode-type charger. This leads, in addition to the otherwise more complicated power supply, to a higher power demand in the high voltage generation to achieve the same ion current. Many designs, such as presented by Liu and Pui (1975) and Biskos et al. (2005b), also use sheath air feed in order to prevent aerosol particles from entering the discharge region. While this complicates the charger design even further, it efficiently prevents the corona discharge electrode from fouling and decreases the need for maintenance. A

triode-type charger is used in many commercial instruments, such as Dekati Mass Monitor (DMM; Lehman et al., 2004), Aerasense NanoTracker (Marra et al., 2009), Testo DisCMini (Fierz et al., 2011) and naneos Partector (Fierz et al., 2014).

An even lower external electric field in the charging region is possible by using high-velocity sheath air flow to introduce the charging ions to the aerosol sample as in the design in figure 2.3c. The first ion source utilising sonic velocity sheath air flow was presented by Whitby (1961) for the use of neutralising powder particles. In this approach, the corona discharge takes place in clean sheath air inside a separate chamber. The ions are transported into contact with the aerosol sample by the sheath air flowing from the discharge region to the charging region. The operation is analogous to the triode-type charger, but in this case there is no applied electric field in the charging region. Because of the lack of electric field, the sheath air–assisted charger operates as close to a true unipolar diffusion charger as possible. As in the triode-type charger, the small particle losses as well as the large particle-charging efficiency are decreased in this design by the lack of electric field. This type of design is used, for instance, in TSI NSAM (Fissan et al., 2007), Choi and Kim (2007), Medved et al. (2000) and Kimoto et al. (2010). Instruments presented in **Paper III** and **Paper IV** are also based on this type of charger.

Regardless of the choice of charger design, to achieve sufficient particle charging a large amount of charged ions is introduced to the aerosol sample. For this reason, the excess ions not taking part in the particle charging need to be prevented from interfering with the current measured from the particles. If the signal from the ions cannot be separated from the signal from the charged particles, the ions need to be removed from the sample. This is typically achieved with an electrical collector, called an ion trap, consisting of a two-electrode system, where the charged ions are collected by the applied electric field. The ion trap is usually a separate electrode system integrated into the charger, but in some charger designs the stray electric field of the corona discharge is sufficient to remove the ions from the sample flow. While the main purpose of the ion trap is ion removal, it also can be used simultaneously for limiting the lowest detectable particle size.

2.4 Particle deposition

Apart from the optical measurement techniques, the particle concentration and size measurements are commonly based on particle deposition. In theory, all deposition mechanisms could be exploited, but the intended operational size range restricts the choice. For instance, diffusion migration can only be used for small particles, while gravitational settling works only for large particles. For the total concentration measurement, the target is ideally to deposit particles of all sizes, and for this filters are commonly used.

In the electrical aerosol instruments, the particle-collecting component needs to be placed inside a Faraday cage in order to enable measurement of the collected charge. The arrangement of a particle-collecting filter inside the Faraday cage is often called a Faraday cup electrometer (FCE). An example of an FCE design can be found, for instance, in Intra and Tippayawong (2015). For example, a simple instrument measuring the total particle concentration can be realised by combining the particle charger and a Faraday cup electrometer (see, e.g., Ntziachristos et al., 2004).

The particle deposition can be expressed as the collection efficiency η_c or the particle penetration P_i. The relation between the two is written as equation 12:

$$P_i = 1 - \eta_c \tag{12}$$

While not necessarily intentionally used for particle collection, particle diffusion often needs to be taken into account in the instrument response to include the effect of particle losses due to diffusion. Even though the structure of the practical instrument can be more complicated, equations derived for transport efficiency through a straight tubular flow channel are often used to model diffusion losses. Particle penetration through a straight cylindrical tube in laminar flow conditions was originally formulated by Gormely and Kennedy (1949). The transport efficiency is characterised by the dimensionless term ξ, which is dependent on the particle diffusion coefficient D_p, the transport line length l_t and the volumetric sample flow rate through the line Q_s:

$$\xi = \pi \frac{D_p L}{Q_s} \tag{13}$$

For laminar flow conditions, the transport efficiency can be approximated with

$$P_d = \begin{cases} 1 - 2.56\xi^{2/3} + 1.2\xi + 0.177\xi^{4/3} & \xi < 0.01 \\ 0.819e^{-3.66\xi} + 0.0975e^{-22.3\xi} + 0.032e^{-57\xi} & \xi \geq 0.01 \end{cases}. \tag{14}$$

Electrical particle deposition or migration is widely deployed in particle classification and collection. For fine-particle classification, a differential mobility analyser (DMA; Knutson and Whitby, 1975) is the most widely used instrument relying on electrical particle migration. By combining the electrical classification and the electrical detection of particles, it is possible to achieve real-time particle size distribution measurement. Mirme et al. (1981), Tammet et al. (2002) and Biskos et al. (2005a) presented real-time instruments measuring the particle size distribution by combining electrical particle classification and electrical particle detection. With more compact instrumentation such as, for instance, presented by Fierz et al. (2011), instead of measuring the full aerosol size distribution, a

median size of the distribution can be obtained by classifying the aerosol into two size classes. In addition to collecting particles for detection, electrical particle collection can be utilised to tailor instrument response for a specific purpose. This approach is used, for example, to modify the diffusion charger response closer to the LDSA concentration (Fissan et al., 2007) and to closer to number concentration (Ranjan and Dhaniyala, 2009).

The simplest electrical particle classifier is the zeroth order mobility analyser (for classification and nomenclature see Tammet, 1970), which was used in **Papers I, III** and **V**. The aerosol particles enter the classification area of the analyser uniformly distributed, and a fraction of the particles is collected to the electrodes by the applied electric field. The particle penetration through the zeroth order mobility analyser depends on the limiting electrical mobility Z_0 and the flow conditions. The term Z_0 equals the minimum electrical mobility for which the geometry has zero penetration. The limiting electrical mobility is specific to the geometry of the analyser; annular mobility analyser geometry can be written as equation 15:

$$Z_0 = \frac{Q_s \ln\left(\frac{s_o}{s_i}\right)}{2\pi l_{ma} V_{ma}} \tag{15}$$

The parameters in equation 15 are the volumetric flow rate Q_s, the inner s_i and outer s_o diameters of the flow channel, the length l_{ma} of the mobility analyser and the applied collection voltage V_{ma}. For laminar flow conditions the particle collection efficiency η_{ma} can be expressed as equation 16:

$$\eta_{ma} = \frac{Z_p}{Z_0}, \tag{16}$$

while in turbulent flow conditions the collection efficiency has the form of equation 17:

$$\eta_{ma} = 1 - e^{-\frac{Z_p}{Z_0}} \tag{17}$$

As seen from equations 15, 16 and 17, the particle collection characteristics of the zeroth order mobility analyser can be easily controlled by varying the applied collection voltage.

Particle inertial deposition can also be used for size measurement. Inertial separation takes place when accelerated aerosol flow is forced to turn around an obstacle in the flow. While the small particles follow the streamlines of the flow, the large particles having high enough inertia are separated from the flow and impact on the obstacle. This phenomenon is utilised in impactors, which are devices that collect particles larger than the

cut point diameter of the impactor. When multiple impactor stages are cascaded in series, each impactor stage collects particles of a certain size range. This technique has been used to measure the particle size distribution since the first cascade impactors were developed in the mid-20th century (Marple, 2004). A real-time aerodynamic size distribution measurement was realised in the ELPI by combining a particle charger, a cascade impactor and a multichannel charge measurement (Keskinen et al., 1992).

The cut point diameter $d_{50\%}$ of the impactor determines the aerodynamic particle size, for which impactor collection efficiency is 50%. While in principle a theoretical value for the cut point of the impactor design could be obtained, usually values obtained from calibration measurements are used in practice. For basic data reduction the cut point values of the used impactor stages are sufficient (Cooper and Guttrich, 1981); however, for more advanced use and for instrument response modelling, a fit for the measured collection efficiency curve is needed. As it is not possible to obtain theoretical expression for the collection efficiency curve, a fit formulated by Dzubay and Hasan (1990) is commonly used instead. The fit, shown in equation 18, takes into account the slope of the curve, which is described by the parameter *s*.

$$h_i = \left[1 + \left(\frac{d_{50\%}}{d_a}\right)^{2s}\right]^{-1} \tag{18}$$

The left pane of figure 2.4 shows particle penetration of the zeroth order mobility analyser used in **Paper I.** The measured values are shown together with curves fitted according to equation 14, for both singly charged particles and particles charged by the ELPI charger. As can be expected from the equation, the particle penetration is lower for the charged particles. The particle penetration fit for the impactor stage according to equation 18 is shown on the right side in figure 2.4. This fit was used in **Paper III** to model the combined effect of the inertial particle losses and the pre-cut cyclone on the instrument response.

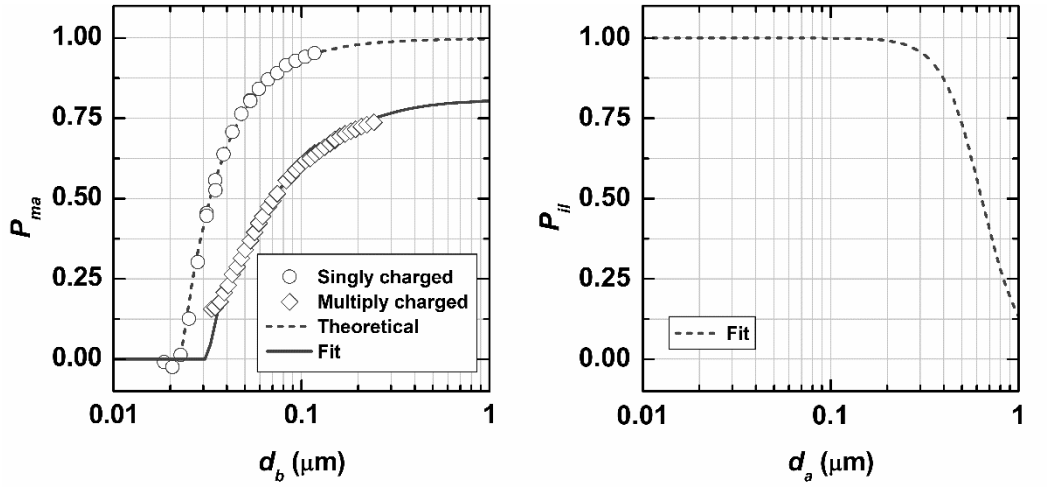

Figure 2.4. Particle penetration of the zeroth order mobility analyser on the left (adapted from **Paper I**), and on the right, the penetration of a pre-cut cyclone modelled as an impactor stage in the response model presented in **Paper III**.

2.5 Charge measurement

Because the charge levels attainable by the aerosol particles in the aerosol charger are low, a high-sensitivity electrometer is required for charge detection. A preamplifier stage realised with an operational amplifier optimised for low input bias current acts as the heart of such electrometer. In this application, the key limiting parameters for the operational amplifier are the input bias current and the input referred voltage and current noises. While the input bias current directly affects the electrometer offset reading, it also contributes to thermal drift. The input offset current is caused by the leakage currents in the semiconductor *pn*-junctions in the input stage of the operational amplifier. While the modern operational amplifiers designed for very low input bias currents are constructed with a metal oxide semiconductor (MOS) input stage, they still need to have protective *pn*-junctions in the input pins to tolerate the electrostatic discharge (Franco, 1998). Generally, with every ten-degree temperature change, the leakage current in the *pn*-junctions doubles. For this reason, the higher the input offset current at the room temperature, the higher the thermal drift of the offset on the absolute scale.

The electrometer preamplifier circuit can be realised with resistive negative feedback in a circuit called the transconductance amplifier or with capacitive negative feedback in the coulombmeter circuit (Keithley, 2004). The ideal circuits are shown in figure 2.5. The transconductance amplifier requires the use of a feedback resistor with very high resistance value. In the simplified circuit, shown on the left side in figure 2.5, the value of

the feedback resistor transfers directly to circuit gain by Ohm's law. For instance, a 1 GΩ feedback resistor corresponds to a gain of 10^9 V/A. In this circuit, the thermal noise of the resistor, called Johnson noise, contributes significantly to the noise performance of the circuit. Additionally, large-valued resistors typically have significant thermal drift, which also needs to be addressed in the practical circuit. In the coulombmeter circuit shown on the right in figure 2.5, the feedback resistor is replaced by a small-valued capacitor, thus eliminating the noise and thermal drift of the resistor. Since the output of this circuit is related to the integrated charge of the input current, the feedback capacitor needs to be discharged repeatedly when measuring DC currents. Additionally, the leakage current through the capacitor needs to be very low for voltages present in the circuit. Although the coulombmeter circuit seems tempting for the low noise application, the transconductance amplifier is in practice more tolerant for the capacitances connected to the input (Keithley, 2004). However, for the fixed operating surroundings of the aerosol instrument, both approaches properly designed give sufficient performance.

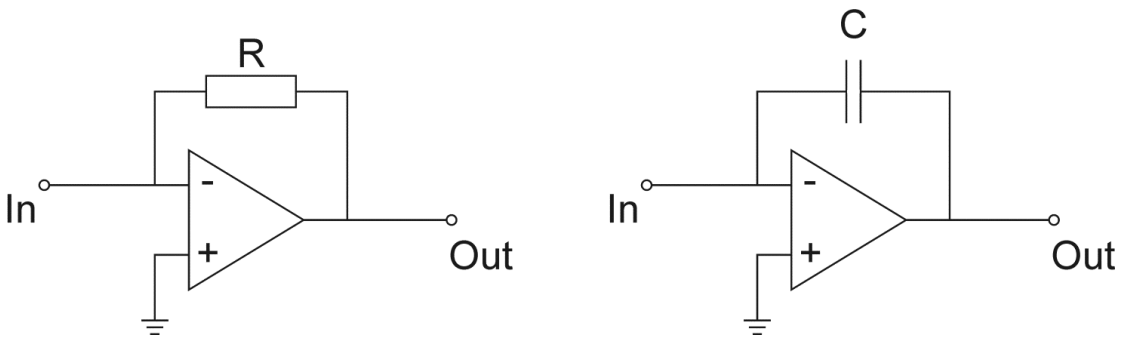

Figure 2.5. Simplified electrometer amplifier circuits: the tranconductance amplifier on the left and the coulombmeter circuit on the right.

While the particle charge measurement methods typically rely on particle collection, it is also possible to construct an electrical aerosol instrument without particle collection. By this method, the pressure drop of the collection element, for instance a filter, is eliminated, providing the possibility to reduce power consumption by the flow system. Additionally, the need for instrument service is reduced, because of the lack of loading effects of particle collecting. Lehtimäki (1983) presented an instrument that accomplished non-collective electrical particle measurement. This same operation principle, called the escaping charge technique (ECT), was used in the instruments studied in **Paper II**, **Paper III** and

Paper IV. In this measurement technique, the high voltage source of the corona discharge particle charger is isolated from the surroundings, and the charge carried away by the particles from the corona source is measured. This approach requires an isolated power source with very high isolation resistance to supply the corona discharge in order to keep the leakage currents below the measured current levels.

While the traditional filter-collection-based electrical measurement determines the total charge of the particles, the ECT method measures the charge particles acquire during the charging process. At first glance, this does not seem to be a major difference, but the situation changes if there is a significant initial net charge on the particles. A schematic picture of the ECT method is presented in figure 2.6, showing the paths of the different current components involved in the measurement. The primary measured current component originates from the charge the charger provides to the particles, marked as current I_{pc}. Some of the particles may deposit inside the instrument causing particle losses, and if the particles carry a charge, they conduct current marked as component I_{pl}. A majority of the ions generated for the charging process, marked as current I_{ch}, do not contribute to the actual charging process but are collected in the ion trap as current I_i. While not desirable, some of the ions may escape the ion trap and contribute to the measured signal by a current component I_{il}. The particle initial charge, marked as current component I_{ic}, also contributes to the measured signal, and the resulting current signal measured, I_m, is the difference between the output current I_{out} and the particle initial charge I_{ic}. The power supply and return currents required for the charger and the ion trap supply current are also marked on figure 3 as I_c, I_c' and It. As stated earlier, the charger's charging efficiency is relatively independent of the initial charge; however, the amount of charge transferred from the corona charger depends on the initial charge state of the particles. When utilising the ECT measurement method, this may need to be taken into account if the measured particles have significant net charge. This situation is, for instance, related to aerosol processes involving high temperatures, such as combustion or high-temperature nanomaterial production processes. The initial net charge levels are, however, typically quite low.

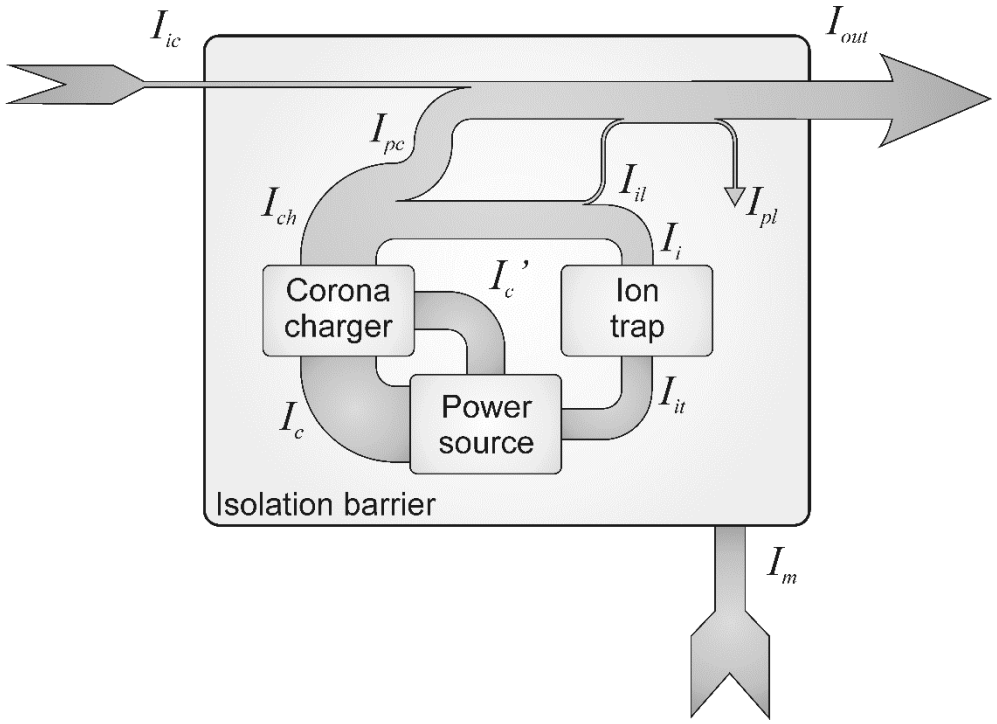

Figure 2.6. The current components related to ECT measurement.

Another way to accomplish non-collective charged particle detection is to use an inductive ring as first presented for single-particle detection by Gajewski and Szaynok (1981). Fierz et al. (2014) utilised this detection method for an aerosol instrument designed for ultrafine particle concentration measurement. The design was based on a charger that is repeatedly switched on and off. This causes the formation of clouds of charged particles in the flow. When these clouds flow through a ring-shaped electrode, an electrical disturbance is induced to the electrode. The magnitude of the disturbance is relative to the total charge of the cloud, which in turn is related to the particle concentration and charging efficiency. This method is also sensitive for the initial charge on the particles if using a conventional unipolar charger, but this shortcoming can be solved, for instance, by using a charger with alternating polarity.

3 Experimental response characterisation

For practical applications, the instrument's overall response needs to be known. Ideally, a complete response model is formulated for the instrument that takes into account the effect of each component included in the design. This response model can be used for instrument development, instrument performance evaluation and measured data processing. While theoretical assumptions can be used for some of the components, it is difficult to obtain an accurate theoretical estimation for charging efficiency. For this reason, experimental response characterisation is required for the instruments based on the electrical detection of aerosol particles. To obtain the instrument response in the characterisation measurements, instrument output is compared to the concentration of the test aerosol. The aerosol total number concentration is most often used for reference. The effect of the particle losses or the effect of the particle-collecting devices on the response can be obtained by measuring the particle penetration or the collection efficiency of the instrument. For the aerosol instruments, the response of the instrument is presented as a function of particle size as the result from the characterisation measurements.

3.1 Methods based on monodisperse test aerosol

The preferred approach for aerosol instrument response measurement is to challenge the instrument to a monodisperse test aerosol of a known particle size and compare the output to the reference measurement. This is then repeated to cover the operational size range of the instrument. The main advantage in this approach is that, in the ideal case, measurement result is directly the instrument response as a function of particle size. On the downside, the available particle concentration is typically quite limited, which requires sufficient sensitivity from the tested instrument.

There are several ways to produce the monodisperse test aerosols (see, for instance, Berglund and Liu, 1973; Iida et al., 2014; Tavankoli et al., 2014). The choice of generation method depends on the particle size range of interest. In the size range from a few nanometres up to one micrometre, perhaps the most widely used method is to use a DMA (Knutson and Whitby, 1975) to select a narrow electrical mobility range for the test aerosol. This method has been used in **Paper I**, **Paper III** and **Paper V**. The measurement setup used in **Paper III**, shown in figure 3.1, represents a typical response measurement setup utilising the DMA. As a first step in the setup, a polydisperse primary test aerosol is generated. For this, a variety of aerosol generation methods can be used, and

the choice of method depends primarily on the preferred particle material. For liquids, droplet-like particles, aerosol nebulisers and atomisers or for narrower primary size distribution, an evaporation-condensation generator (Liu and Lee, 1975) can be used. As for solid particle materials, thermal generation methods are suitable. After aerosol generation, the primary aerosol is classified by the DMA to get the monodisperse test aerosol. A dilution air feed needs to be added to the classified aerosol flow after the DMA if the total sample flow required by the instruments exceeds the polydisperse flow of the DMA. After dilution, the sample flow needs to be thoroughly mixed before it is divided to the instruments. A proper mixing and a good quality flow divider ensure equal concentrations for all flow branches. Although a dilution air feed is not always required, it is always a good practice to use a flow mixer before the flow divider. From the flow divider, one extra flow branch is used for the excess flow. Producing monodisperse test aerosol in excess helps to maintain the flow balance of the setup.

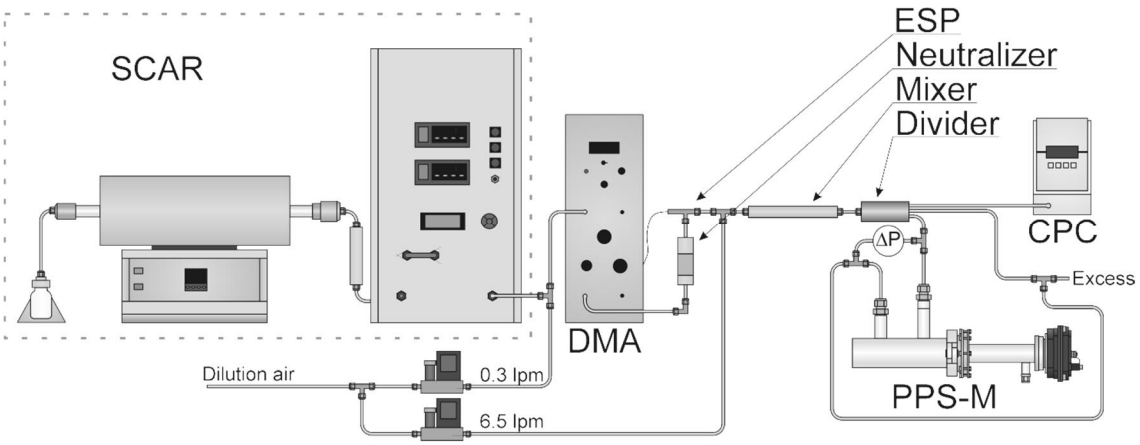

Figure 3.1. An example of a measurement setup for the response characterisation with monodisperse test aerosol (**Paper III**).

The two main problems in the DMA method arise from its operation principle. The DMA does not classify the particles according to their size, but their electrical mobility. Firstly this means that all the neutral particles and also, because of the DMA construction, particles of opposite polarity are lost. This limits the maximum available concentration of the classified test aerosol. This is especially problematic for small particle sizes, since the charging efficiency of the aerosol neutraliser used in the DMA decreases sharply with decreasing particle size. The second problem is also related to charging probabilities. As seen in equation 7, electrical mobility links the particle size and charge. Because the particles entering the DMA are typically in charge equilibrium, the particles have a charge

distribution. For each particle size, there are certain amounts of neutral, singly, doubly etc. charged particles and the ratios depend on particle size. Based on this, for a given particle size there exists a certain amount of multiply charged particles in addition to singly charged particles. The ratio between the singly charged and multiply charged particles in the DMA output depends on the median size and geometric standard deviation (GSD) of the primary aerosol size distribution. For the smallest particle sizes this is not a major concern, as the probability for multiply charging is very low for small particles. However, for particles larger than approximately 30 nm, multiple charging may need to be taken into account.

In the example setup shown in figure 3.1, the single charged aerosol reference (SCAR; Yli-Ojanperä et al., 2009) was used for the primary aerosol generation. The SCAR is based on the condensational growth of mobility classified small seed particles, which leads to a narrow particle size distribution and singly charged particles. While the generated aerosol is not as monodisperse as with the DMA method, the distribution would be sufficiently narrow for the response measurement even without the added DMA. However, when combining the SCAR and the DMA in the monodisperse test aerosol generation, a truly monodisperse test aerosol can be obtained.

3.2 Method based on polydisperse test aerosol

In many cases, it is not possible to produce monodisperse test aerosols in sufficient concentrations for the response measurement. In this case, the polydisperse calibration method needs to be used. In this method the tested instrument is challenged to different polydisperse test aerosol size distributions and the output is recorded together with the size distribution measurement. In this approach, there are several possibilities for test aerosol generation and the size distribution measurement. However, a narrow size distribution in the test aerosol and a good size resolution in the size distribution measurement are preferred. The polydisperse response characterisation method was used in **Paper II** and **Paper IV**. As an example, the measurement setup used in **Paper IV** is presented in figure 3.2. In this setup, a modified diesel fuel–burning air heater (Högström et al., 2012) was chosen for the aerosol generator because the characterised instrument was intended primarily for measuring soot-like exhaust emission particles. For the size distribution measurement, a scanning mobility particle sizer (SMPS; Wang and Flagan, 1990) was used in the example setup. As the generated test aerosol concentration may be very high, a dilution system is usually required for the reference instruments. In the measurement setup shown in figure 3.2, two ejector diluters before the SMPS and an additional third before the CPC were required to bring the test aerosol concentration within the measurement range of the instruments.

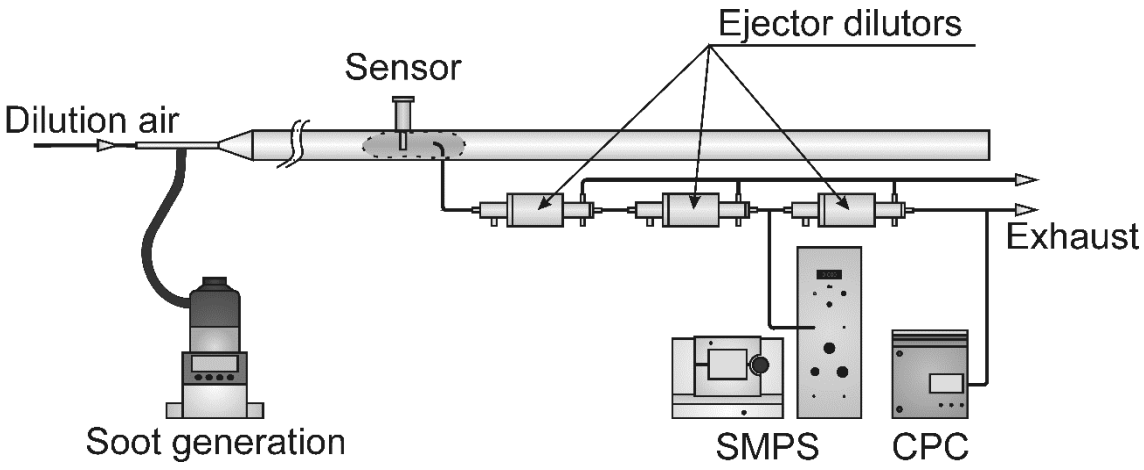

Figure 3.2. Response measurement setup used in **Paper IV**, for obtaining the instrument response with polydisperse test aerosol.

While it is also usually possible to obtain the total number concentration from the particle size distribution measurement, it is a good practice to use a separate instrument for the total number concentration measurement. For instance, the accuracy of the SMPS in the concentration measurement is sensitive to the flow balance of the DMA. While not significantly affecting size distribution measurement accuracy, a small imbalance in the DMA sheath flow can lead to a significant error in the total concentration measurement. When using a separate and preferably calibrated CPC parallel to the SMPS, the concentration measurement accuracy can be greatly improved.

The main problem in the polydisperse calibration method is that the measurement result does not directly describe the instrument response as a function of the particle size. In order to obtain the response, a model for instrument operation is needed together with a fitting routine, where the modelled instrument output is compared to the measured output. The best fitting values for the response model parameters are determined, for instance, by minimising the squares sum of the difference.

3.3 Temporal performance characterisation

The time resolution of an instrument can be expressed either as the time constant τ or as the rise time t_r. The former corresponds to the relaxation time constant of the exponential decay. The latter is usually expressed as the 10–90% rise time, which corresponds to the time required for the signal to change from 10% to 90% of the final value when challenged to a step input. For an exponentially changing signal output, these two values are proportional. These numbers describe the instrument time response sufficiently for cases in which measured signal changes are much slower than instrument time response. When the time scale of the signal change approaches the time constant of the instrument, or when the exact temporal nature of the signal is of interest, more detailed information on the instrument time response is required. With the help of the instrument's impulse response, the instrument time response effect can be compensated for in the measured output by deconvolution. This applies to cases in which the signal changes are slower than the instruments' time response.

The instrument's impulse response can be obtained by measuring the instrument output during fast signal impulses. For aerosol instruments, this could be accomplished by generating a narrow burst of aerosol particles, by spark ignition (Schwyn et al., 1988) or laser ablation (Ullmann et al., 2002), for instance. Since the primary particle size produced by both of these methods is typically quite small, it might be challenging to get sufficient signal for measurement. For this reason, it is often more practical to obtain the impulse response by first measuring the instrument's step response. To produce the step response, a sharp step in the measured aerosol concentration is required; then the instrument impulse response can be obtained by differentiating the measured step response.

An example of the temporal performance characterisation was presented in **Paper IV**, in which instrument time resolution was evaluated by the step response measurement. In the measurement setup, a sharp step in aerosol concentration was obtained by introducing a high velocity dilution air stream towards the sensor inlet. The used dilution air feed setup is shown in figure 3.3, in which the dilution air feed was controlled by a fast-acting magnetic valve. The dilution air feed rate was set high enough to ensure fast transient in the test aerosol concentration.

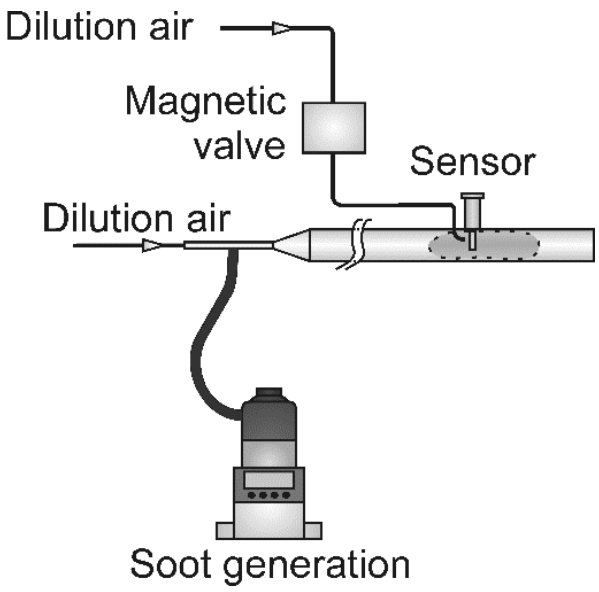

Figure 3.3. Dilution air feed setup used in the step response measurements presented in **Paper IV**.

4 Instrument design and performance

The instrument design and performance evaluation are important steps in the instrument design process. Aspects, such as the operational surroundings, the targeted application and the desired measurement performance needs to be taken into account. Performance characterisation is needed to verify the correct operation of the instrument and to find out the instrument response. In the following the key design aspects and the performance of the instruments included in this thesis are discussed.

4.1 Real-time particle effective density measurement

The particle effective density combines three different parameters describing the morphology of fractal-like particles: bulk density, primary particle size and fractal dimension. With the help of effective density, one of these parameters can be obtained if the two other parameter values are known or can be approximated. For effective density measurement, mobility and aerodynamic particle diameters must both be measured. This can be accomplished, for instance, by using DMA and an impactor in series (Kelly and McMurry, 1992) or by using SMPS and ELPI in parallel (Ristimäki et al., 2002). Both of these methods require a rather complicated setup for the measurement.

In **Paper I**, a new add-on module for the Electrical Low-Pressure Impactor was introduced to allow real-time particle effective density measurement. The designed module replaces the Classic ELPI's (Dekati ltd., Finland) upper impactor stages with a mobility analyser, which adds mobility size information to the ELPI's aerodynamic size distribution measurement. The mobility analyser and the impactor arrangement is shown in figure 4.1. Particle effective density is obtained, with the help of equation 19, by comparing the mobility median size d_{im}, acquired from the mobility measurement, to the aerodynamic median size d_{ia} from the impactor measurement. All the necessary signals are recorded in one-second time resolution, and the data processing can be done online, which enables real-time effective density measurement.

$$r_{eff} = \frac{d_{ia}^2 C_c\left(d_{ia}\right) r_0}{d_{im}^2 C_c\left(d_{im}\right)} \tag{19}$$

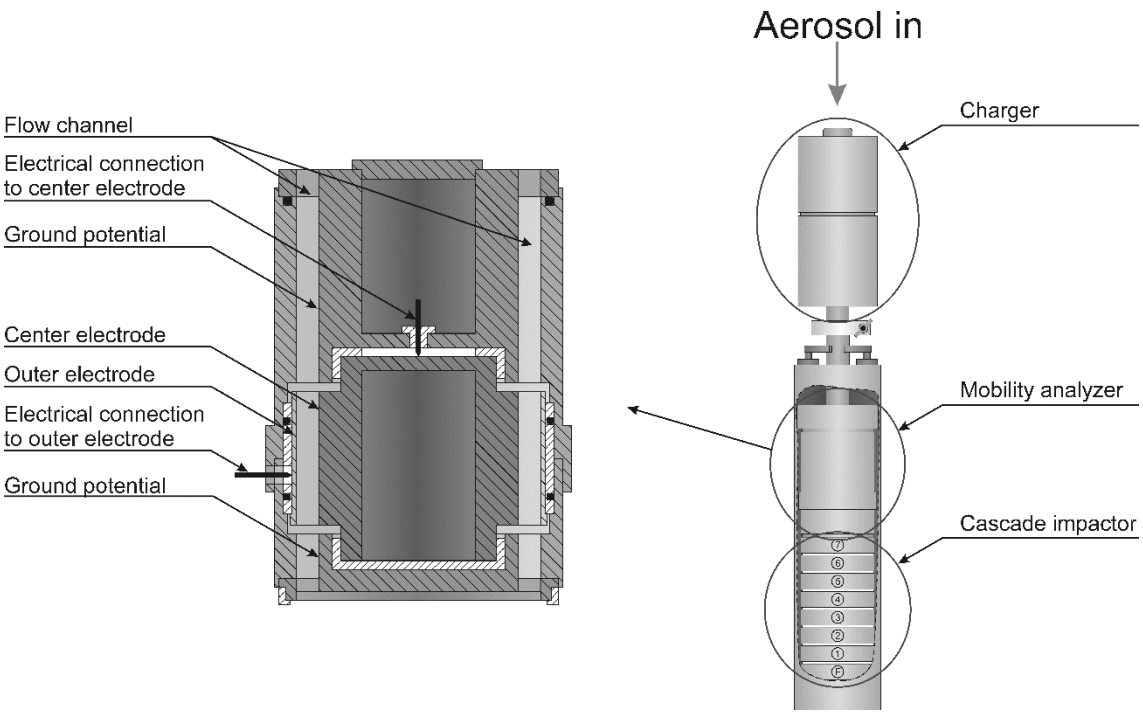

Figure 4.1. Cross section of the mobility analyser and the ELPI impactor arrangement designed for the real-time particle effective density measurement. (Adapted from **Paper I**)

The mobility median size measurement is based on measurement of the current from the particles collected in the mobility analyser and comparing that to the total current measured. To link this measured mobility analyser current fraction to particle mobility median size, the mobility analyser's particle collection efficiency is needed. Since the mobility analyser is placed after the ELPI charger, the increased charge level of the particles' effect on collection efficiency needs to be taken into account. To accomplish this, mobility analyser collection efficiency was first measured for singly charged particles classified by a DMA. The measured collection efficiency was compared to the theoretically predicted collection efficiency to verify mobility analyser operation, then the collection efficiency measurement was repeated for monodisperse particles charged by the ELPI charger. From this, a fit for the particles' effective average charge was obtained. With this information, it was possible to find a relation between the measured mobility analyser current fraction and the polydisperse size distribution mobility median size.

A flow chart of the data processing routine is presented in figure 4.2, showing the instrument components and the key parameters related to the measurement. As the aerosol

flows through the ELPI charger and the particles are charged, the number size distribution marked as $N(d_b)$ converts to the current size distribution $I'(d_b)$. Both these size distributions can be expressed either as the function of the mobility particle size d_b or as the function of the aerodynamic particle size d_a. After the charger, a fraction of the particles is collected in the mobility analyser, and the current from the collected particle fraction is measured. The remaining particles, marked as current size distribution $I(d_b)$, continue to the impactor, where they are classified, and as a result, current size distribution $I(d_a)$ is obtained. The charger efficiency $E_{ch}(d_b)$, the average number of charges per particle $n_{ave}(d_b)$ and the mobility analyser collection efficiency $\eta_{ma}(d_b)$ are all functions of the particle mobility diameter, whereas the impactor classifies the particles according to their aerodynamic diameter. To obtain particle effective density, the mobility analyser's current fraction is first converted to the mobility median diameter d_{im} with the help of the simulated relation between the two. This median diameter is related to the current size distribution $I'(d_b)$. To find the corresponding aerodynamic median diameter, the mobility analyser collection efficiency needs to be compensated for in the impactor's current size distribution. From the compensated aerodynamic current size distribution $I'(d_a)$, the aerodynamic median diameter d_{ia} is obtained, and the resulting particle effective density is obtained with the help of equation 19. Since particle effective density is required in order to link mobility analyser collection efficiency to the impactor's aerodynamic current distribution, an iterative calculation is required. For the iteration, unit density is used for the initial approximation; the last iteration round's effective particle density is returned as the result.

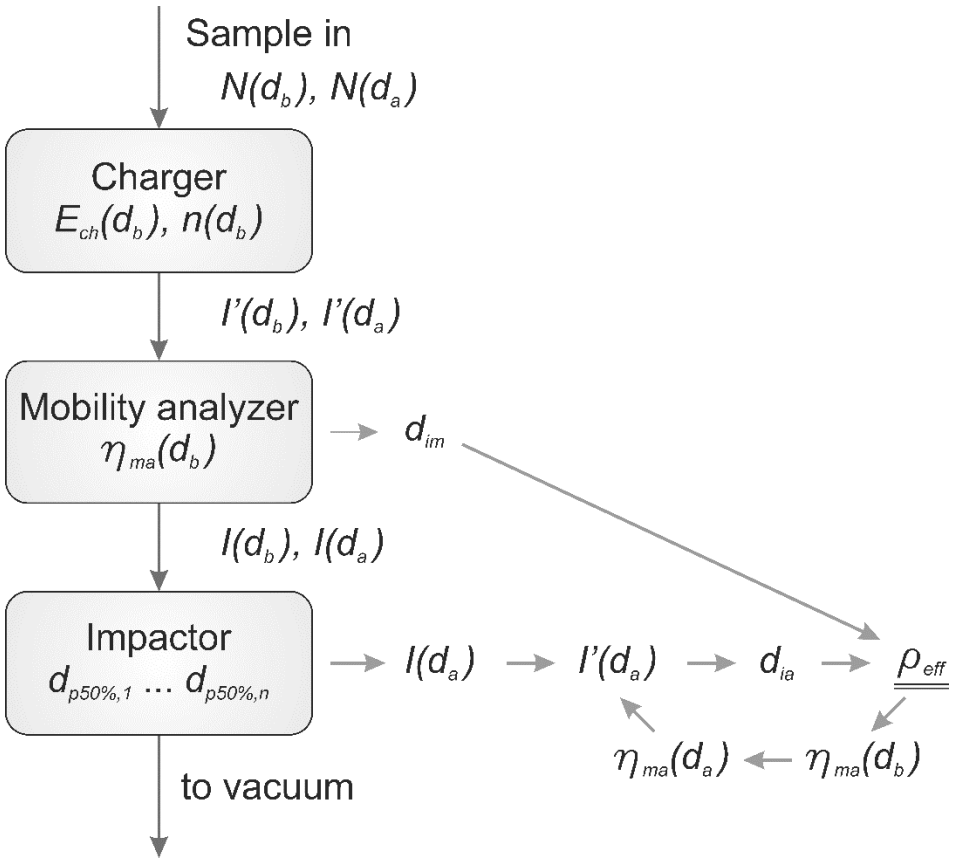

Figure 4.2. A flow chart of the data processing routine used in the particle effective density measurement in **Paper I**.

As the added mobility analyser replaces the impactor's upper stages, the operational aerodynamic size range is narrower than in the original ELPI instrument. The mobility measurement's size range is limited by the particle-charging properties of the ELPI charger. With increasing particle size, the the rate of increase in the average number of charges per particle is greater than the rate of the decrease in the particle mechanical mobility; this leads to a loss of resolution in the mobility analyser measurement at large particle sizes. Because of these limitations, the instruments operational particle size range is from 30 nm up to 200 nm for mobility size distribution count median size. Furthermore, this method is only applicable for single modal size distributions, and an approximation of the distribution GSD is needed for the data processing.

Example data from the real-time effective density measurement for different laboratory test aerosols are presented in figure 4.3. As seen from the figure, the obtained effective density values correlate well with the reference density measurement. For the liquid aerosol particles (DOS, Santovac, Fomblin), variation in both density measurements was very low and the obtained values are close to the material bulk values. For the solid silver

particles, variation was increased in both measurement methods, and the obtained values differ from the bulk density. This difference may result from the non-spherical shape of the particles or from impurities, such as those caused by particle surface oxidation. Since the developed method is sensitive for detecting particle morphology changes, the same operating principle was used in a simplified instrument developed for monitoring a nanoparticle production process stability (Juuti et al., 2016).

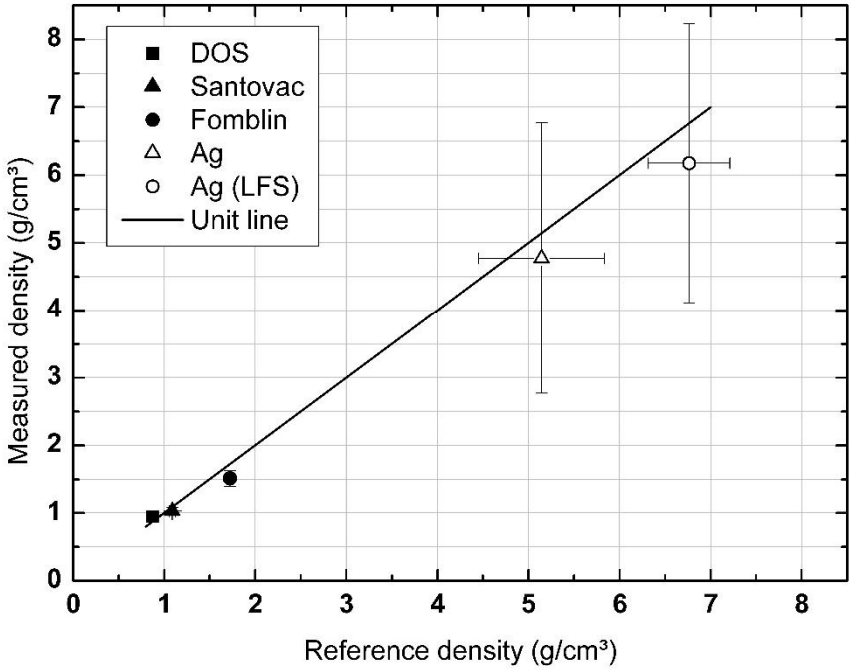

Figure 4.3. Measured particle effective densities for different laboratory test aerosols. The real-time effective density measurement is compared to the reference density measurement. (**Paper I**)

4.2 Exhaust emission measurement

The exhaust gas flow of an engine or a vehicle is at an elevated temperature and contains water from the combustion. Because of the high temperature, sample conditioning systems are required for particle emission measurement, in order to bring the sample

temperature to the particle measuring instruments' operational range. These systems usually lower the temperature by diluting the sample, to avoid water condensation and thermophoretic particle losses. The use of sample conditioning systems adds to measurement setup complexity considerably.

The Electrical Tail Pipe Sensor (ETaPS, Tikkanen et al., 2007), introduced in **Paper II**, and the PPS-M sensor (Ntziachristos et al., 2011, Lanki et al., 2011), characterised in **Paper III**, are both initially designed for particle emission measurement directly from the exhaust gas flow. A schematic view of the sensor construction and of key operational components are shown in figure 4.4. While both instruments are based on the ECT measurement method, the designs are somewhat different. The ETaPS is based on a sensor probe, which installs directly into the exhaust flow. This probe consists of a diode-type corona discharge charger surrounded by perforated walls. When placed in the exhaust flow, a part of the flow travels through the sensor probe. The particles in the flow are charged inside the probe, and the charge carried away by the particles is measured. On the other hand, the PPS-M is an instrument that connects to the exhaust line by two flow connections, one for the sample inlet and the other for returning the sample and excess flows to the exhaust line. By returning the flow back to the exhaust line, the pressure difference and the power demand required for the sample flow is minimised. Inside the PPS-M, there is a sheath air-assisted corona discharge charger, which also supplies the necessary pump flow for the integrated ejector pump. The design also includes an integrated mobility analyser acting simultaneously as an ion trap.

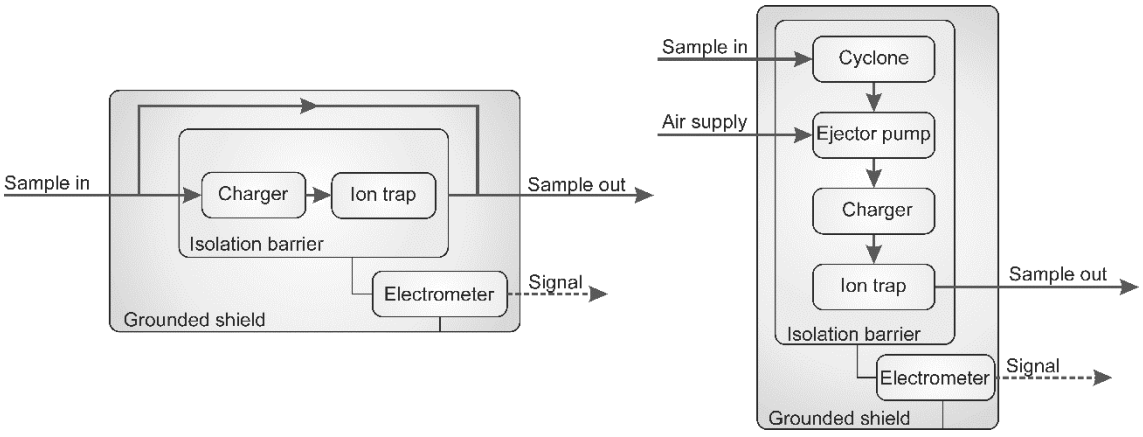

Figure 4.4. A schematic view of the instrument construction showing the key components of the ETaPS and PPS-M instruments. The ETaPS is on the left and the PPS-M is on the right (adapted from **Paper III**).

Response characterisation measurements and a response model was presented for both sensors. For the ETaPS, the response was measured in a flow circulating measurement setup, using polydisperse test aerosol. This arrangement was chosen because the sensor's high flow velocity range required a high volumetric flow rate. The response was characterised over the flow velocity range of 1 to 36 m/s. The fitted response model was based on the combined effect of the particle diffusion and field charging (equations 9 and 10) with a volumetric flow rate approximation through the charging zone of the sensor, according to equation 20.

$$R_{ETaPS} = \tfrac{1}{4} p d_{duct}^{2} R \left(V_{flow} - V_{\min}\right)\left(n_d + n_f\right) e \qquad (20)$$

In equation 20, the volumetric flow rate approximation through the charging region was based on the assumption that the flow velocity in the charging region follows the flow velocity inside the flow duct V_{flow} but is decreased by the factor R. An additional term V_{min} was included to simulate particle losses inside the sensor with low flow velocities. The remaining parameters in equation 20 are flow duct diameter d_{duct} and the elementary charge e. The $N_i t$ product, required by the charge number estimation, was obtained according to equation 21 by using the approximated flow velocity inside the charging region, the effective length of the charging region L_{eff} and the estimated ion concentration N_i.

$$N_i t = \frac{N_i L_{eff}}{R\left(V_{flow} - V_{\min}\right)} \qquad (21)$$

Additionally, an estimate for an average electrical field E_{ave} during the particle charging was required for field charging. Table 4.1 shows the fitted parameter values required for the response model. The effect of the exhaust flow velocity to the ETaPS sensor response is shown in figure 4.5, which is simulated with the response model for single modal lognormal size distributions with count median diameters of 0.06, 0.08 and 0.10 µm.

Table 4.1 Fitted parameter values in the ETaPS sensor response (**Paper II**)

Description	Symbol	Value
Effective length of the charging region	L_{eff}	$6.8 \cdot 10^{-3}$ m
Average electric field	E_{ave}	$2.07 \cdot 10^{-5}$ V/m
Ion concentration	N_i	$1.28 \cdot 10^{15}$ 1/m^3
Minimum flow velocity	V_{min}	1.6 m/s

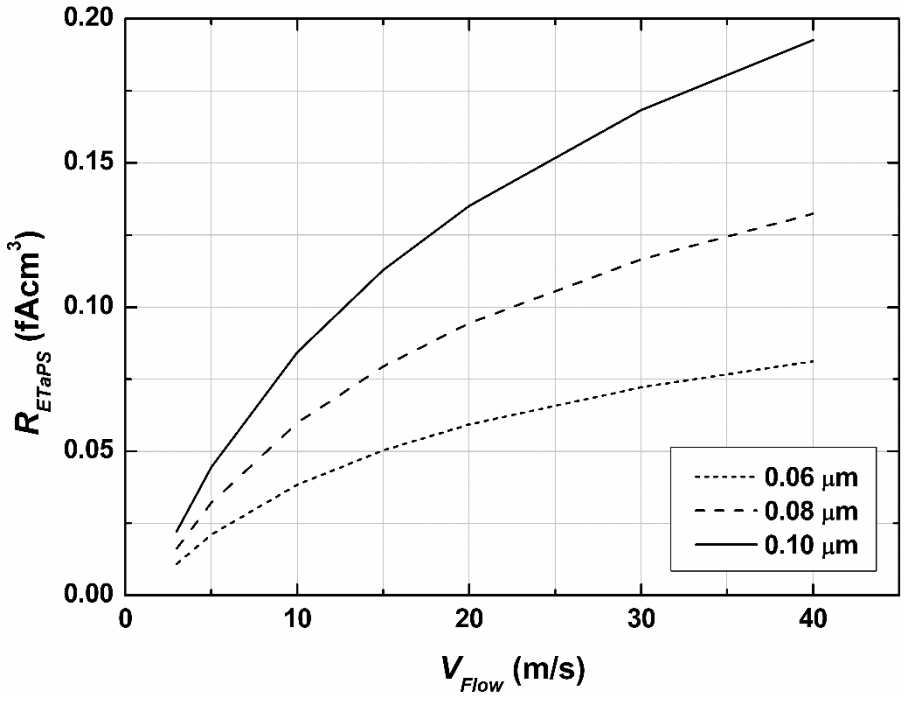

Figure 4.5. The flow velocity dependence of the ETaPS sensor response for lognormal size distributions. The response of three different size distributions having count median sizes of 0.06, 0.08 and 0.10 µm are shown. The geometric standard deviation used in the simulation was 1.8. (Adapted from **Paper II**)

In the case of the PPS-M sensor, the response was characterised by using monodisperse test aerosol. In the measurement setup, the monodisperse particles were neutralised prior to the measurement and a calibrated CPC was used as the reference instrument. Since the PPS-M mobility analyser was integrated to the instrument, it was not possible to separate the analyser from the instrument for the response measurement. Instead, analyser response was measured by using singly charged monodisperse particles and measuring the charge collected by the mobility analyser with the charger switched off and comparing the measured current to the number concentration measured by the reference CPC. The response model of the PPS-M was based on charger efficiency and particle penetration through the sensor, as written in equation 22

$$R_{PPS-M} = P_d P_{ma} P_{il} E_{ch} e Q_s \tag{22}$$

Charging efficiency E_{ch} is a major contributor in the instrument response. For the response model, a power function fit of equation 23 was used to describe the effect of the charger. Since in the PPS-M, the mobility analyser is also used as the ion trap and it is not operated at a fixed collection voltage, the effect of changing collection voltage to charging efficiency was included in the fit.

$$E_{ch}\left(d_p, V_{ma}\right) = \left(1.05\times10^{6} - 7.23\times10^{4}\ln\left(1+1.12\times10^{-2}V_{ma}\right)\right)d_p^{\,1.05} \tag{23}$$

In order to model particle penetration, the effects of the diffusion losses, mobility analyser penetration and the combined effect of the pre-cut cyclone and the inertial particle losses were taken into account. An estimation for the diffusion losses was obtained with a computational fluid dynamics (CFD) simulation. A transport efficiency P_d based on equation 14, was fitted to the simulation results with a value of $1.79\cdot10^5$ s/m^2 used for u_0.

$$P_d = \begin{cases} 1 - 2.56\left(u_0 D_p\right)^{2/3} + 1.2u_0 D_p + 0.177\left(u_0 D_p\right)^{4/3} & u_0 D_p < 0.03 \\ 0.819e^{-3.657u_0 D_p} + 0.097e^{-22.3u_0 D_p} + 0.032e^{-57u_0 D_p} & u_0 D_p \geq 0.03 \end{cases} \tag{24}$$

A voltage-dependent fit for the measured mobility analyser penetration, P_{ma}, was constructed according to the turbulent mobility analyser penetration shown in equation 17. For practical reasons, the parameters related to the mobility analyser's mechanical design combined to a single constant K, leaving the sample and pump flow rates Q_s and Q_p for the equation. A value of 1.37 1/m was fitted to the constant K, based on the mobility analyser collection efficiency measurements.

$$P_{ma}\left(Z_p\right) = e^{-\frac{Z_p V_{ma}}{(Q_s+Q_p)K}} \tag{25}$$

Since the particles are charged before the mobility analyser, the effective average charge affects mobility analyser penetration. A particle average charge approximation, shown in equation 26, was constructed from the charger efficiency fit by approximating the particle penetration through the charging zone to one. Because of the electrical detection, the average charge minimum value was limited to one.

$$n_{ave}\left(d_p\right) = \begin{cases} 1, & d_p < 1.63\times10^{-8}\,m \\ 6.13\times10^{7}\,d_p^{\,1.05}, & d_p \geq 1.63\times10^{-8}\,m \end{cases} \tag{26}$$

The pre-cut cyclone's inertial losses and penetration were modelled with the term P_{il}. The fit, shown in equation 27, is based on equation 18, which is an approximation used to describe the operation of inertial impactors.

$$P_{il}\left(d_a\right) = 1 - \frac{1}{1+\left(\frac{6.36\times10^{-7}\,m}{d_a}\right)^{2.06}} \tag{27}$$

The components of the response model are shown in figure 4.6 for unit density particles, with a mobility analyser collection voltage of 400 V. The components included in the particle penetration fit are shown separately on the left side, and the combined total particle penetration P_{tot} and the charger efficiency fit are shown on the right side.

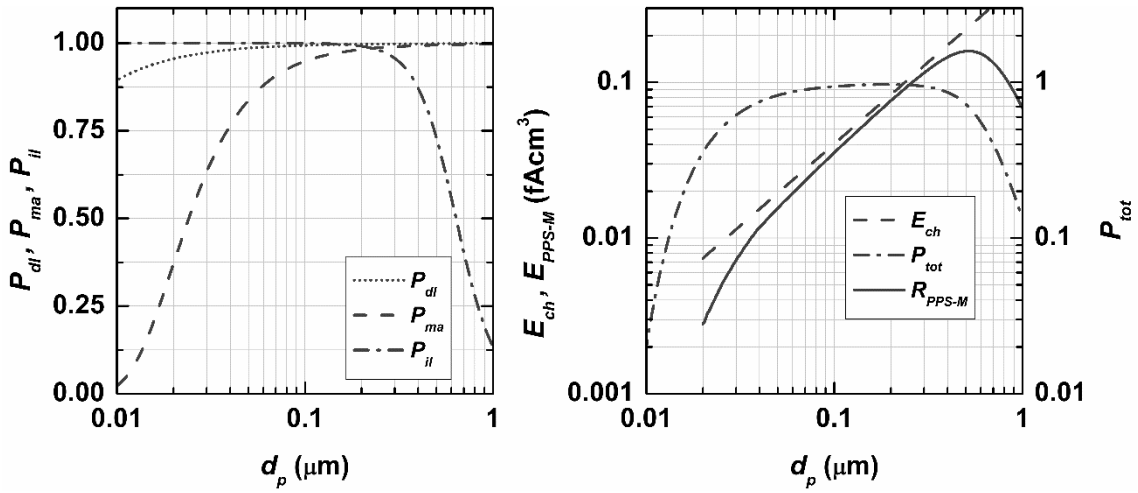

Figure 4.6. The components used in the response model of the PPS-M sensor. The diffusion losses P_{dl}, inertial losses P_{il} and the mobility analyser collection efficiency, all expressed as penetrations, are shown on the left. The charger efficiency E_{ch}, the total particle penetration P_{tot} and the resulting instrument response R_{PPS-M} are shown on the right.

A comparison between the characterisation measurement results and the fitted response model is presented in figure 4.7. The measured data are shown as points for three different mobility analyser collection voltages, and the response model is shown as a solid line. Despite the approximations made in the response model, the fitted model is in good agreement with the experimental measurement results.

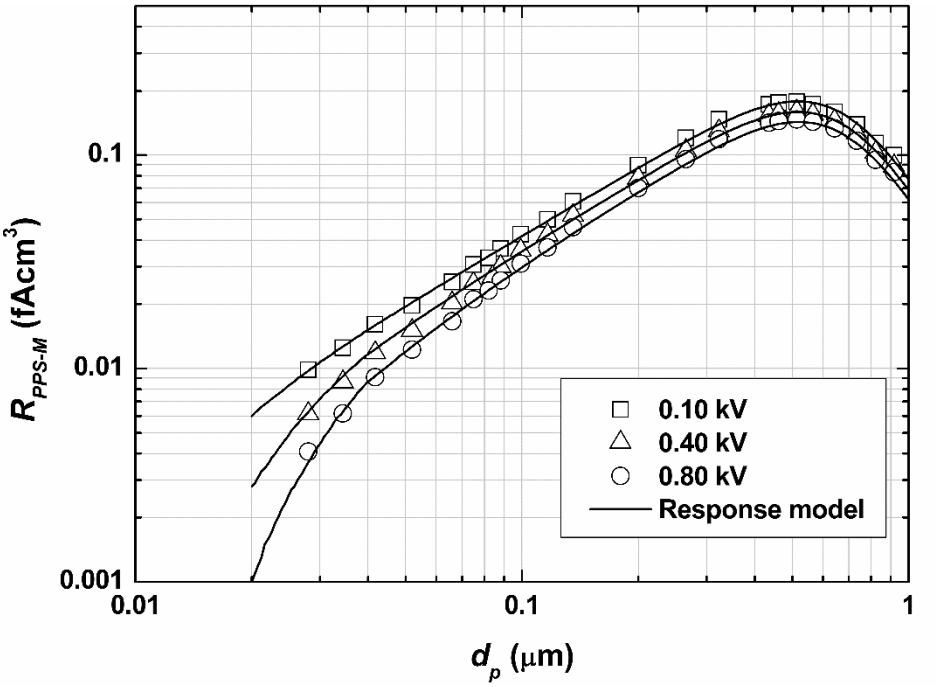

Figure 4.7. The measured response of the PPS-M sensor shown together with the fitted response model. Both are shown for different mobility analyser collection voltages (adapted from **Paper III**).

The obtained models for both instruments are useful in interpreting the measurement results. Since the regulatory limits set for engines and vehicle particle emissions are expressed as number and mass emission, it is practical to convert the measurement results to units compatible with regulations. With the help of the models, it is possible to obtain conversion factors needed for this conversion for the approximated particle size distributions. A good approximation for the distributions can be obtained, since the size distributions in this application remains in a relatively narrow range (see, e.g., Harris and Maricq, 2001). Another approach was presented in Amanatidis et al. (2014), in which a method using two PPS-M sensors in parallel with different mobility analyser collection voltages for obtaining a real-time estimation on the size distribution median size was presented.

4.3 Ultra-fast on-board emission measurement

The emission regulations require the in-use monitoring of the operation of the exhaust after treatment devices; this creates a demand for emission-related instrumentation for on-board use. The prototype instrument presented in **Paper IV** targets an on-board diagnostics (OBD) sensor to measure particle emissions. The presented OBD sensor is essentially a miniaturised version of the PPS-M and is based on the same operation principle. In **Paper IV**, the response characterisation, together with vehicle and engine dynamometer test measurements, was presented. The sensor design showing the components and operational parameters is presented in figure 4.8. The prototype's overall dimensions were 190 mm in length and 36 mm in diameter at the largest point.

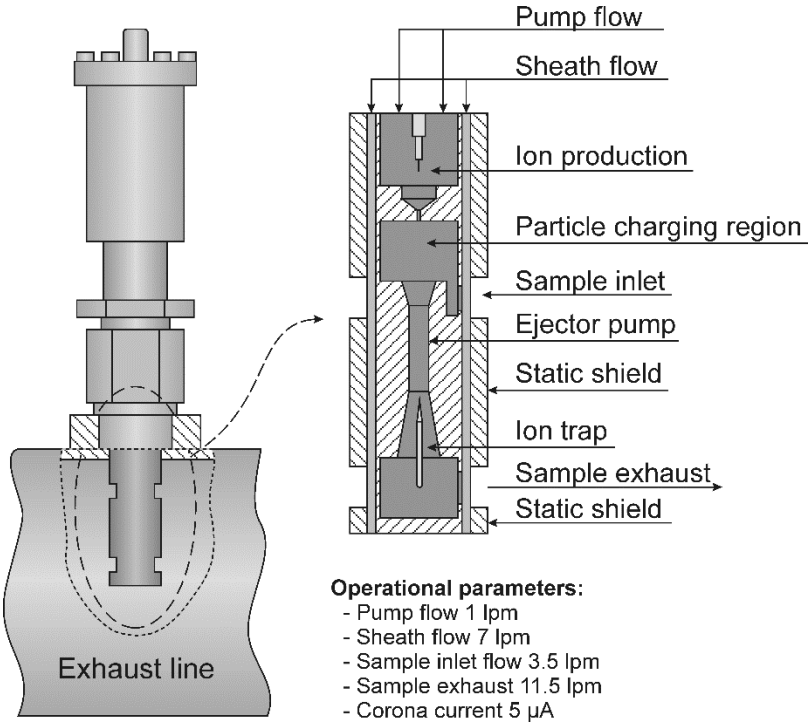

Figure 4.8. Cross section of the high speed OBD sensor showing the key components and operational parameters (**Paper IV**)

As a side effect of the minimisation, the sample volume inside the sensor decreased substantially. This led to a faster gas exchange rate inside the sensor, which in turn enabled a faster time response for the sensor measurement. The temporal performance of the sensor was characterised in the laboratory measurements by the step response measurement. The instrument impulse response fit was constructed from the measured step response. Both the measured step response and the impulse response fit are shown

in figure 4.9. Based on these results, the time constant of the prototype sensor was 18 ms, which corresponds to a value of 40 ms for 10–90% rise time. While comparable temporal performance was demonstrated by de la Mora et al. (2017), the obtained time resolution exceeds that of conventional aerosol instruments significantly.

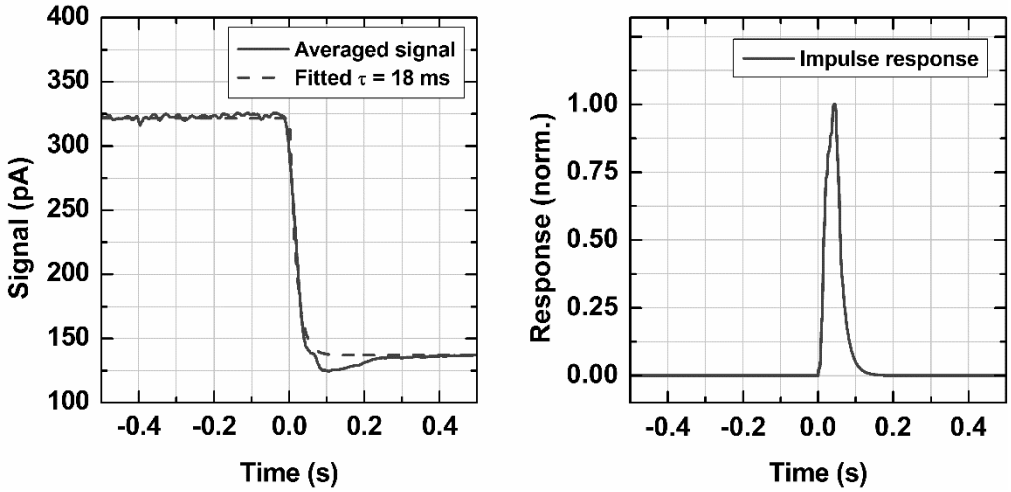

Figure 4.9. Step (left) and impulse (right) responses for the high-speed OBD sensor. (**Paper IV**)

The fast time response was also demonstrated in the engine dynamometer measurements presented in **Paper IV**. With the sensor measurement, it was possible to distinguish the poor burning caused by a deliberately delayed fuel injection in one cylinder when running a six-cylinder diesel engine at 350 revolutions per minute (RPM). The effect of the delayed injection is shown in figure 4.10, which shows a clear difference in the signal waveform when comparing signals measured from the delayed injection conditions to the engine's normal operation conditions. The individual power stroke emission burst measurement required unconventional data processing compared to conventional aerosol instrumentation. To obtain the average, the raw data was divided into sections and the sections were aligned together on the time axis with the help of the timing signal, which was measured from the engine. After this, an average waveform was calculated from the sections to form the result, shown in figure 4.10, for both normal engine operation and for delayed injection. The points of the exhaust peaks of the different cylinders are marked in the figure with the dashed vertical lines. As a result of the poor burn, an increased signal from one cylinder and an increase in the average signal can be seen in waveforms presented in the figure.

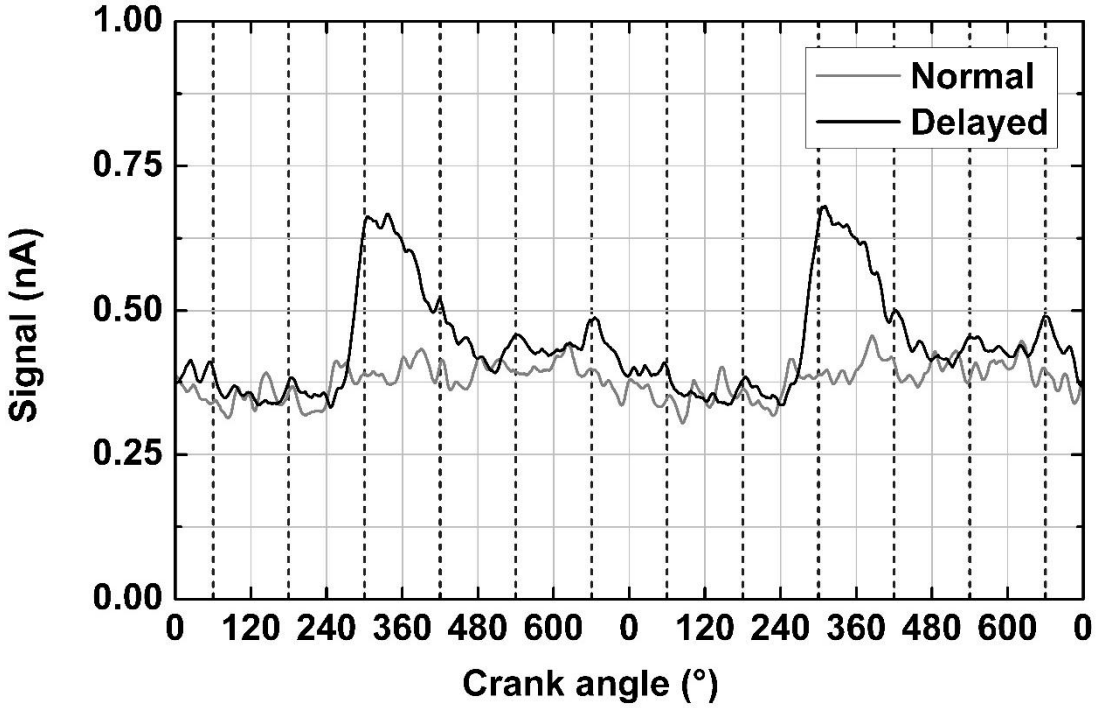

Figure 4.10. Demonstration of the high speed OBD sensor's temporal performance. The effect of the delayed injection in one cylinder compared to the engine's normal operation. Measured for a medium speed diesel engine running at 350 RPM with 62 kW load. The exhaust peak times from the different cylinders are marked with the vertical dashed lines. (Adapted from **Paper IV**)

4.4 Flow independent concentration measurement

In conventional diffusion charging–based instruments, the measured signal is dependent on the sample's volumetric flow rate. For this reason, the instruments typically operate with a fixed sample flow rate, which requires the means to stabilise the flow rate. Looking at the response of the diffusion charger (equation 2), it seems that instrument response is linear to the sample flow rate. On the other hand, based on equations 16 and 17, a simple mobility analyser's particle collection characteristics are inversely proportional to the sample flow rate when the collection efficiency is below one. This implies that the mobility analyser's measured current connected after the diffusion charger would be independent of the sample flow rate. While the direct effect of the sample flow rate cancels

out from the instrument response, secondary effects on charging efficiency remains. With increased flow rate, the charger's particle residence time decreases. This decreases the average charge on the particles n_{ave}, but at the same time, it increases the particle penetration through the charger.

As the particle charge also affects collection efficiency, the resulting response of the diffusion charger and the mobility analyser combination can be approximated to be proportional to the product of $P_{ch}n_{ave}^2$. Since the effect of the varying sample flow rate affects in opposite directions in the particle penetration and the particle average charge, a flow rate range can be found, where the response is relatively independent of the flow rate. Following this thought, normalised instrument response approximations are plotted in figure 4.11 for both conventional filter–based instrument R_f and mobility analyser-based instrument R_{ma}. In these response plots, mobility analyser collection efficiency was approximated according to equation 16 and charging efficiency approximation was based on the diffusion charging (equation 9) and by modelling charger electrical particle losses with a mobility analyser operated in turbulent flow conditions (equation 17). Based on these very rough estimations, the instrument response flow dependence for the diffusion charger and mobility analyser combination is reduced to approximately ±10% over the normalised flow rate range from 0.4 to 3.

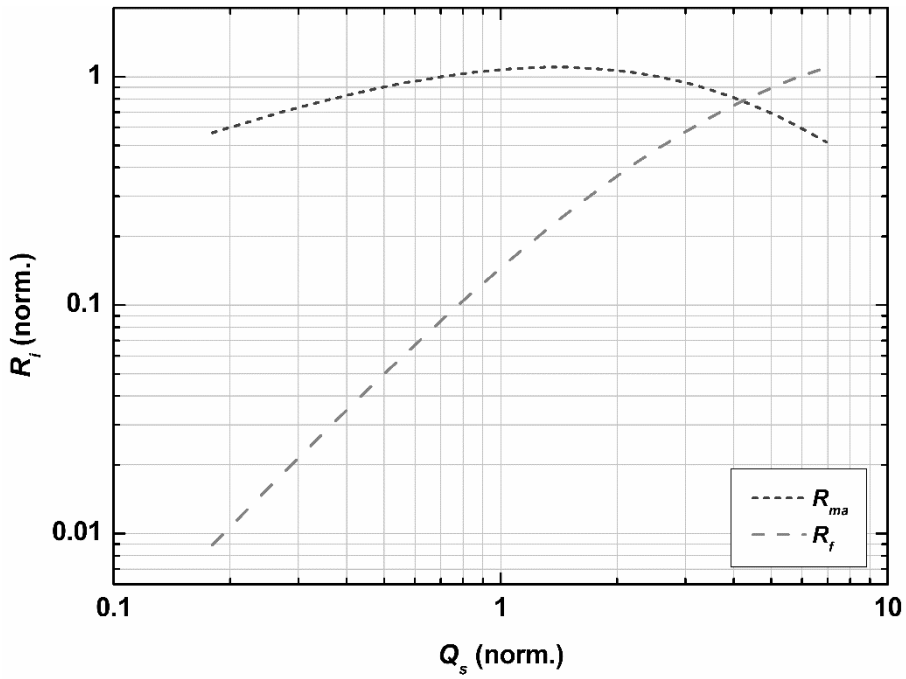

Figure 4.11. Normalised approximations on the instrument response as a function of the sample flow rate for two different diffusion charger–based instruments. The response of an instrument using a Faraday cage filter the particle detection (R_f) compared to the instrument, where particle charge is detected by a mobility analyser (R_{ma}).

The discovery of a possible nearly flow rate–independent response led to the flow independent electrical aerosol sensor (FIAS) prototype, which was presented in **Paper V**. A schematic view on the instrument construction is shown in figure 4.12. The constructed instrument prototype consisted of a small-sized diode type corona discharge diffusion charger, an ion trap and the mobility analyser used in **Paper I**. Like the other instruments treated in this thesis, this design was tested and characterised in laboratory measurements and the instrument response's flow rate dependence was studied.

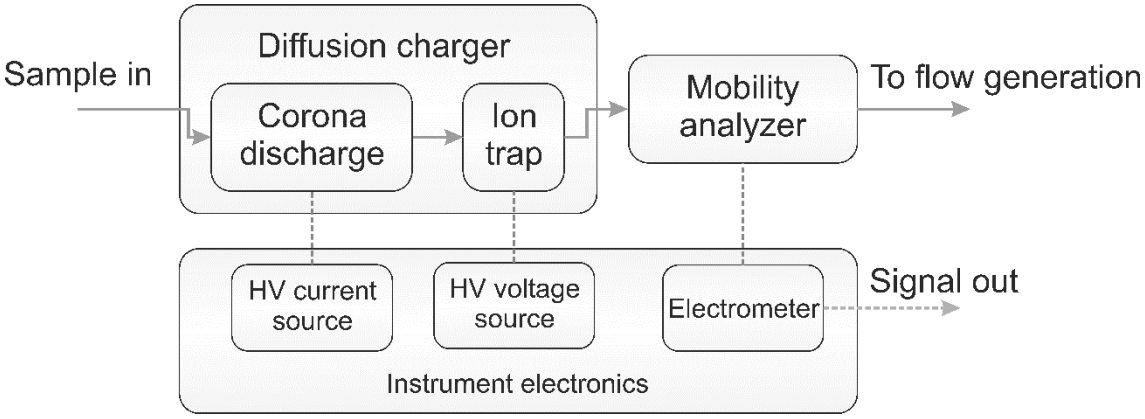

Figure 4.12. Schematic view of the FIAS instrument construction (**Paper V**).

The performance of the instrument and the effect of the sample flow rate on the response are shown in figure 4.13. The left side of the figure shows the measured response for different sample flow rates ranging from 3.0 to 10 lpm. The fitted response obtained from the response characterisation measurement results is shown for reference. The right side shows the normalized instrument response as the function of the sample flow rate for selected particle sizes. The shaded area in both plots represents ±15% deviation from the average response. As shown in the right panel, the instrument response remains within 15% in the tested sample flow rate range apart from the lowest particle size with the lowest flow rate.

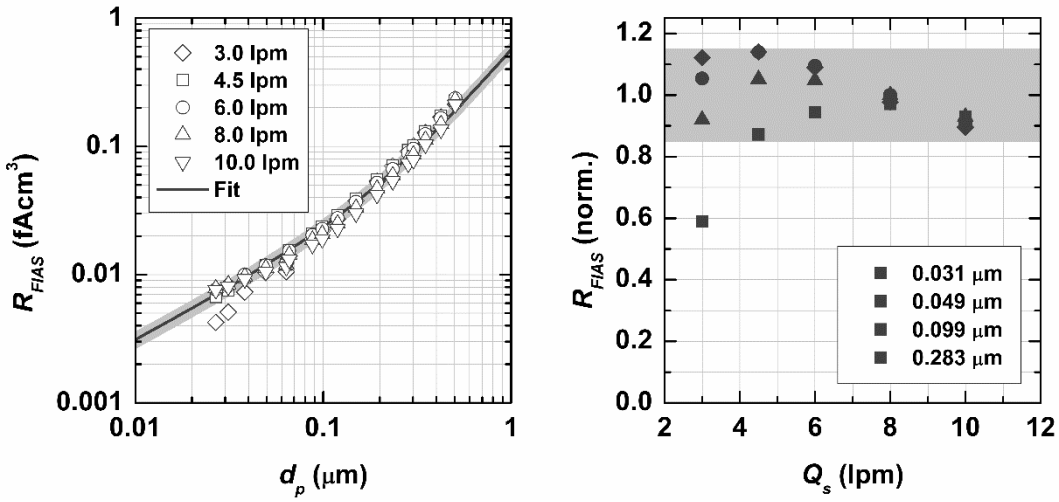

Figure 4.13. On the left side: Response of the FIAS prototype, measured for different sample flow rates. On the right side: The flow dependence of the normalised FIAS response for selected particle sizes. (Adapted from **Paper V**)

Instrument sensitivity is sacrificed in this design, since only part of the particles participate in the measurement. This is, however, acceptable for low-cost aerosol instrumentation, where flow generation and monitoring cost may be an issue. The flow rate independence and the open flow through sensor construction promotes the use of a low cost fan for providing the necessary sample flow, even without flow rate monitoring. The detection limit of the demonstrated prototype sensor for 100 nm particles with a one-second time resolution was approximately 400 1/cm³, which corresponds to a 10 fA signal. This is sufficient for instance for practical outdoor air quality monitoring.

5 Summary

Corona discharge–based diffusion charger, combined with particle charge measurement, is a straightforward way to produce simple and affordable instruments to measure the concentration of ultrafine aerosol particles. The operating principle allows real-time measurement with a good temporal resolution, which makes it possible to use these instruments even for monitoring fast concentration transients. The diffusion charging–based instruments typically offer good repeatability and reliability with a sensitivity adequate for most applications. For the aerosol instruments based on electrical detection of particles, instrument response is the link between measured aerosol concentration and the electrical current measured as output. The response provides useful information on for instrument development, performance evaluation and processing of the measured data.

In order to obtain instrument response, characterisation measurements are required. In these measurements, the instrument is challenged to a test aerosol, and the measured output is compared to the reference measurement. In a typical outcome, the measured response as the function of particle size is obtained. Ideally, the test aerosol should be truly monodisperse for data processing simplicity, but polydisperse test aerosols can also be used in the characterisation measurements. With polydisperse test aerosols, a fitting routine and an approximation on the functional form of the response are usually required for data processing.

The market for cost-effective instruments to measure ultrafine particle concentration is growing. The increased interest towards the air quality measurement networks, driven by the concern on the air quality of urban areas, increases the demand for reliable and cost-effective ultrafine particle concentration monitoring instruments. The requirements for portable and in-use vehicle emission measurements, which are set by regulation, further increases the demand for simplified aerosol instruments. In addition to the air quality–related aerosol measurement, many applications require more detailed information on ultrafine particles. For instance, applications involving engineered nanoparticles would benefit from instruments providing key information on the produced nanomaterial. To support simplified aerosol instrumentation development, the publications included in this thesis studied five different instruments, ranging from commercial instruments to early prototypes.

In **Paper I**, the presented modification to the ELPI added the possibility of real-time measurement of particle effective density; this was accomplished by adding a mobility analyser as a part of the ELPI impactor. This new instrument was tested in laboratory measurements, in which the resulting particle effective density values were in good agreement with the reference method. A further development of this operating principle resulted in a sensor-type instrument for monitoring the nanoparticle synthesis processes.

Three sensor-type instruments were studied in the following three publications, which were targeted for particle concentration measurement directly from the exhaust flow. In **Papers II** and **III**, the instrument design targeted engine laboratory work and portable emission measurement applications. For both instruments, a response model based on theoretical instrument response was constructed and fitted to the laboratory characterisation measurement results. The miniaturised instrument presented in the **Paper IV** sensor was in turn targeted for OBD applications. As a side effect of miniaturisation, this sensor had very good temporal performance. This performance was characterised in the laboratory measurements and was demonstrated in the engine laboratory measurements.

Paper V presented a new approach for building a diffusion charging–based aerosol instrument with a response that is relatively independent of the sample flow rate. Based on the laboratory test measurements for the prototype instrument, the response remained within ±15% of the sample flow rate, ranging from 3.0 to 10 lpm. This new approach has the potential to be a starting point for low-cost sensor development for aerosol concentration monitoring.

References

Agarwal, J. K., Sem, G. J., 1980. Continuous flow, single-particle-counting condensation nucleus counter, J. Aerosol Sci., Vol. 11, pp. 343-357, doi: 10.1016/0021-8502(80)90042-7.

Allen, M. D. and Raabe, O. G., 1982. Re-evaluation of millikan's oil drop data for the motion of small particles in air. J. Aerosol Sci., 13, pp. 537 – 547, doi: 10.1016/0021-8502(82)90019-2

Alonso, M., Martin, M. I. and Alguacil, F. J., 2006. The measurement of charging efficiencies and losses of aerosol nanoparticles in a corona charger, Journal of Electrostatics 64, pp. 203–214, doi: 10.1016/j.elstat.2005.05.008

Amanatidis, S., Maricq, M. M., Ntziachristos, L. and Samaras, Z., 2016. Measuring number, mass, and size of exhaust particles with diffusion chargers: The dual Pegasor Particle Sensor, J. Aerosol Sci. 92, pp. 1–15, doi: 10.1016/j.jaerosci.2015.10.005

Berglund, R.N., and Liu, B.Y. H., 1973. Generation of monodisperse aerosol standards. Environ. Sci. Technol., 7, pp. 147–153, doi: 10.1021/es60074a001

Biskos, G., Reavell, K. and Collings, N., 2005a. Description and Theoretical Analysis of a Differential Mobility Spectrometer, Aerosol Sci. Technol., 39:6, 527-541, doi: 10.1080/027868291004832

Biskos, G., Reavell, K. and Collings, N., 2005b. Unipolar diffusion charging of aerosol particles in the transition regime, J. Aerosol Sci. 36, pp. 247–265, doi: 10.1016/j.jaerosci.2004.09.002

Boelter, K. J. and Davidson, J. H, 1997. Ozone Generation by Indoor, Electrostatic Air Cleaners, Aerosol Science and Technology, 27:6, 689-708, doi: 10.1080/02786829708965505

Bricard, J., Delattre, P., Madelaine, G., and Pourprix, M., 1976. Detection of Ultra-Fine Particles by Means of a Continuous Flux Condensation Nuclei Counter. In Fine Particles, Liu, B.Y.H. ed. Academic Press, New York, 565 – 580, ISBN: 978-0124529502

Brown, D., Wilson, M., MacNee, W., Stone, V., Donaldson, K., 2001. Size-dependent proinflammatory effects of ultrafine polystyrene particles: a role for surface area and oxidative stress in the enhanced activity of ultrafines. Toxicol. Appl. Pharmacol. 175 (3), 191-199, doi: 10.1006/taap.2001.9240

Buonanno, G., Morawska, L. and Stabile, L., 2011. Exposure to welding particles in automotive plants J. Aerosol. Sci., 42, pp. 295 – 304, doi: 10.1016/j.jaerosci.2011.02.003

Büscher, P., Schmidt-Ott, A. and Wiedensohler, A, 1994. Performance of a unipolar ”square wave” diffusion charger with variable nt-product, J. Aerosol Sci., 25, pp. 651-663, doi: 10.1016/0021-8502(94)90006-X

Cheng, S.H., Ranade, M.B. and Gentry, J.W., 1997. Experimental Design of High Volume Electrostatic Charger. Aerosol Sci. Technol. 26:5 pp. 433–446, doi: 10.1080/02786829708965443

Choi, Y. and Kim, S. (2007). An Improved Method for Charging Submicron and Nano Particles with Uniform Charging Performance. Aerosol Sci. Technol. 41:3 pp. 259–265, 10.1080/02786820601148262

Chow, J. C., 1995. Measurement Methods to Determine Compliance with Ambient Air Quality Standards for Suspended Particles, J. Air Waste Manag. Assoc., 45:5, 320-382, doi: 10.1080/10473289.1995.10467369.

Cooper, D. W., and Guttrich, G. L., 1981. A study of the cut diameter concept for interpreting particle sizing data. Atmos. Environ., 15, pp. 1699–1707, doi: 10.1016/0004-6981(81)90156-6

Cunningham, E., 1910. On the Velocity of Steady Fall of Spherical Particles through Fluid Medium. Proc. R. Soc. Lond. A, 83, pp. 357 - 365, doi: 10.1098/rspa.1910.0024

Davison, S. W., Hwang, S. Y., Wang, J., and Gentry, J. W., 1985. Unipolar Charging of Ultrafine Particles by Diffusion of Ions: Theory and Experiment. Langmuir 1985:1, pp. 150-158, doi: 10.1021/la00061a027

Dzubay, T. G., and Hasan, H., 1990. Fitting Multimodal Lognormal Size Distributions to Cascade Impactor Data. Aerosol Sci. Technol., 13:2, pp. 144–150, doi: 10.1080/02786829008959432

EU, 2008. Directive 2008/50/EC of the European Parliament and the Council of 21 May 2008 on Ambient Air Quality and Cleaner Air for Europe.

Fierz, M., Houle, C., Steigmeier, P., and Burtscher, H., 2011. Design, Calibration, and Field Performance of a Miniature Diffusion Size Classifier. Aerosol Sci. Technol., 45:1, pp. 1–10, doi:10.1080/02786826.2010.516283

Fierz, M., Meier, D., Steigmeier, P., and Burtscher, H., 2014. Aerosol Measurement by Induced Currents. Aerosol Sci. Technol., 48:4, pp. 350–357, doi:10.1080/02786826.2013.875981

Fissan, H., Neumann, S., Trampe, A., Pui, D., Shin, W., 2007. Rationale and principle of an instrument measuring lung deposited nanoparticle surface area. J. Nanopart. Res. 9 (1), pp. 53-59, doi: 10.1007/s11051-006-9156-8

Flagan, R. C., 1998. History of Electrical Aerosol Measurements. Aerosol Sci. Technol. 28:4, pp. 301-380, doi: 10.1080/02786829808965530

Franco, S., 1998. Design with operational amplifiers and analog integrated circuits, 2nd ed., International ed. McGraw-Hill companies Inc., USA, ISBN: 0-07-115722-0

Gajewski, J. B. and Szaynok, A., 1981. Charge Measurement of Dust Particles in Motion. J. Electrostat., 10, pp. 229 – 234, doi: 10.1016/0304-3886(81)90047-4

Geiss, O., Bianchi, I. and Barrero-Moreno, J., 2016. Lung-deposited surface area concentration measurements in selected occupational and non-occupational environments. J. Aerosol Sci., 96, pp. 24 – 37, doi: 10.1016/j.jaerosci.2016.02.007

Gormely, P. G., and Kennedy, M., 1949. Diffusion from a Stream Flowing through a Cylindrical Tube. Proc. R. Irish Acad., 52, pp. 163–169

Harris, S. J. and Maricq, M. M., 2001. Signature size distributions for diesel and gasoline engine exhaust particulate matter, J. Aerosol Sci. 32, pp. 749 – 764, doi: 10.1016/S0021-8502(00)00111-7

Hering, S. V., Stolzenburg, M. R., Quant, F. R., Oberreit, D. R. and Keady, P. B., 2005. A Laminar-Flow, Water-Based Condensation Particle Counter (WCPC), Aerosol Sci. Technol., 39:7, pp. 659-672, doi: 10.1080/02786820500182123

Hewitt, G. W., 1957. The Charging of Small Particles for Electrostatic Precipitation, AIEE Trans. 76, pp. 300–306, doi: 10.1109/TCE.1957.6372672

Hinds, W. C., 1999. Aerosol technology: Properties, behaviour and measurement of airborne particles, 2nd ed., Wiley, New York, ISBN: 978-0-471-19410-1

Hu, S., Fruin, S., Kozawa, K., Mara, S., Paulson, S. E. and Winer, A. M., 2009. A wide area of air pollutant impact downwind of a freeway during pre-sunrise hours. Atm. Env. 43 pp. 2541-2549, doi: 10.1016/j.atmosenv.2009.02.033

Högström, R., Karjalainen, P. Yli-Ojanperä J., Rostedt, A., Heinonen, M., Mäkelä, J. M., and Keskinen, J., 2012. Study of the PM Gas-Phase Filter Artifact Using a Setup for Mixing Diesel-Like Soot and Hydrocarbons, Aerosol Sci. Technol., 46:9, pp. 1045-1052, doi: 10.1080/02786826.2012.689118

ICCT, 2016. A technical summary of Euro 6/VI vehicle emission standards. International Council on Clean Transportation, Washington, D.C

Iida, K, Sakurai, H., Saito, K. and Ehara, K., 2014. Inkjet Aerosol Generator as Monodisperse Particle Number Standard, Aerosol Sci. Technol., 48:8, pp. 789-802, doi: 0.1080/02786826.2014.930948

Iida, K., Stolzenburg, M., R. and McMurry, P. H., 2009. Effect of Working Fluid on Sub-2 nm Particle Detection with a Laminar Flow Ultrafine Condensation Particle Counter. Aerosol Sci. Technol. 43:1, pp. 81-96, doi: 10.1080/02786820802488194

Intra, P. and Tippayawong, N., 2009. Progress in Unipolar Corona Discharger Designs for Airborne Particle Charging: A Literature Review. J. Electrostat., 67(4):605–615, doi: doi:10.1016/j.elstat.2008.12.018

Intra, P and Tippayawong, N., 2015. Development and Evaluation of a Faraday Cup Electrometer for Measuring and Sampling Atmospheric Ions and Charged Aerosols, Particul. Sci. Technol., 33, pp. 257 - 263, doi: 10.1080/02726351.2014.952392

Juuti, P., Arffman, A., Rostedt, A., Harra, J., Mäkelä, J. M. and Keskinen, J., 2016. Real-time effective density monitor (DENSMO) for aerosol nanoparticle production, Aerosol Science and Technology, 50:5, pp. 487-496, doi: 10.1080/02786826.2016.1168511

Järvinen, A., Kuuluvainen, H., Niemi, J., Saari, S., Dal Maso, M., Pirjola, L., Hillamo, R., Janka, K., Keskinen, J., Rönkkö, T., 2015. Monitoring Urban Air Quality with a Diffusion Charger Based Electrical Particle Sensor. Urban Climate 14, 3, pp. 441–456, doi: 10.1016/j.uclim.2014.10.002

Kaminski, H., Kuhlbusch, T., Fissan, H., Ravi, L., Horn, H.-G., Han, H.-S., Caldow, R., and Asbach, C., 2012. Mathematical Description of Experimentally Determined Charge Distributions of a Unipolar Diffusion Charger. Aerosol Sci. Technol., 46:6, pp. 708–716, doi: 10.1080/02786826.2012.659360

Keithley, 2004. Low Level Measurements Handbook, 6th edition, Keithley Instruments Inc., Cleveland, OH, USA.

Kelly, K. E., Whitaker, J., Petty, A., Widmer, C., Dybwad, A., Sleeth, D., Martin, R. and Butterfield, A., 2017. Ambient and laboratory evaluation of a low-cost particulate matter sensor, Environ. Pollution, Vol. 221, pp. 491-500, doi: 10.1016/j.envpol.2016.12.039.

Kelly, W. P. and McMurry, P. H., 1992. Measurement of Particle Density by Inertial Classification of Differential Mobility Analyzer–Generated Monodisperse Aerosols, Aerosol Sci. Technol., 17:3, pp. 199-212, doi: 10.1080/02786829208959571

Keskinen, J., Pietarinen, K., and Lehtimäki, M. (1992). Electrical low pressure impactor. J. Aerosol Sci., 23, pp. 353–360, doi: 10.1016/0021-8502(92)90004-F

Kimoto, S., Saiki, K., Kanamaru, M. and Adachi, M., 2010. A Small Mixing-Type Unipolar Charger (SMUC) for Nanoparticles, Aerosol Sci. Technol., 44:10, pp. 872-880, doi: 10.1080/02786826.2010.498796

Knutson, E. O. and Whitby, K. T., 1975 Aerosol classification by electric mobility: apparatus, theory, and applications. J. Aerosol Sci. 6, pp. 443-451, doi: 10.1016/0021-8502(75)90060-9

Kuhlbusch, T. A. J., Quincey, P., Fuller, G. W., Kelly, F., Mudway, I., Viana, M., Querol, X., Alastuey, A., Katsouyanni, K., Weijers, E., Borowiak, A., Gehrig, R., Hueglin, C., Bruckmann, P., Favez, O., Sciare, J., Hoffmann, B., EspenYttri, K., Torseth, K., Sager, U., Asbach, C., Quass, U., 2014. New Directions: The future of European urban air quality monitoring. Atm. Environ., 87, pp. 258-260, doi: 10.1016/j.atmosenv.2014.01.012

Kulkarni, P., Baron, P. A., and Willeke, K., 2011. Aerosol Measurement: Principles, Techniques, and Applications, John Wiley & Sons, Hoboken, NJ, pp. 3–13, ISBN: 978-0-470-38741-2

Kumar, P. Morawska, L., Martani, C., Biskos, G., Neophytou, M., Di Sabatino, S., Bell, M., Norford, L., Britter, R., 2015. The rise of low cost sensing for managing air pollution in cities. Environment International 75, pp. 199–205. doi: 10.1016/j.envint.2014.11.019

Künzli, N., Kaiser, R., Medina, S., Studnicka, M., Chanel, O., Filliger, P., Herry, M., Horak F., Puybonnieux-Texier, V., Quénel, P., Schneider, J., Seethaler, R., Vergnaud, J.-C. and Sommer, H., 2000. Public-health impact of outdoor and traffic-related air pollution: a European assessment. Lancet 2000; 356, pp. 795–801, doi: 10.1016/S0140-6736(00)02653-2

Kuuluvainen, H., Rönkkö, T., Järvinen, A., Saari, S., Karjalainen, P., Lähde, T., Pirjola, L., Niemi, J. V., Hillamo, R. and Keskinen, J., 2016. Lung deposited surface area size distributions of particulate matter in different urban areas. Atm. Env. 136 (2016) pp. 105-113, doi: 10.1016/j.atmosenv.2016.04.019

Lanki, T., Tikkanen, J., Janka, K., Taimisto, P., and Lehtimäki, M. (2011). An electrical sensor for long-term monitoring of ultrafine particles in workplaces. J. Phys.: Conf. Ser., 304:012013. doi: 10.1088/1742-6596/304/1/012013

Lee, D.-D. and Lee D.-S., 2001. Environmental Gas Sensors. IEEE Sensors J. Vol. 1, No. 3, pp. 214-224, doi: 10.1109/jsen.2001.954834

Lehman, U., Niemelä, V., and Mohr, M., 2004. New method for time-resolved diesel engine exhaust particle mass measurement. Environ. Sci. Technol., 38, pp. 5704–5711, doi: 10.1021/es035206p

Lehtimäki, M., 1983. In Modified Electrical Aerosol Detector. in Aerosols in the Mining and Industrial Work Environments, Vol. 3, V. A. Marple, and B. Y. H. Liu, eds., Ann Arbor Science Publishers, Ann Arbor, pp. 1135–1143, ISBN: 978-0250405336

Liu, B. Y. H. and Lee, K. W., 1975. An aerosol generator of high stability. Am. Ind. Hyg. Assoc. J., 36, pp. 861–865, doi: 10.1080/0002889758507357

Liu, B. Y. H. and Lee, K. W., 1976. Efficiency of Membrane and Nuclepore Filters for Submicrometer Aerosols. Environ. Sci. Technol. 10(4) pp. 345 – 350, doi: 10.1021/es60115a002

Liu, B.Y.H. and Pui, D.Y.H., 1975. On the Performance of the Electrical Aerosol Analyzer. J. Aerosol Sci. 6, pp. 249–264, doi: 10.1016/0021-8502(75)90093-2

Liu, X., Cheng, S., Liu, H., Hu, S., Zhang, D., and Ning, H., 2012. A Survey on Gas Sensing Technology Sensors. Sensors 2012, 12, pp. 9635-9665, doi: 10.3390/s120709635

Marra, J., Den Brink, W., Goossens, H., and Kessels, S., 2009. Nanoparticle Monitoring for Exposure Assessment Nanotechnology Magazine. IEEE 3:6–13, doi: 0.1109/MNANO.2009.932417

Marjamäki, M., Keskinen, J., Chen, D.-R., and Pui, D. Y. H., 2000. Performance evaluation of electrical low pressure impactor (ELPI). J. Aerosol. Sci., 31, pp. 249–261, doi: 10.1016/S0021-8502(99)00052-X

Marjamäki, M., Ntziachristos, L., Virtanen, A., Ristimäki, J., Keskinen, J., Moisio, M., Palonen, M. and Lappi, M., 2002. Electrical filter stage for the ELPI, SAE Technical paper 2002-01-0055, doi: 10.4271/2002-01-0055

Marjovi, A., Arfire, A. and Martinoli, A., 2015. High Resolution Air Pollution Maps in Urban Environments Using Mobile Sensor Networks, International Conference on Distributed Computing in Sensor Systems, doi: 10.1109/DCOSS.2015.32

Marple, V. A., 2004. History of Impactors — The First 110 Years, Aerosol Sci. Technol. 38:3, pp. 247-292, doi: 10.1080/02786820490424347

Marquard, A., Meyer, J., and Kasper, G., 2005. Characterization of unipolar electrical aerosol chargers — Part I: A review of charger performance criteria, J. Aerosol Sci., 37, pp. 1052-1068, doi: 10.1016/j.jaerosci.2005.09.001

McMurry, P. H., 2000. The History of Condensation Nucleus Counters, Aerosol Sci. Technol., 33:4, pp. 297-322, doi: 10.1080/02786820050121512

Medved, A., Dorman, F., Kaufman, S.L. and Pocher, A., 2000. A New Corona-Based Charger for Aerosol Particles. J. Aerosol Sci. 31: s616–s617, doi: 10.1016/S0021-8502(00)90625-6

Mirme, A., Tamm, E. and Tammet, H., 1981. An Aerosol Electrogranulometer with a Wide Measuring Range. Acta et comm. Univ. Tartuensis, 588, pp. 84-92 (in Russian, with English abstract)

de la Mora, J. F., Perez-Lorenzo, L. J., Arranz, G., Amo-Gonzalez, M and Burtscher, H., 2017. Fast high-resolution nanoDMA measurements with a 25 ms response time electrometer, Aerosol Sci. Technol. 51, pp. 724 - 734, doi: 10.1080/02786826.2017.1296928

Ntziachristos, L., Fragkiadoulakis, P., Samaras, Z., Janka, K. And Tikkanen, J., 2011. Exhaust Particle Sensor for OBD Application, SAE Technical Paper 2011-01-0626, 2011, doi: 10.4271/2011-01-0626.

Ntziachristos, L., Giechaskiel, B., Ristimäki, J. and Keskinen, J., 2004. Use of a corona charger for the characterisation of automotive exhaust aerosol, J. Aerosol Sci., 35, pp. 943-963, doi: 10.1016/j.jaerosci.2004.02.005

Ntziachristos, L., Polidori, A., Phuleria, H., Geller, M. D. and Sioutas, C., 2007. Application of a Diffusion Charger for the Measurement of Particle Surface Concentration in Different Environments, Aerosol Sci. Technol., 41:6, pp. 571-580, doi: 10.1080/02786820701272020

Oberdörster, G., Oberdörster, E., Oberdörster, J., 2005. Nanotoxicology: an emerging discipline evolving from studies of ultrafine particles. Environ. Health Perspect. 113 (7), pp. 823-839, doi: 10.1289/ehp.7339

Park, C. O., Fergus, J. W., Miura, N., Park, J. and Choi, A., 2009. Solid-state electrochemical gas sensors. Ionics 15, pp. 261–284 doi: 10.1007/s11581-008-0300-6

Patashnick, H. and Rupprecht, E. G., 1991. Continuous PM-10 Measurements Using the Tapered Element Oscillating Microbalance, J. Air Waste Manag. Assoc., 41:8, pp. 1079-1083, doi: 10.1080/10473289.1991.10466903

Piedrahita, R., Xiang, Y., Masson, N., Ortega, J., Collier, A., Jiang, Y., Li, K., Dick, R. P., Lv, Q., Hannigan, M. and Shang, L., 2014. The next generation of low-cost personal air quality sensors for quantitative exposure monitoring. Atmos. Meas. Tech., 7, pp. 3325–3336, doi: 10.5194/amt-7-3325-2014

Ranjan, M. and Dhaniyala, S., 2009. A novel electrical-mobility-based instrument for total number concentration measurements of ultrafine particles, J. Aerosol Sci. 40, pp. 439-450, doi: 10.1016/j.jaerosci.2009.01.007

Ristimäki, J., Virtanen, A., Marjamäki, M., Rostedt, A., and Keskinen, J., 2002. On-line measurement of size distribution and effective density of submicron aerosol particles, J. Aerosol Sci., 33, pp. 1541–1557, doi: 10.1016/S0021-8502(02)00106-4

Schmid, O., Karg, E., Hagen, D. E., Whitefield, P. D., and Ferron, G. A., 2007. On the effective density of non-spherical particles as derived from combined measurements of aerodynamic and mobility equivalent size. J. Aerosol Sci., 38, pp. 431–443, doi: doi:10.1016/j.jaerosci.2007.01.002

Schwyn, S., Garwin, E. and Schmidt-Ott, A., 1988. Aerosol generation by spark discharge, J. Aerosol. Sci. 19, pp. 639-642, doi: 10.1016/0021-8502(88)90215-7

Shin, W. G., Wang, J., Mertler, M., Sachweh, B., Fissan, H. and Pui, D. Y. H., 2010. The effect of particle morphology on unipolar diffusion charging of nanoparticle agglomerates in the transition regime. J. Aerosol Sci. Vol. 41, pp. 975 – 986, doi: 10.1016/j.jaerosci.2010.07.004

Snyder, E. G., Watkins, T. H., Solomon, P.A, Thoma, E. D., Williams, R. W., Hagler, G. S. W., Shelow, D., Hindin, D. A., Kilaru, V. J. and Preuss P. W., 2013. The Changing Paradigm of Air Pollution Monitoring. Environ. Sci. Technol. 47, pp. 11369−11377, doi: 10.1021/es4022602

Sousana, S., Koehlerb, K., Halletta, L. and Petersa, T. M, 2017. Evaluation of consumer monitors to measure particulate matter. J. Aerosol Sci. Vol. 107, pp. 123–133, doi: 10.1016/j.jaerosci.2017.02.013

Tammet, H. F., 1970. The aspiration method for the determination of atmospheric-ion spectra, Israel Program of Scientific Translations, Jerusalem, 1970.

Tammet, H., Mirme, A. and Tamm, E., 2002. Electrical aerosol spectrometer of Tartu University, Atm. Res., 62, 3–4, pp. 315–324, doi: 10.1016/S0169-8095(02)00017-0

Tavakoli, F., Symonds, J. P. R. and Olfert, J. S., (2014) Generation of a Monodisperse Size-Classified Aerosol Independent of Particle Charge, Aerosol Sci. Technol., 48:3, pp. 1-4, doi: 10.1080/02786826.2013.877121

Tikkanen, J., Moisio, M., Janka, K., Pietarinen, K., Keskinen, J. and Rostedt, A., 2007. Method and a Sensor Device for Measuring Particle Emission from the Exhaust Gases of a Combustion Engine. Finnish Patent FI118278, US patent 7406855.

Ullmann, M., Friedlander, S. K. and Schmidt-Ott, A., 2002. Nanoparticle formation by laser ablation, J. Nanopart. Res. 4, pp. 499–509, doi: 10.1023/A:1022840924336

Viana, M., Rivas, I., Reche, C., Fonseca, A. S., Pérez, N., Querol, X., Alastuey, A., Álvarez-Pedrerol, M. and Sunyer, J., 2015. Field comparison of portable and stationary instruments for outdoor urban air exposure assessments Atm. Env. 123, pp. 220 – 228, doi: 10.1016/j.atmosenv.2015.10.076

Virtanen, A., Marjamäki, M., Ristimäki, J. and Keskinen, J., 2001. Fine particle losses in electrical low-pressure impactor, J. Aerosol Sci. 32, pp. 389–401, doi: 10.1016/S0021-8502(00)00087-2

Whitby, K. T., 1961. Generator for Producing High Concentrations of Small Ions. Rev. Sci. Instrum., 32, pp. 1351–1355, doi: 10.1063/1.1717250

Wilson, W., Stanek, J., Han, H.-S., Johnson, T., Sakurai, H., Pui, D., Turner, J., Chen, D.-R., Duthie, S., 2007. Use of the electrical aerosol detector as an indicator of the surface area of fine particles deposited in the lung. J. Air Waste Manag. Assoc. 57(2), pp. 211-220, doi: 10.1080/10473289.2007.10465321

Wang, S. C. and Flagan, R. C., 1990. Scanning Electrical Mobility Spectrometer, Aerosol Sci. Technol., 13:2, pp. 230-240, doi: 10.1080/02786829008959441

Yli-Ojanperä, J., Mäkelä, J. M., Marjamäki, M., Rostedt, A., and Keskinen, J., 2010. Towards Traceable Particle Number Concentration Standard: Single Charged Aerosol Reference (SCAR). J. Aerosol Sci., 41, pp. 719–728, doi: 10.1016/j.jaerosci.2010.04.012

Publications

Paper I

Rostedt, A., Marjamäki, M., and Keskinen, J., 2009. *Modification of the ELPI to Measure Mean Particle Effective Density in Real-Time*. J. Aerosol Sci., 40:823–831, doi: 10.1016/j.jaerosci.2009.05.002.

Aerosol Science 40 (2009) 823 – 831

Contents lists available at ScienceDirect

Aerosol Science

journal homepage: www.elsevier.com/locate/jaerosci

Technical note

Modification of the ELPI to measure mean particle effective density in real-time

Antti Rostedt*, Marko Marjamäki, Jorma Keskinen

Aerosol Physics Laboratory, Department of Physics, Tampere University of Technology, P.O. Box 692, FIN-33101 Tampere, Finland

ARTICLE INFO

Article history:
Received 22 August 2008
Received in revised form
6 May 2009
Accepted 12 May 2009

Keywords:
Impactor
Density
Mobility

ABSTRACT

A new modification of electrical low pressure impactor (ELPI) for the particle effective density measurement is presented. The system is capable of real-time operation and it is based on the serial measurement of mobility and aerodynamic diameter. In the studied configuration, a zeroth order mobility analyser is installed inside of the ELPI-instrument. The system is feasible for single modal distributions. For several particle materials and varying size distributions, the measured average density values were within 15% of the values obtained with a reference method.

1. Introduction

Particle effective density is an important quantity affecting the mechanical dynamics of aerosol particles. Several methods have been applied to the measurement of the effective density. As reviewed by Schmid, Karg, Hagen, Whitefield, and Ferron (2007), one of the most popular methods is the combined measurement of aerodynamic and mobility equivalent diameter (e.g. Hering & Stolzenburg, 1995; Kelly & McMurry, 1992; Maricq, Podsiadlik, & Chase, 2000; Schleicher, Künzel, & Burtscher, 1995). Usually the methods are based on having a differential mobility analyser (DMA) and an impactor in series, i.e. measuring the aerodynamic size of the mobility classified particles. Covering a size distribution this way is relatively time consuming, as one particle size at a time needs to be passed through the DMA. As an alternative to the serial method is parallel size distribution measurement using two instruments, one classifying the particles according to their mobility equivalent size and the other according to the aerodynamic size. Effective density is then acquired by using some kind of fitting procedure to the two size distributions. Parallel measurement methods have been applied previously to aerodynamic particles sizer (APS) and cascade impactor measurement (Brockmann & Rader, 1990). Kerminen, Mäkelä, Hillamo, and Rantanen (1999) used scanning mobility particle sizer (SMPS; Wang & Flagan, 1990) and cascade impactor data to calculate the effective density. Ristimäki, Virtanen, Marjamäki, Rostedt, and Keskinen (2002) introduced a computational method to acquire the effective density from the parallel measurement with the electrical low pressure impactor (ELPI; Keskinen, Pietarinen, & Lehtimäki, 1992) and SMPS on-line. Although several methods to measure the effective density have been published previously, none of them are fast enough to allow real-time measurement of the effective density. The knowledge of the changes in the effective density of the particles in real-time may be very useful when for example monitoring different industrial aerosol processes and diesel engine exhaust measurements.

A variant of the serial method, capable of real-time measurement of particle density was introduced by Keskinen, Moisio, Marjamäki, Virtanen, and Ristimäki (2001). The serial method has been applied to convert electrical impactor signals to mass concentration (Dekati Mass Monitor (DMM-230, Dekati Ltd.), as reported by Lehman, Niemelä, and Mohr (2004). In this paper, a simple serial setup is for the first time applied to the measurement of the effective density of the particles in real-time. Here, the

* Corresponding author. Tel.: +358 3 3115 2529.
E-mail address: antti.rostedt@tut.fi (A. Rostedt).

0021-8502/$ - see front matter © 2009 Elsevier Ltd. All rights reserved.
doi:10.1016/j.jaerosci.2009.05.002

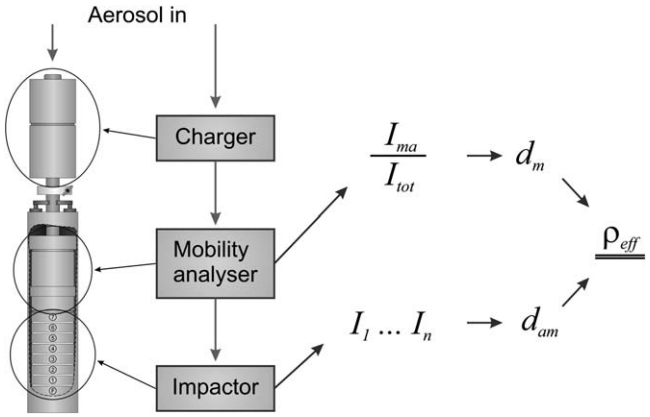

Fig. 1. Schematic view of the measurement setup.

serial method is implemented by introducing a zeroth order mobility analyser between the charger and the impactor of the ELPI. The mobility analyser is placed after the corona charger and it replaces the upper stages of the impactor. The design is such that the additional parts will easily fit inside the existing ELPI unit. This makes it possible to attach the mobility analyser as a part of existing equipment without any major modifications. Thus the designed setup serves also as an add-on measurement feature to the already existing ELPI system.

2. Description of the method

2.1. Operation principle

The measurement method combines the electrical mobility measurement and the aerodynamic size classification by connecting a zeroth order mobility analyser in series with a cascade impactor. The electrical mobility measurement is used to obtain a mobility median of the measured size distribution, whereas the aerodynamic classification gives the size distribution as a function of aerodynamic particle size. From the measured aerodynamic size distribution we calculate the median of the distribution. The effective density is a parameter linking mobility equivalent particle size to aerodynamic particle size (e.g. Kelly & McMurry, 1992; Ristimäki et al., 2002) with the following equation:

$$\rho_{eff} = \rho_0 \frac{C_{c,aerodyn} d_a^2}{C_{c,mobility} d_b^2}, \tag{1}$$

where $C_{c,aerodyn}$ and $C_{c,mobility}$ are the slip correction factors corresponding for the aerodynamic and mobility particle sizes d_a and d_b, respectively. In this case we use the mobility equivalent median diameter d_m and corresponding aerodynamic median diameter d_{am} to estimate the effective density.

To achieve real-time response, the mobility analyser is actually located inside of the ELPI-instrument. It is installed inside the impactor casing to replace the upper stages 8–12. This configuration makes it possible to use one of the on board electrometers of the ELPI to measure the current signal of the mobility analyser. Additionally in this configuration, it is possible to detect all of the collected particles as a current signal with an electrometer. Schematic view of the measurement setup is shown in Fig. 1.

As shown in the figure, the measurement consists of three different phases; the charging of the aerosol, the mobility classification and the aerodynamic classification of the charged particles. The charging of the aerosol is carried out by the standard corona charger of the ELPI unit. The charge, which the particles acquire inside the charger, is determined by the mobility equivalent diameter. The mobility analyser collects a part of the particles from the flow. The amount of particles collected can be measured as a fraction of the total current that is measured from the analyser. The mobility median is determined from this fraction. After the mobility classification the measured aerosol is classified in the cascade impactor. The aerodynamic median diameter is calculated from the measured impactor currents and the effective density is calculated with Eq. (1) using the measured mobility and aerodynamic median diameters.

2.2. Mobility analyser

The geometry of the analyser was chosen to be cylindrical, because of the shape of the existing ELPI impactor casing. The actual design of the analyser is shown in Fig. 2. The two coaxial cylinders form the zeroth order mobility analyser and the aerosol flows through the analyser as a thin annular stream between the two cylinders (inner diameter 45 mm and outer diameter 55 mm). The collection of the particles takes place in between the measuring and voltage electrodes, which are placed at the bottom of

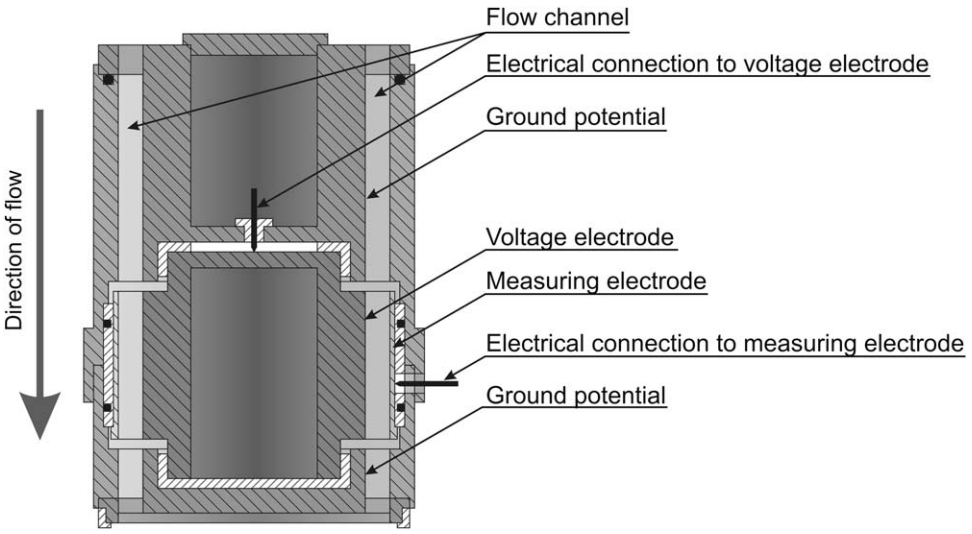

Fig. 2. Cross section view of the mobility analyser.

the analyser. The length of the collection region is 30 mm. In the upper part of the analyser, the flow channel is same as inside the actual classification region (i.e. between the electrodes) to ensure stable flow pattern in between the electrodes. The geometry is dimensioned so that the flow stays laminar. This was also verified with Computational Fluid Dynamics package of Comsol Multiphysics software.

The design of the mobility analyser is such that the onboard trap voltage source of the ELPI unit can be used as a power source for the analyser. The electric field inside the analyser was also modelled and verified with Comsol Multiphysics. The range of operating voltage that can be used with the setup varies from 50 to 400 V. The optimum voltage of the analyser depends on the size distribution measured, the higher the median size of the distribution, the higher the optimum voltage. The operational size range of the setup is from 30 to 200 nm.

The collection efficiency of the used geometry depends on the diameters of both inner and outer cylinders D_i and D_o, the length of the electrodes l_e, the applied voltage between the electrodes V and the volumetric flow rate passing through the analyser Q. The collection efficiency, η, is determined as follows (e.g. Fuchs, 1964).

$$\eta = \frac{2\pi Z V l_e}{Q \ln\left(\frac{D_o}{D_i}\right)} \tag{2}$$

The property of the particles, which affects to the collection efficiency, is the electrical mobility Z of particles. This depends on the mobility diameter of the particles d_b, gas viscosity μ, elementary charge e and the number of elementary charges on the particle n and can be written as (Hinds, 1999)

$$Z = \frac{neC_c}{3\pi\mu d_b} \tag{3}$$

where the term C_c is the slip correction factor.

2.3. Impactor

Since the mobility analyser replaces ELPI stages 8–12, only the stages 1–7 and the filter stage can be used for size classification. In this configuration impactor can be used for size classification for particles smaller than 0.62 μm. In theory, size range could be adjusted for larger particles by changing the stages. However, owing to the limitations of the zeroth order mobility classification this is not practically feasible as will be seen later. The operation of the impactor is described by cutpoints $d_{50\%}$ of the individual impactor stages. A cutpoint of the impactor stage refers to an aerodynamic particle diameter from which 50% are collected by the stage in question. In this study we use the cut diameter concept (e.g. Cooper & Guttrich, 1981) to carry out the necessary size distribution calculations. In this concept, it is assumed that all of the particles larger than the cutpoint are collected and all of the particles smaller than the cutpoint pass on to the next stage.

The pressure drop of stages 8–12 is less than 1 kPa (Marjamäki, Keskinen, Chen, & Pui, 2000). Since the mobility analyser has also very small pressure drop, we can assume that replacing stages 8–12 with the mobility analyser does not affect the operation of the stages 1–7, i.e. impactor stages 1–7 operate as in original ELPI setup. The last stage of the impactor is a filter

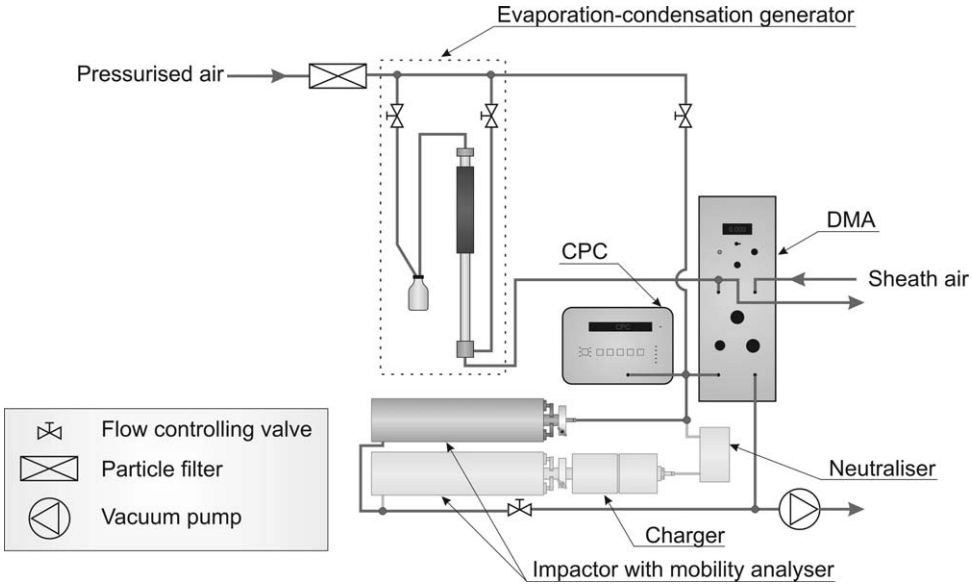

Fig. 3. Experimental setup for the collection efficiency measurements.

stage, which collects the rest of the particles, which are smaller than the lowest cut point of the impacting stages. The operation of the filter stage differs from the other stages: For the filter stage, the upper size limit of the collected particles depends on the lower size limit of the previous stage, but the lower limit of the filter stage originates from the charger charging efficiency, i.e. it is defined by the point in the charging efficiency curve, where the measured signal becomes too low to measure (Marjamäki et al., 2002). In the presented configuration, the lower limit depends also on the collection efficiency of the mobility analyser, since it cannot be lower than the particle size where the mobility analyser collects 100% of the particles. In practice the lower limit of the filter stage is defined by the mobility analyser since the size corresponding to 100% collection is higher than the charging efficiency limit. The lower limit is different for different mobility analyser voltages, because of the changing collection efficiency curve.

3. Response of the components

The calibration setup (Fig. 3) is very similar to the one used to calibrate ELPI (Marjamäki et al., 2000). As a calibration aerosol, monodispersed dioctylsebacate (DOS) particles were used. First a narrow, but polydisperse, aerosol distribution was generated using evaporation–condensation generator (Liu & Lee, 1975). Generated size distribution was monitored with a scanning mobility particle sizer (TSI 3934). The generated narrow distribution was further classified with differential mobility analyser (TSI 3071) to generate monodisperse particles.

The collection efficiency, η, measured with the singly charged particles can be compared to the theoretical predictions calculated with Eq. (2). The comparison between the measured collection efficiency and the theoretical collection efficiency with an analyser voltage of 400 V is shown on the left side of Fig. 4. From the comparison it can be seen that the measured collection efficiency fits perfectly to the theoretically calculated efficiency. This result confirms that the design is working as theory predicts and no corrections are needed for the calculation of the collection efficiency.

In this application, particles entering the analyser will be charged by the ELPI charger before entering the analyser. The charger changes the charge distribution of the particles, which changes the electrical mobility of the particles (see Eq. (3)). This changes the collection efficiency of the mobility analyser as a function of the particle size. For this reason collection efficiency for the particles charged with the ELPI charger is essential knowledge when calculating the densities. As particles have a distribution of charges, we characterize the operation of the charger and mobility analyser using the average (arithmetic mean) value for the charge per particle. The efficiency of the ELPI charger has been defined (Marjamäki et al., 2000) as a product of the penetration of the charger and average number of charges per particle. In this case we are not interested in the charging efficiency as a whole; instead we need to know the average number of charges per particles, so that we can link the measured collection efficiency of the mobility analyser to the particle size. The average number of charges carried by the particles after the ELPI charger can be obtained by measuring the collection efficiency of the analyser with monodisperse particles charged with the ELPI charger. The measurement setup is the same as presented in Fig. 3, except that now the monodispersed particles are first passed through a neutraliser before entering the ELPI charger. The neutraliser is added because the initial charge level of the aerosol can affect the operation of the charger. The use of neutraliser is also recommended for normal measurement situations, especially if the aerosol is not expected to be in charge equilibrium.

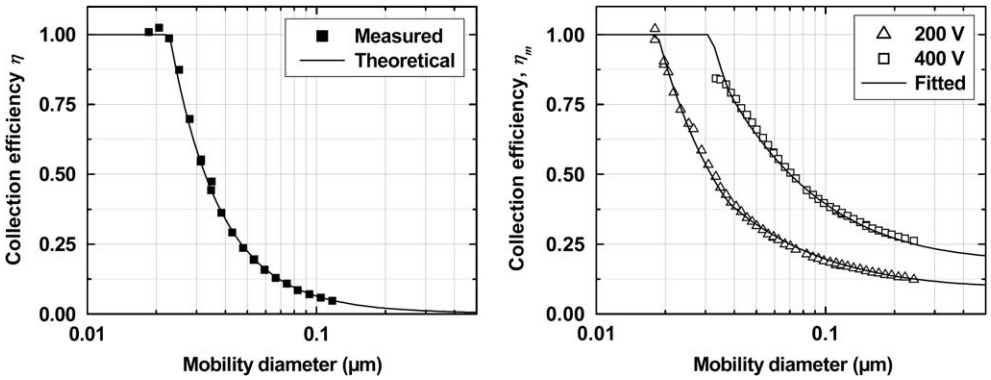

Fig. 4. On the left measured and theoretical collection efficiencies with singly charged particles η measured at analyser voltage of 400 V. On the right measured collection efficiencies for multiply charged particles η_m with two different analyser voltages. The solid line on the right is the collection efficiency calculated with fitted average number of charges per particle.

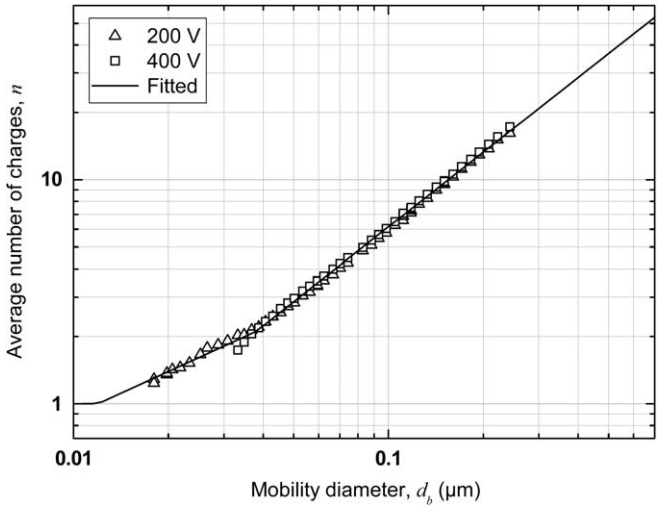

Fig. 5. Measured average charges per particle, n, generated by the ELPI charger as a function of particle mobility diameter d_b together with a power function fit to the data.

From the DMA we know the particle mobility size and we acquire the electrical mobility of the particles from the measured collection efficiency η_m. From the electrical mobility and the particle size we can calculate the average number of charges per particle with the use of Eq. (2). Results can be calculated only for the particle sizes that have a collection efficiency of less than 100%. A power function, Eq. (4), was then fitted to the calculated average number of charges.

$$n(d_b) = \begin{cases} 1, & d_b \leq 0.0119\,\mu\text{m} \\ 17.325 d_b^{0.6440}, & 0.0119 < d_b \leq 0.0379\,\mu\text{m} \\ 78.898 d_b^{1.1076}, & 0.0379\,\mu\text{m} < d_b \end{cases} \quad (4)$$

Average number of charges is limited to one, because only the charged particles are detected. The resulting average number of charges per particle together with the power function fit is plotted to Fig. 5. The resulting calculated collection efficiency for particles charged by the ELPI charger together with measured point is presented on the right side in Fig. 4.

Since the charging efficiency of the ELPI charger (Marjamäki et al., 2000, 2002) and the collection efficiencies of the impactor stages are known (Marjamäki et al., 2000), we know the response of every component in the density measurement setup.

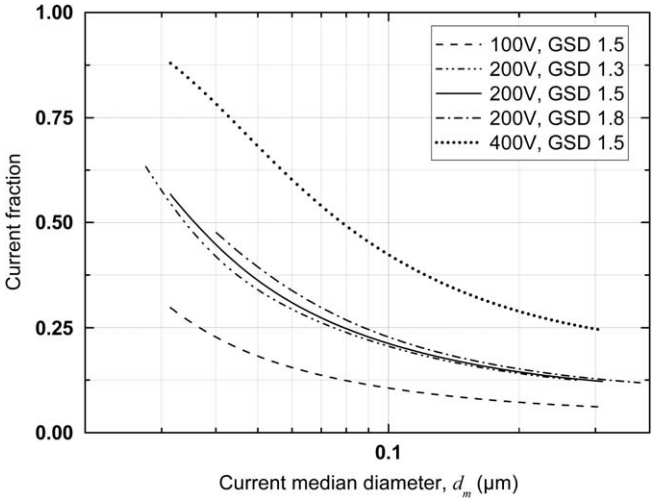

Fig. 6. Simulation of the current fraction of mobility analyser current from the measured total current as a function of the current median diameter d_m of the size distribution with different GSDs at a analyser voltage of 200 V.

4. Calculation of the effective density

4.1. Response to polydisperse aerosols

In the case of a polydisperse aerosol, the fraction of the mobility analyser current from the total current (I_{ma}/I_{tot}, see Fig. 1) corresponds to the same fraction of the charge weighted mobility size distribution of the charged aerosol. We name the charge weighted size distribution as current distribution. A 50% current fraction would therefore correspond to the current median diameter of the mobility size distribution. For other measured current fractions, the current median diameter can be calculated, if the shape of the size distribution is known. In practice, this is not known and therefore we need to make approximations that cause limitations. The method is limited to cope only with unimodal size distributions on a certain size range. The operational size range that can be used can be slightly varied by changing the operating voltage of the mobility analyser. With the current setup, the usable size range of the method is from 30 to 200 nm. The upper limit of the size range is caused by the collection efficiency of the mobility analyser. For particles larger than 200 nm, collection efficiency curve is so flat (right side of Fig. 4) that it cannot be used to measure the mobility median size reliably. The lower limit is imposed by the characteristics of the impactor. Although the size range of the ELPI impactor is down to 7 nm, at sizes below 30 nm the aerodynamic median of the distribution cannot be calculated reliably, since the most of the signal is on the filter stage.

In the following calculation we assume that the distribution is lognormal with a geometric standard deviation (GSD) of 1.50. The relationship between the mobility median diameter of the size distribution and the measured current fraction of the analyser current from the total current was numerically simulated. As a first step in the simulation the number size distribution $N(d_b)$ entering the system was generated. The used count median diameter range was from 25 to 250 nm and the GSD of the distributions was set to constant 1.50. Then with the help of the charging efficiency, Pn, the number size distribution was converted to a current size distribution using Eq. (5) (see Ristimäki et al., 2002). The terms e and Q are the elementary charge (1.6022×10^{-19} C), and volumetric flow rate at the inlet of the charger. Both the generated number size distribution and the resulting current distribution are functions of the particle mobility diameter.

$$I(d_b) = Pn(d_b)eQN(d_b) \tag{5}$$

Next, the mobility analyser current fraction as a function of the current median mobility diameter, d_m, of the size distribution is calculated by integrating the product of the current distribution, $I(d_b)$, and the fitted collection efficiency of the mobility analyser, $\eta_m(d_b)$ (right side of Fig. 4)

$$I_{ma} = \int I(d_b)\eta_m(d_b)dd_b$$

and dividing the result with the total current I_{tot}. The result of the calculation is shown in Fig. 6 for different collection voltages. There are also curves calculated for different GSD values with one collection voltage for comparison.

Table 1
Average effective densities of the tested aerosols, together with results from reference method and bulk densities of the aerosol material.

	Bulk (g/cm^3)	Reference (g/cm^3)	Measured (g/cm^3)	Deviation from reference (%)
DOS	0.91	0.87	0.95	9.0
Santovac 5	1.20	1.09	1.03	−5.4
Fomblin	1.90	1.72	1.51	−12.2
Ag (furnace)	10.5	5.14	4.77	−7.2
Ag (LFS)	10.5	6.76	6.18	−8.7

4.2. Effective density

As electrical current is the primary signal measured, it is convenient to use the current distributions, i.e. charge weighted size distributions, in the calculations. The effective density can be calculated with the Eq. (1) from the current medians of the aerodynamic and mobility size distributions. The current median mobility size d_m of current distribution is obtained from the fit shown in Fig. 6 for the measured current fraction value. The current median aerodynamic diameter is calculated from the impactor current distribution with the aid of an iteration routine. Firstly, the diffusion losses of fine particles to the impactor stages are corrected from the raw current signals in a manner similar to that used in the normal operation of the ELPI (Moisio, 1999). Then the current distribution is corrected again with the collection efficiency of the mobility analyser. As a result from this the obtained current distribution corresponds to the current distribution before the mobility analyser, and now the median of this distribution corresponds to the median measured with the mobility analyser. Unfortunately, for this correction we need to know the effective density of the particles, hence we need the iteration. From the corrected impactor current distribution the current median aerodynamic diameter d_{am} is calculated. From these two median diameters new effective density is calculated. Then the iteration routine to calculate the new aerodynamic median diameter is repeated to get new effective density. This iteration is repeated for 10 times. As a result the effective density from the last iteration round is given.

5. Laboratory experiments

5.1. Different aerosol materials

The method was tested in the laboratory using aerosols with different densities. The test aerosol materials chosen were DOS, which was also used for calibration, Santovac 5, Fomblin and silver. From these aerosols DOS, Santovac 5 and Fomblin are liquid and silver is a solid metal. The DOS aerosol was generated with the same evaporation–condensation generator that was used in the calibration. Santovac 5, Fomblin and silver aerosols were generated using a tube furnace. Silver particles were also generated using liquid flame spray (LFS) technique (Mäkelä, Keskinen, Forsblom & Keskinen, 2004). DOS, Santovac and Fomblin produce spherical liquid particles. The median of the generated number distribution for the oil aerosols was in the size range of 40–120 nm and the GSD varied between 1.35 and 1.65. The median and GSD of the generated silver aerosols varied between 10–60 nm and 1.4–1.8, respectively. The bulk densities of the tested materials together with measurement results are collected to Table 1. The results include all of the different distributions, i.e. they include distributions with variable median sizes and geometric standard deviations.

The mobility analyser voltage was varied during tests according to the size of the particles. Results of the present method were compared to the densities calculated from the parallel measurement with the ELPI and SMPS. This reference method is based on fitting the ELPI and SMPS distributions by varying the effective density. Method is described fully in a paper by Ristimäki et al. (2002). In the parallel reference method, the same ELPI unit, in which the mobility analyser was fitted, was used to measure the ELPI current distributions. During the reference measurements the mobility analyser voltage was set to zero and the fitting routine was used only for the remaining eight size channels of the ELPI. The results of the comparison between the developed method and reference method are presented in Fig. 7 and Table 1. The error bars in the figure represent the standard deviation for the measured density values for both methods.

For the liquid particles the measured values are quite close to the bulk values. For the solid silver particles the values for both methods are significantly lower than the bulk values. Density values much lower than the bulk density have been reported for silver particles in several studies, and they have been attributed to impurities in the generator or the carrier gas (e.g. Fernandez de la Mora, de Juan, Liedtke, & Schmidt-Ott, 2003; Virtanen, Ristimäki, & Keskinen, 2004). In some of the presented distributions, the particles were probably agglomerated. Nevertheless, the agreement between the presented method and the reference is relatively good. The error bars include the effect of differences between the measured size distributions for each material. For the liquid aerosols the error bars are small due to homogenous spherical structure of the particles. For the silver aerosols, part of the variation is caused by real differences in the effective density caused, e.g. by varying degree of agglomeration.

5.2. Changing aerosol size distribution

The real time response of the method was tested with DOS aerosol with changing median diameter. The aerosol was generated with the same generation system as in calibration, but now the operation parameters of the generator were changed so that the median size of the size distribution changed. The system was first operated with a constant small median diameter and

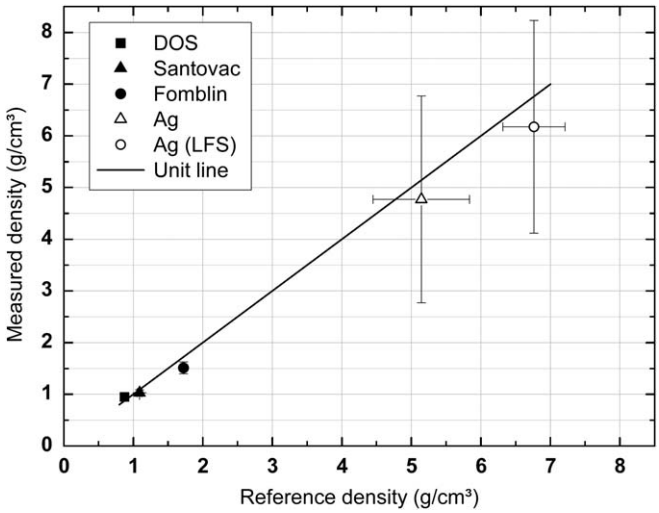

Fig. 7. Acquired densities for the reference method (*x*-axis) and developed method (*y*-axis) for DOS, Santovac, Fomblin and two different silver aerosols. Results shown are arithmetic mean values from the measurements. The error bars represent the standard deviation values.

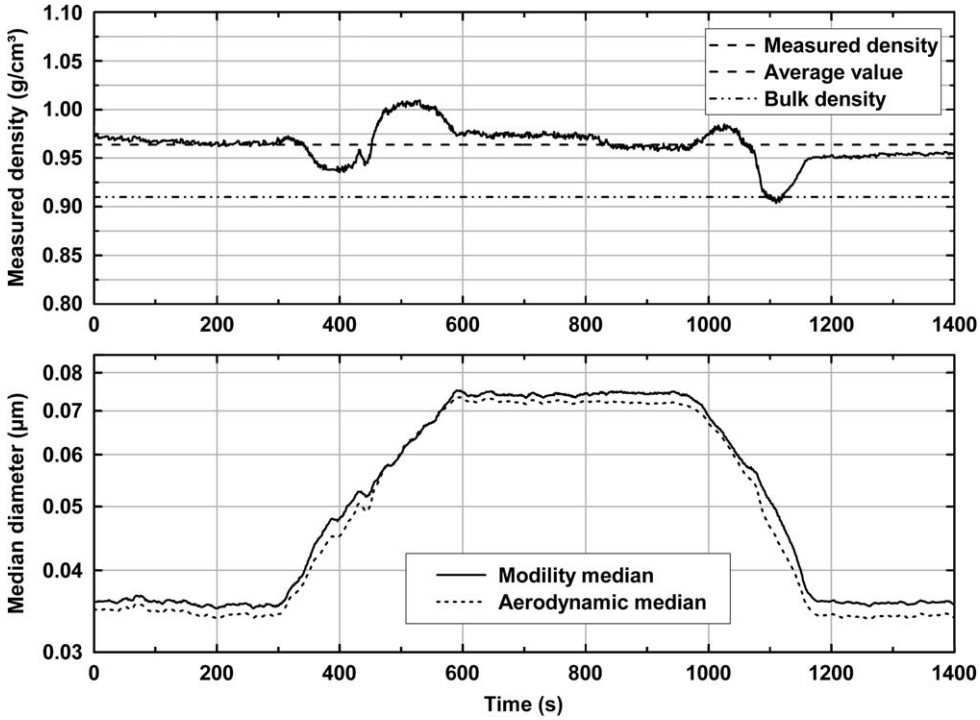

Fig. 8. Density measurement for changing aerosol. The calculated density values as a function of time on the top and the calculated current median diameters on the bottom.

then the parameters were changed slowly to increase the median size. Then at the maximum median size, the generation was kept constant for a while followed by a decrease in the median size. The ELPI with the mobility analyser was measuring all the time saving the data with one second intervals. The resulting density values were calculated from the ELPI data and are plotted together with the mobility and aerodynamic medians of the current distribution to Fig. 8.

The data in the figure shows that the density measurement gives constant density for stable conditions and that there is a small variation in the density during transitions. However the variations in the resulting density values are small. The density values are calculated assuming the GSD of the distribution to be constant 1.5, and if the GSD value changes during the transitions,

it could lead to a change in to the calculated density value. With SMPS measurement made during the stable conditions it can be seen that GSD varies from 1.5 with the small median diameters to 1.6 with increased median diameter.

6. Conclusions

The presented method is simple to use and can be used in real-time to measure the effective density of the particles. The presented setup can be installed inside the ELPI unit and therefore it can be used in a same way as a regular ELPI. Method could be applied for example to monitor industrial aerosol processes or engine exhaust aerosols or it could be used to increase the number concentration accuracy of the ELPI. Laboratory measurements show that the effective density of the particles measured with the developed method was in good agreement with the reference method of parallel measurement with ELPI and SMPS.

Owing to the simple measurement principle, the presented setup has limitations. It is limited to unimodal size distributions. Another limitation is that the setup can only be used to obtain one previously unknown quantity about the density of the aerosol. In most cases this quantity is the average effective density for the distribution. For best accuracy in effective density, the geometric standard deviation of the particle size distribution must be known at least approximately. The method could, in principle, be used to estimate the fractal dimension if the bulk density and primary particle size of the aerosol is known. However, both theoretical considerations and the limited instrument resolution (see. e.g. Virtanen et al., 2004) would limit this to fractal dimension values greater than 2.

Although several approximations were needed to be able to calculate the effective density they do not significantly hinder the usability of the method for unimodal distributions. Reliability of the method could be improved by developing the data reduction further, for example the GSD of the distribution could be estimated from the measured impactor currents and taken into account in data reduction.

Acknowledgement

Dr. Marjamäki was funded by the Academy of Finland Grant no. 109124.

References

Brockmann, J. E., & Rader, D. J. (1990). APS response to nonspherical particles and experimental determination of dynamic shape factor. *Aerosol Sci. Technol.*, *13*, 162–172.
Cooper, D. W., & Guttrich, G. L. (1981). A study of the cut diameter concept for interpreting particle sizing data. *Atmos. Environ.*, *15*, 1699–1707.
Fernandez de la Mora, J., de Juan, L., Liedtke, L., & Schmidt-Ott, A. (2003). Mass and size of nanometer particles by means of mobility analysis and focused impaction. *J. Aerosol Sci.*, *34*, 79–98.
Fuchs, N. A. (1964)). *The mechanics of aerosols*. Oxford: Pergamon Press.
Hering, S. V., & Stolzenburg, M. R. (1995). On-line determination of particle size and density in the nanometer size range. *Aerosol Sci. Technol.*, *23*, 155–173.
Hinds, W. C. (1999)). *Aerosol technology. Properties, behaviour and measurement of airborne particles*. New York: Wiley.
Kelly, W. P., & McMurry, P. H. (1992). Measurement of particle density by inertial classification of differential mobility analyser-generated monodisperse aerosol. *Aerosol Sci. Technol.*, *17*, 199–212.
Kerminen, V.-M., Mäkelä, T., Hillamo, R., & Rantanen, L. (1999). Relation between particle number and mass size distribution in the diesel car exhaust. *J. Aerosol Sci.*, *30*(S1), S777–S778.
Keskinen, J., Moisio, M., Marjamäki, M., Virtanen, A., & Ristimäki, J. (2001). *Method of measuring density properties of a particle distribution*. Finnish patent FI115075, US Patent 7131343.
Keskinen, J., Pietarinen, K., & Lehtimäki, M. (1992). Electrical low pressure impactor. *J. Aerosol Sci.*, *23*, 353–360.
Lehman, U., Niemelä, V., & Mohr, M. (2004). New method for time-resolved diesel engine exhaust particle mass measurement. *Environ. Sci. Technol.*, *38*, 5704–5711.
Liu, B. Y. H., & Lee, K. W. (1975). An aerosol generator of high stability. *Am. Ind. Hyg. Assoc. J.*, *36*, 861–865.
Mäkelä, J. M., Keskinen, H., Forsblom, T., & Keskinen, J. (2004). Generation of metal and metal oxide nanoparticles by liquid flame spray process. *J. Materials Sci.*, *39*, 2783–2788.
Maricq, M. M., Podsiadlik, D. H., & Chase, R. (2000). Size distributions of motor vehicle exhaust PM: A comparison between ELPI and SMPS measurements. *Aerosol Sci. Technol.*, *33*, 239–260.
Marjamäki, M., Keskinen, J., Chen, -R., & Pui, D. Y. H. (2000). Performance evaluation of electrical low pressure impactor (ELPI). *J. Aerosol. Sci.*, *31*, 249–261.
Marjamäki, M., Ntziachristos, L., Virtanen, A., Ristimäki, J., Keskinen, J., Moisio, M., et al. (2002). *Electrical filter stage for the ELPI*. Society of Automotive Engineers (SAE), Technical paper series 2002-01-0055.
Moisio, M. (1999). *Real time size distribution measurement of combustion aerosols*. Ph.D. thesis, Tampere University of Technology.
Ristimäki, J., Virtanen, A., Marjamäki, M., Rostedt, A., & Keskinen, J. (2002). On-line measurement of size distribution and effective density of submicron aerosol particles. *J. Aerosol Sci.*, *33*, 1541–1557.
Schleicher, B., Künzel, S., & Burtscher, H. (1995). In situ measurement of size and density of submicron aerosol particles. *J. Appl. Phys.*, *78*, 4416–4422.
Schmid, O., Karg, E., Hagen, D. E., Whitefield, P. D., & Ferron, G. A. (2007). On the effective density of non-spherical particles as derived from combined measurements of aerodynamic and mobility equivalent size. *J. Aerosol Sci.*, *38*, 431–443.
Virtanen, A., Ristimäki, J., & Keskinen, J. (2004). Method for measuring effective density and fractal dimension of aerosol agglomerates. *Aerosol Sci. Technol.*, *38*, 1–10.
Wang, S. C., & Flagan, R. C. (1990). Scanning electrical mobility spectrometer. *Aerosol Sci. Technol.*, *13*, 230–240.

Paper II

Rostedt, A., Marjamäki, M., Yli-Ojanperä, J., Keskinen, J., Janka, K., Niemelä,V. and Ukkonen, A., 2009. *Non-Collecting Electrical Sensor for Particle Concentration Measurement.* AAQR, 9:470–477, doi: 10.4209/aaqr.2009.03.0023

Aerosol and Air Quality Research, 9: 470-477, 2009

ISSN: 1680-8584 print / 2071-1409 online
doi: 10.4209/aaqr.2009.03.0023

Non-Collecting Electrical Sensor for Particle Concentration Measurement

Antti Rostedt[1*], Marko Marjamäki[1], Jaakko Yli-Ojanperä[1], Jorma Keskinen[1], Kauko Janka[2], Ville Niemelä[2], Ari Ukkonen[2]

[1] *Tampere University of Technology, Department of Physics, Aerosol Physics Laboratory, P.O.Box 692, FI-33101 Tampere, Finland*
[2] *Dekati Ltd, Osuusmyllynkatu 13, FI-33100 Tampere, Finland*

ABSTRACT

A novel particle emission sensor based on particle charging and electrical detection is presented. The sensor charges the particles and measures the current carried by the particles exiting the sensor. The measurement is carried out without collecting the particles. Thanks to this principle, the mechanical construction of the sensor can be such that the sensor is not prone to fouling. The intended application of the sensor is the measurement of particle emission of diesel vehicles. The sensor is placed directly in to the exhaust flow of the tested vehicle, and because of that there is no need for any sampling or dilution of the exhaust gas. This together with the electrical measurement method allows rapid time response, and consequently, real time measurement of test cycles or on-road driving.

The sensor was tested in the laboratory and a theoretical model was build to predict the response of the instrument. The model can be used for converting the measured signals to the particle concentration or emission rate. Good correlation with a reference instrument was obtained in a diesel test cycle measurement.

***Keywords*:** Particle; Sensor; Diesel exhaust; Real time.

INTRODUCTION

The need to measure aerosols has increased substantially in recent years–mainly because of the undesirable effects they have on our health and the environment and the role particles play in atmospheric processes and climate change. Particle emissions and ambient and workplace particle concentrations and exposure are measured to ensure that the limits set by the legislation are met and that the public is not exposed to undesirable concentrations of aerosols. The health of the employees needs to be considered, as the number of manufacturing processes where materials pass through an aerosol phase is increasing rapidly, in areas from pigments, powders, and pharmaceuticals to optical fibers. Such applications require constant monitoring at many different locations or portable instrumentation that can be easily transferred between the locations of interest. In addition, with low cost portable instrumentation the particle emission sources could be monitored more easily and more extensively. Although the information obtained with a simple sensor type measurement can be quite limited compared to a full featured measurement set-up, there are some clear advantages. Usually most modern fine particle instruments can provide a lot of detailed information about the aerosol measured, but the cost and complexity of these devices is a major concern. Furthermore when using these devices, there is commonly need for sampling and sample conditioning systems. They not only add on to the cost and complexity, but they can also have some unwanted side effects to the measured sample. Despite its limitations a simple sensor type measurement could be very useful, when monitoring relatively well known aerosol or in particularly when monitoring changes in the aerosol content.

In engine exhaust particle emission measurement, which is the application for the sensor presented in this study, several different measurement techniques have been used. Mohr *et al*. (2005) lists various particle measurement instruments for particle emissions of modern vehicles. Those utilize the most commonly used measurement techniques, including mass based, optical and electrical techniques. A common feature of the listed instruments is that they need sampling and sample conditioning before the actual measurement. Most commonly used sample conditioning includes some kind of a dilution system to dilute and to lower the sample temperature and water content. The use of a dilution system adds delay and averaging to the sample and for comparative results similar dilution system and operational parameters must be used (e.g. Mathis *et al*., 2004). A dilution system also slows the time response of the measurement system. This may be a significant disadvantage when rapid transient phenomena are investigated.

Simple sensor type solutions, such as opacimeter and filter smoke number (FSN), are especially well suited for engine development, inspection and maintenance related particle measurements, where often only relative quantities of the emission are required. The opacimeter (e.g. ISO 3173, SAE J1667), commonly used in inspection tests, measures extinction of light in the exhaust gas in the visible or near infrared wavelength regions and it has been commonly used in the past. The FSN is also widely used as a simple technique to measure diesel particle emission, where the particles are first collected to a filter surface and then the blackening of the filter is measured optically. Although requiring particle collection for the measurement, only simple equipment is needed. A more modern technique capable of on-line soot measurements is laser induced incandescence (LII, Quay *et al*., 1994). The measured soot containing flow is illuminated with a pulsed laser source and the blackbody radiation from the heated soot particles is detected. LII can be used as an imaging measurement, enabling both spatial and temporal measurement of the soot volume fraction and primary particle size of the soot as demonstrated by Will *et al*.

* Corresponding author. Tel.: 358-3-3115-11;
Fax: 358-3-3115-2600
E-mail address: antti.rostedt@tut.fi

(1995). The measurement can be used to study the soot formation inside the flame region of a combustion process.

Other promising and relatively simple instruments are the photoacoustic sensor (Petzold and Niessner, 1996) and the diffusion charger (e.g. Ntziachristos *et al.*, 2004). The photoacoustic sensor utilizes the high absorption coefficient of the soot and measures acoustic signals originating from the particles heated by pulsed light source. With the diffusion charger measurement the particles are usually charged using an unipolar corona discharge charger after which the particles are collected with a Faraday cup filter and the charge on the particles is measured as a current signal. The outcome of the diffusion charger measurement is related to the total active surface of the aerosol measured.

In general, electrical measurement methods seem promising, when aiming towards a simple sensor solution for aerosol measurement. The simplicity and ruggedness of the electrical measurement methods are the key properties. Electrical measurement methods also provide fast response times, which make it possible to use them in real time measurements of a changing aerosol. With electrical methods, the particle size or the concentration cannot be measured directly. If the measured aerosol and the properties of the sensor are known, the measured electrical signals can be converted for instance into a number or mass concentration. In emission measurement, the temporal concentration values need to be converted into temporal emission rate values (#/s, mg/s), integrated over time and divided by the produced energy or travelled distance. The current regulations for particle emissions are based on total mass (mg/km, mg/kWh). A proposal for particle number emission measurements (#/km, #/kWh) is included in future Euro V/Euro VI regulations (Regulation (EC) No 692/2008).

In this paper, an aerosol particle sensor capable for measuring particle emission of a diesel vehicle is presented and evaluated (Janka *et al*., 2007; Niemelä *et al*., 2007; Tikkanen *et al*., 2007). The sensor is placed directly in contact with the measured exhaust flow ensuring simple and easy to use measurement set-up. Although the presented sensor is tailored to a focused application, the same principle could easily be used for other purposes as well; in fact a similar measurement method has been previously used in monitoring the air quality in work environments (Lehtimäki, 1983). The sensor presented here is named the Electrical Tail Pipe Sensor (ETaPS) and it is commercially available from Dekati Ltd, Finland.

SENSOR DESIGN

The operation principle of this sensor is based on a non-collective electrical measurement. The system consists of an electrically isolated corona discharge circuit and an electrometer to measure the leakage current from the discharge. In operation, the corona discharge unit, i.e. the probe, is placed inside the flow channel, so that the flow containing particles to be measured flows around and through the probe. A fraction of the particles in the flow pass through the sensor volume where they are charged by the corona discharge. While some of particles may deposit on the sensor's surfaces, the majority exit, and thereby remove charge, from the sensor volume. Because the corona discharge circuit is electrically isolated from the surroundings, this loss of charge can be seen as a leakage current from the system and it is measured by an electrometer. Since we want only the particles to contribute to the measured signal, escaping of ions from the system must be prevented. This is done with the corona electrodes, which also form an ion trap inside the sensor probe. Particles collected inside the probe do not contribute to the measured current; only the charge carried away from the probe with particles will be measured. In this way, the passage of particles through the sensor can be recorded without additional sampling and collection of the particles. The resulting small detection volume located directly in the exhaust stream enables fast response time.

The sensor is placed directly in contact with the measured aerosol flow to simplify the measurement set-up. As a disadvantage this exposes the sensor to a harsh environment where it must tolerate high variations in temperature and flow velocity. The aerosol concentration inside the tailpipe can be really high, of the order of 10^9 1/cm³ at the most. To withstand all this, the sensor must be build so that it is rugged and not prone to fouling. In addition, the electrical measurement method needs good insulators to operate correctly. Insulators need to stay clean and inside the operating temperature range of the insulating materials. For this, the use of cooling and sheath flows must be used. The total sheath air flow rate is 50 L/min, which is less than five percent of the flow rate inside the exhaust line at the most. Based on the tests done, this has negligible effect on the measurement. The designed operation limits of the presented sensor are collected to the Table 1.

The operational concentration range depends on the particle size and flow velocity inside the flow channel. This is due to velocity dependent residence time in charger. The values shown in Table 1 are calculated to cover the whole flow velocity range of 3-50 m/s and particle number median size range of 40-100 nm. For instance for constant flow velocity of 20 m/s, the concentration range is 4×10^3-7×10^8 for a lognormal size distribution with a median size of 100 nm and a GSD of 1.8.

The response time of the sensor is not practically restricted by physical properties of the charging process involved, which makes the method ideal for real time measurement. In the actual sensor the response time is electrically limited to 1 s, but even faster response times could be used if needed. A cross section view of the sensor probe together with an equivalent electrical circuit is presented in Fig. 1.

EXPERIMENTAL SET-UP

The laboratory measurements were made using a measurement setup presented in Fig. 2. The set-up consisted of a channel system, where a ducted fan circulated the air through the tested sensors and an air filter. There were two identical sensor prototypes fitted to the flow channel one after the other. The first sensor (Sensor 1) was primarily used in the tests and the second one (Sensor 2) was used just for comparison. All data presented here is measured with the first sensor. For both sensors the sheath air flow rate was set to 50 L/min. The filter in the set-up cleaned the test flow from particles. An exhaust port was needed, because the feed of the test particles and the sheath flows of the sensors led to an excess flow from the system. During the tests the flow velocity was measured with a flow sensor and it could be varied by the rotation speed of the fan in the range of 1-35 m/s. The channel size, where the sensors were fitted, was 100 mm in diameter and to reduce pressure drop in the system the diameter was 250 mm elsewhere. To ensure stable flow profile around the sensor probes, they were fitted so that there was enough free space in before and after the sensors for the flow to stabilize.

The aerosol sample for the reference measurement was taken from the flow before the sensors and it was diluted with an

Table 1. Designed operation limits of the sensor.

Parameter	Range
Temperature	0-400°C
Flow velocity	3-50 m/s
Particle concentration	10^5-10^8 1/cm³
Sheath air flow rate (total)	50 L/min

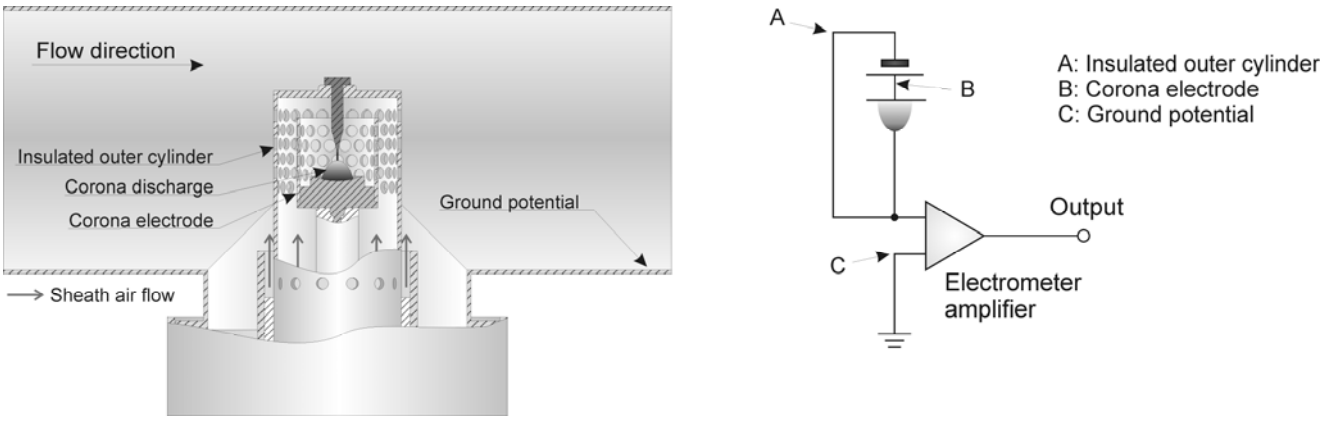

Fig. 1. Cross section view of the ETaPS sensor probe on the left. On the right the equivalent electrical circuit of the sensor.

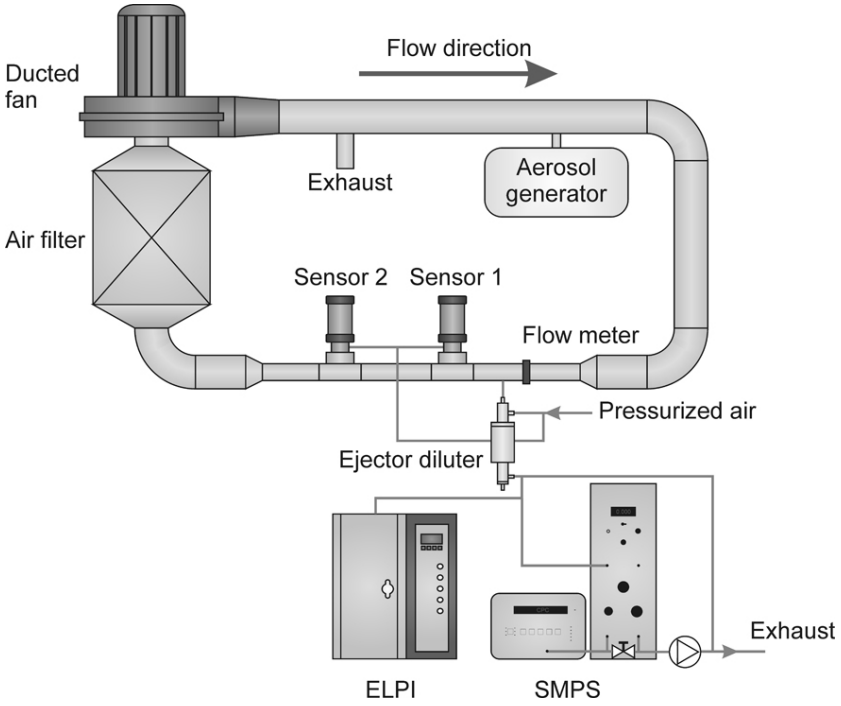

Fig. 2. Measurement set-up for laboratory tests. The DOS aerosol used in the tests was generated with a condensation-evaporation generator. As reference measurement ELPI and SMPS systems were used.

ejector diluter with a dilution ratio of 10.5. As reference instruments an Electrical Low-Pressure Impactor (ELPI, Keskinen *et al*., 1992) and a Scanning Mobility Particle Sizer (SMPS, Wang and Flagan 1990) were used. With these instruments the number size distribution of the test aerosol could be monitored together with the total concentration. The SMPS system was run with flow rates of 0.6 L/min of aerosol and 6 L/min of sheath air, which gave the measurement size range of 10-420 nm. The operational size range of the ELPI system was 7 nm-10 μm. The sample time of the SMPS was set to 120 s, whereas the ELPI size distribution was saved with 1 s interval. The data from the sensors was also saved with 1 s interval. All tests were performed in normal laboratory conditions and temperatures.

The test aerosol was generated from dioctyl sebacate (DOS) with an evaporation-condensation generator (e.g. Liu and Lee, 1970). With the generator, the median size of the test aerosol could be adjusted from 40 to 120 nm, while the geometric standard deviation was typically around 1.5. An example of a normalized and averaged size distribution used in the measurements is shown in Fig. 3. The ELPI was used to monitor the stability of the test aerosol in real time during the measurements. The particle concentration in the test flow could be varied by controlling the flow rate of the generated aerosol into the test flow. The generated aerosol was fed to the system 4 m before the tested sensors. The Reynolds number in the test flow was 26000 at the minimum. This indicates a high turbulence level, ensuring a complete mixing of the test aerosol.

INSTRUMENT RESPONSE

The charge level of the particles as such is not detected, only the charge particles acquire and carry away from the probe is detected. Therefore the initial charge of the particles does not affect the measurement, as long as it is well below the level acquired inside the probe. The measured current is proportional to the particle flux through the sensor and the charge that particles acquire inside the charger. For a charging process

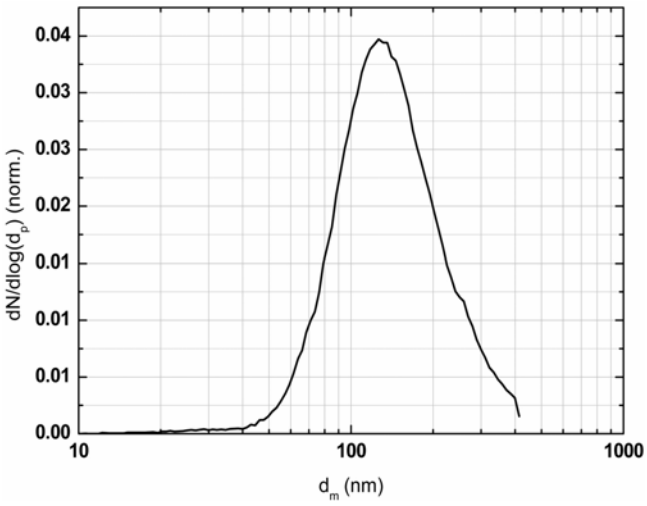

Fig. 3. Normalized average size distribution of the linearity test.

independent of the exhaust flow velocity and particle size, the output would be a direct measure of particle emission rate (#/s). However, the change in the charging efficiency with different flow velocities causes some nonlinearity to the sensor output compared to the actual particle flux in the measured flow. In addition, the amount of charge the particles acquire while travelling through the sensor depends on particle size through the so called active surface of the particles. That dependence has been used previously to measure the surface area content of aerosols by using conventional diffusion chargers. (Ntziachristos *et al*., 2007).

Linearity

First of all we have to have a look on the sensor linearity to test the correct operation of the sensor. If the shape of the particle size distribution and the flow velocity do not change, the sensor output should be linear as a function of the particle concentration. To test this, the dependence of the sensor output signal on the particle concentration in the flow was measured with two flow velocities 10 m/s and 35 m/s. During the measurements only the concentration of the aerosol was varied, particle size distribution was kept constant and monitored with SMPS and ELPI. During the measurements the number median size of the aerosol distribution was 134 nm with GSD of 1.56. The measured sensor output signal was compared to the total number and surface area concentrations measured with SMPS in Fig. 4. From the comparison it can be seen that the sensor output is linear as a function of the particle concentration and the slope of the response curve depends on the flow velocity inside the channel and probe. The slight curvature seen on the number concentration correlation (left side of Fig. 4.) is caused by a small variation on the number median size of the distribution during the measurements. The effect of the variation does not show on the surface area correlation (right side of Fig. 4), since the particle charging and the sensor correlates better to the surface area concentration than to number concentration. Based on Fig. 4, we can use the ratio of the measured signal to the particle concentration in the following data analysis.

Effect of Particle Size and Flow Velocity

Because the sensor output signal originates from the charging of the particles with a corona discharge, both the properties of the particles (mainly the particle size) and their velocity through the charging region affects the measured signal. To understand the effect of these parameters, the sensor output signal needed to be studied with different particle sizes and flow velocities.

The effect of particle size could be studied using monodisperse particles, but in this case the required volumetric flow rates were so high that monodisperse particles could not be generated in sufficient concentrations for the measurement. Therefore the effect of particle size was studied with lognormal polydisperse distributions having different median diameters. The effect of particle size distribution with different flow velocities are shown in Fig. 5. In the figure, sensor output normalized with particle number concentration is plotted against the median size of the measured size distribution with different but constant flow velocities. The coordinate axis on the figure represents the response of the sensor to particle number concentration, and it has the same units as the charging efficiency of the ELPI (Keskinen *et al.*, 1992.).

Modeling of the Response

To gain understanding on the operation of the charger, a model is built based on the measurements. To explain the measured output signal, we have to look on the charging processes involved. Because the particle size range in this application is around 100 nm, the particle charging processes involved are primarily diffusion and secondly field charging. The total number of elementary charges per particle is approximated as the sum of the charges acquired by diffusion charging and field charging, i.e.

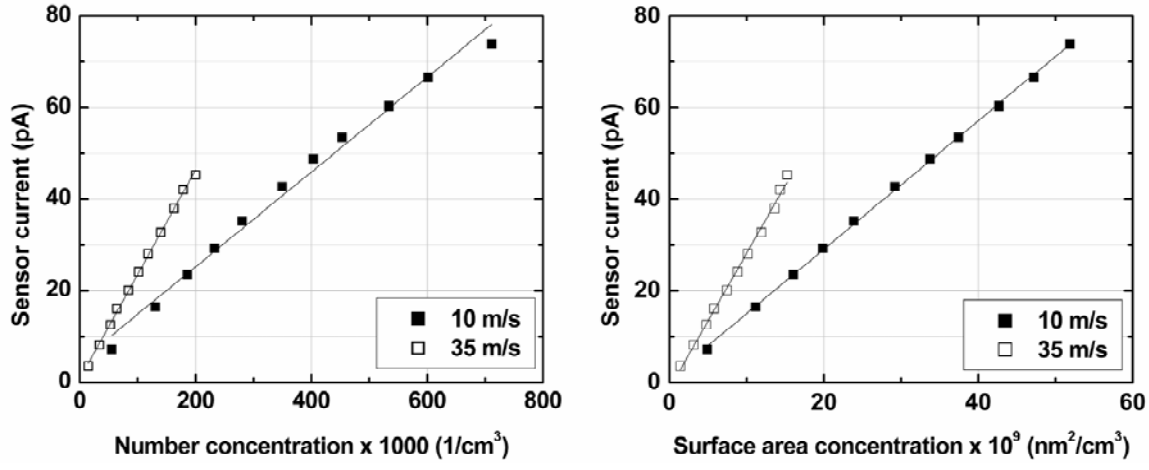

Fig. 4. Concentration dependence: Comparison of the sensor signal and total number concentration on the left and comparison of sensor signal and the total surface area concentration.

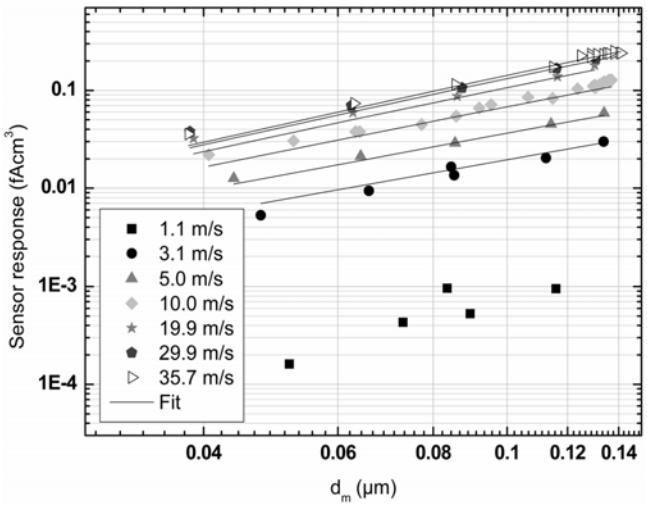

Fig. 5. Dependence of the sensor output on the median diameter of the size distribution. The sensor output is normalized to SMPS total number concentration for comparison. The solid line is simulated sensor output with fitted charger efficiency (Eq. (4)).

$$n = n_d + n_f = \frac{2pe_0 d_p kT}{e^2}\ln\left|\frac{d_p \bar{c}_i e^2 N_j t}{8e_0 kT}\right| + \left|\frac{3e}{e+2}\right|\left|\frac{E_{ave} d_{p\,pe_0}^2}{e}\right| \left|\frac{eZ_i N_i t}{4e_0\left|1+\frac{1}{4e_0}eZ_i N_i t\right|}\right| \quad (1)$$

where ε_0 is the permittivity of vacuum 8.85 × 10^{-12} F/m, ε is the relative permittivity of the particles 4, d_p is the particle mobility diameter, k is the Boltzmann constant 1.38 × 10^{23} J/K, T is the temperature of the gas 293 K, e is the charge of the elementary charge 1.602 × 10^{-19} C and $\bar{c}_i$ is the average thermal velocity of the charging ions 240 m/s, E_{ave} is the fitted average electrical field in the charging region and Z_i is the mobility of the charging ions 1.5 × 10^{-4} m²/s. The diffusion charging of the particles depends on the particle size and the $N_i t$ product, which is a product of the ion concentration and the residence time of the particles inside the charging region. Field charging depends also on the $N_i t$ product, but it also depends on the average electrical field inside the charging region and the permittivity of the particles.

The increase in the velocity of the measured flow should also increase the current which is measured from the sensor, since the amount of particles traveling through the charging region per second increases. However the flow velocity V_{flow} also affects the residence time t: an increase in the flow velocity reduces the residence time and the $N_i t$ product. Therefore the increase in the measured current is not linear to the flow velocity. The residence time depends on the flow velocity inside the charging region. Since the sensor probe can be considered as a porous medium in the flow, the flow velocity inside is smaller by a factor R. This gives for the residence time the approximate form shown in the Eq. (2)

$$t = \frac{L_{eff}}{V_{ch}}, \quad V_{ch} = R(V_{flow} - V_{\min}) \quad (2)$$

An artificial term V_{min} is added to the equation to simulate the fact that below a certain minimum flow velocity no charged particles can exit the charger, i.e. all of the particles are collected inside the charger by electrical forces. L_{eff} is the fitted effective length of the charging region in the flow direction. The ratio R describes the ratio of flow velocities inside and outside of the charging region. Theoretical calculation of the ratio R ("effective porosity") gives a value of 0.29. The calculation has been performed according to the following principles and assumptions: Since the detection volume is inside of two perforated cylinders, the aerosol flows through four perforated plates – two plates prior and two after the charging region. Because of this the total pressure drop between the inlet and outlet faces of the sensor is the sum of the pressure drop of each perforated plate. Following estimations and approximations have been made: 1) The curvatures of the plates are assumed to be negligible in the streamlines following through the charging region. 2) The discharge coefficient C_d of each hole of the perforated walls is assumed to be 0.7. 3) The flow field reaches a fully developed state prior to each wall.

The resulting response of the charger, E_{ch}, can be written as

$$E_{ch} = \frac{1}{4} p d_{duct}^2 R(V_{flow} - V_{\min}) ne \quad (3)$$

where the diameter of the flow channel is d_{duct}, R is the ratio of the flow velocity inside the charging region and e is the elementary charge. For practical use of the sensor, the output signal should be converted to a relevant concentration or emission value. Presented model can be used for this purpose, if the flow velocity and size distribution of the measured aerosol is known.

As seen in Fig. 5 the response of the particles increases with increasing particle size, which is expected since charging efficiency increases with increasing particle size. The response also increases with the increasing flow velocity. This is attributed to the fact that the amount of particles passing through the sensor increases increasing the charge carried away by the particles. The actual charging efficiency for individual particles decreases with increasing flow velocity, since the residence time inside the charging region decreases.

We can use the theoretical approach presented to build a fit for the response of the instrument. The fit can then be used to predict the response of the instrument for different aerosol size distributions. The output current of the sensor is the integral equation of the response of the charger and the size distribution as follows:

$$I_s = \int \mathrm{E_{ch}}(\mathrm{d_p}, \mathrm{V_{flow}})\,\mathrm{N}(\mathrm{d_p})\,\mathrm{dd_p} \quad (4)$$

The term $N(d_p)$ is the number concentration as a function of particle size, E_{ch} is the response of the charger as a function of particle size and flow velocity as derived in Eq. (3). The fit is constructed so that the parameters for the theoretical model are fitted to minimize the difference between the measured current and the current simulated from the measured size distribution using the theoretical model.

Now selected parameters from the equations of the average charge number (Eq. (1)) are fitted so that the simulated currents agree with the corresponding measured currents. Parameters used for the fitting are ion concentration, average electric field, minimum flow velocity and effective length of the charging region. The fitted parameter values are collected to Table 2. It has to be remembered that values are not thought to be physically accurate; they are just values that give the best prediction for the operation and response of the instrument. Even so, all of the fitted values are realistic and feasible for the used construction.

Table 2. Fitted parameters to particle charging model.

Description	Symbol	Value
Effective length of the charging region	L_{eff}	6.8×10^{-3} mm
Average electric field	E_{ave}	2.07×10^{5} V/m
Ion concentration	N_i	1.28×10^{15} 1/m³
Minimum flow velocity	V_{min}	1.6 m/s

The resulting response with different flow velocities are plotted to Fig. 6. All of the measurements for this study were used to generate the fit. In Fig. 7, the simulated sensor outputs using the fit are plotted against corresponding measured values. As can be seen from the figure the fit predicts the measurements nicely, suggesting that the fit is reliable and can be used to predict results. Size dependence of the response predicted by the fit is also plotted with solid line in Fig. 5.

The fit can be used to estimate the response of the instrument for different size distributions, as plotted in Fig. 8. Only number concentration response is shown in the figure, but mass concentration and number or mass emission rate responses could be easily constructed for any given aerosol size distribution. With the aid of the obtained response, the current signal from the sensor can be converted to a number or mass concentration value, if the flow velocity and properties of the size distribution of the measured aerosol are known. The emission rate responses do not depend on the flow velocity of the measured flow as much as the number or mass concentration response. This makes it possible for a narrow flow velocity range to convert the sensor output to an emission rate value by using a simple conversion factor without the need of measuring the flow velocity.

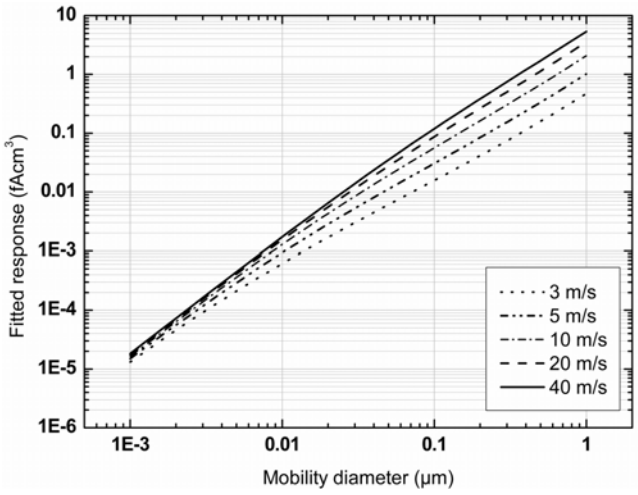

Fig. 6. Fitted charging efficiency curves for the sensor with different flow velocities.

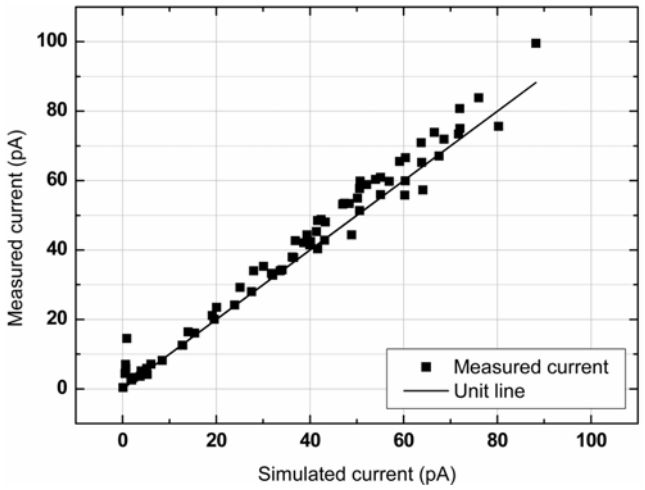

Fig. 7. Simulated sensor output as a function of the measured output.

TEST MEASUREMENTS WITH DIESEL EXHAUST

The designed sensor is intended to measure the particle concentration of a diesel engine exhaust. Moreover, the whole sensor is intended to be mounted so that the raw exhaust gases flow through the sensor probe. To test the sensor design, diesel exhaust measurements were made. Fig. 9 demonstrates the operation of the sensor in a real life measurement. The figure shows how the particle mass concentration inside the exhaust line changes during an engine test cycle. The measured sensor signal is first converted to a number concentration value with the aid of Eq. (4) by assuming the particle size distribution to be constant with a median size of 80 nm and a GSD of 1.75. After that the number concentration was converted to a mass concentration.

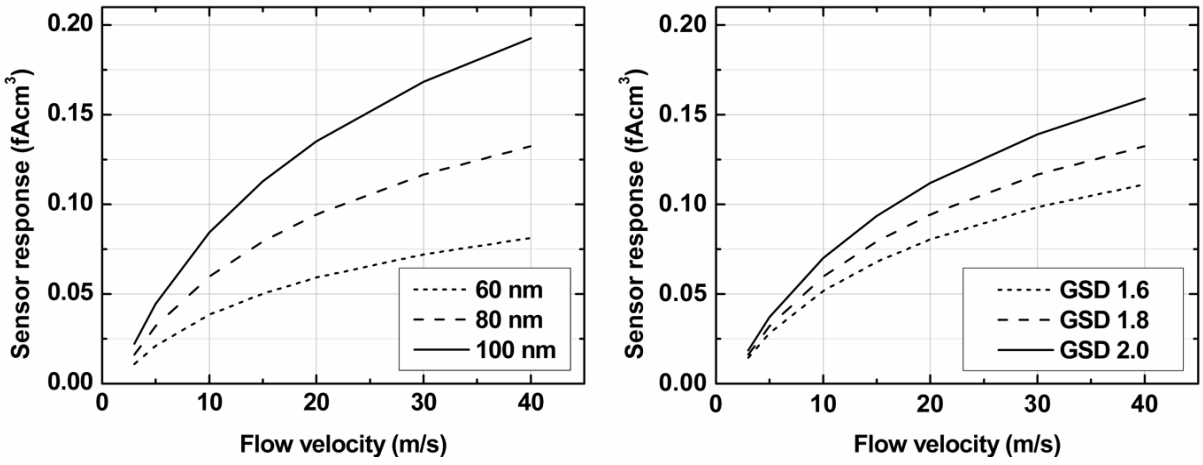

Fig. 8. Sensor response for different lognormal size distributions as a function of the flow velocity. On the left the effect of the median diameter with constant GSD of 1.80 and on the right the effect of the GSD with a constant median size of 80 nm is shown.

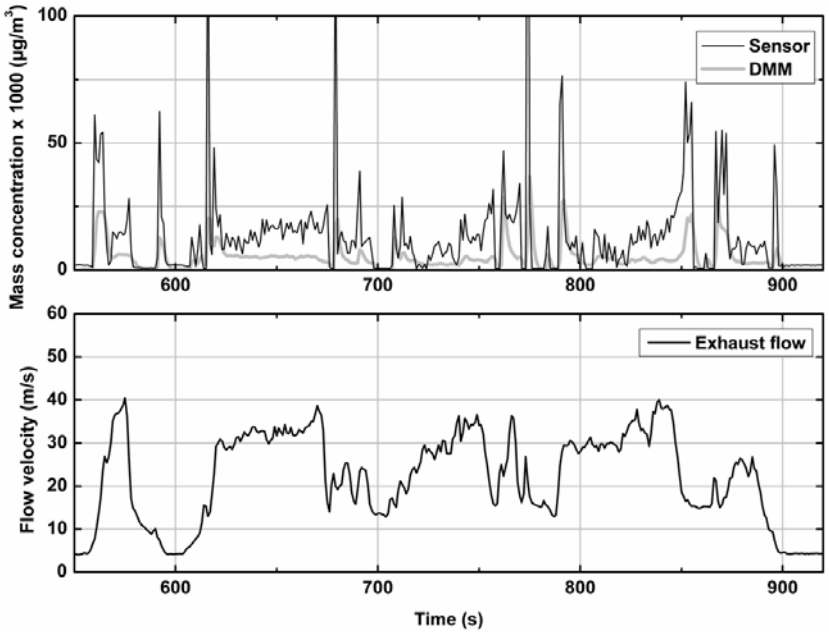

Fig. 9. Mass concentration of a diesel exhaust during a test cycle measured with ETaPS sensor and DMM together with a flow velocity inside the exhaust line.

The effective density of the particles was assumed to obey a fractal law, with a mass fractal dimension of 2.6 (e.g. Virtanen *et al.*, 2002). The resulting mass concentration is plotted to Fig. 9 as a function of time. Corresponding mass concentration values obtained with a Dekati Mass Monitor (DMM-230, Lehmann *et al.*, 2004) are shown for comparison.

It can be seen from Fig. 9, that the mass concentration measured with the sensor follows the reference measurement. We can see that the emission peaks from the changes in the engine load are much sharper in the ETaPS data than what measured with the DMM. This shows the effect of slower response time of the dilution system used in the DMM measurement. ETaPS can distinguish the short concentration peaks during engine loading transients, while the diluter-DMM combination smoothes the peaks significantly. Fig. 10 shows a correlation plot, where the mass concentration measured with the sensor is plotted against the reference measurement. Since the instruments have a different time responses, an additional time constant of 1.8 seconds was artificially added to the ETaPS sensor signal to have similar time responses in both instruments. The correct time alignment of the data was found by cross correlation. Finally a time constant of 10 s was added to both measurement data to add averaging and to reduce the effects of timing misalignments in the sensor and flow velocity measurements. Then the correlation between the instruments was calculated and the resulting correlation plot is shown in Fig. 10. With the diesel engine measurements the mechanical structure withstood the extreme conditions inside the exhaust line. The operation of the sensor has been successfully tested in temperatures ranging up to 400°C with a flow velocity ranging up to 50 m/s. Although the operation times of the sensor depends on the concentrations measured, with modern diesel engines having low emissions the sensor can be operated without need for cleaning.

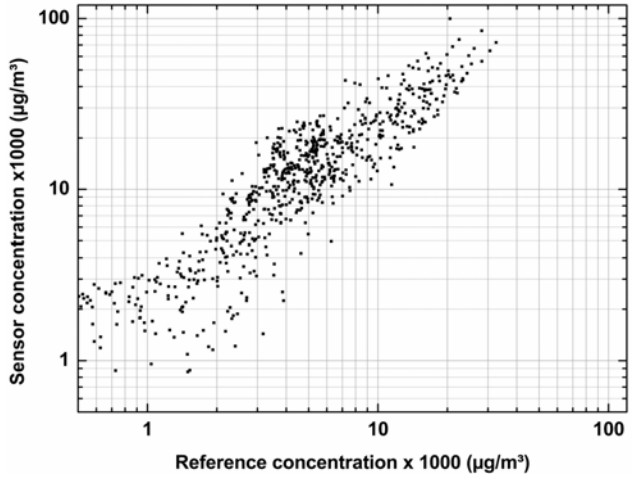

Fig. 10. Mass concentration measured with the sensor as a function of reference mass concentration measured with DMM. The minimum value of the y-axis is limited to the detection limit of the sensor, caused by the data logging and selected sensor sensitivity range for the measurements.

DISCUSSION AND CONCLUSIONS

The presented sensor design allows in situ measurement of aerosol concentration without any dilution or sampling systems. This allows faster response time and simpler measurement setup compared to traditional aerosol instrumentation. With the sensor events such as engine start ups and sudden changes of engine load can be easily monitored. The measured particles are not collected by the sensor allowing longer operation times without service.

The response of the sensor depends primarily on the particle flux through the sensor and the presented theoretical model can be used to predict the response of the instrument in different measurement conditions. If the size distribution of the measured aerosol is known, the model can also be used to convert the measured sensor signal into a concentration value. The model is useful in predicting the operation of the sensor and it can be used as an aid when the measurement principle is used in other applications. Depending on the application, the quantity that is sought after can be different. It can be for example number or mass concentration or active surface of the particles.

In the studied configuration, the response of the sensor is affected by the flow velocity in the measured exhaust flow. This is a trade off with the simplicity of the measurement set-up. This same type of measurement method can also be used with a forced constant flow system to overcome this dependence of the flow velocity. The operational concentration range of the sensor is 10^4-10^8 1/cm³ with a flow velocity range of 3-50 m/s. The operation of the designed sensor was tested successfully in the conditions of the exhaust line of a running diesel engine.

The calibration measurements presented here were made at room temperature. In order to increase the accuracy in diesel exhaust measurements, the effect of the elevated temperature of the exhaust gases must be included into the developed model. In the exhaust gas measurements, although the effect of temperature was not taken into account, the correlation in the mass concentration of the sensor to the reference measurement was good.

ACKNOWLEDGEMENTS

The vehicle test measurements were done during New York State Energy Research and Development Authority (NYSERDA) programme "Evaluation of On-Board Real-Time Particulate Emissions Measurement Technologies". William "Butch" Crews from Southern Research Institute and Jill Hendren and the test cell personnel from Environmental Canada are acknowledged for their help during the measurements.

Dr. Marjamäki was funded by the Academy of Finland grant number 109124.

REFERENCES

Janka, K., Niemelä, V., Lamminen, E., Keskinen, J., Rostedt, A. and Lemmetty, M. (2007). Design and Performance Evaluation of a New Non-Collective Electrical Aerosol Sensor. European Aerosol Conference 2007, Salzburg, Abstract T02A037.

Keskinen, J., Pietarinen, K. and Lehtimäki, M. (1992). Electrical Low Pressure Impactor. *J. Aerosol Sci.* 23: 353-360.

Lehman, U., Niemelä, V. and Mohr, M. (2004). New Method for for Time-Resolved Diesel Engine Exhaust Particle Mass Measurement. *Environ. Sci. Technol.* 38: 5704-5711.

Lehtimäki, M. (1983). In *Modified Electrical Aerosol Detector. Aerosols in the Mining and Industrial Work Environments*, Vol. 3, Marple, V.A. and Liu, B.Y.H. (Eds.), Ann Arbor Science Publishers, Ann Arbor, p. 1135-1143.

Liu, B.Y.H. and Lee, K.W. (1975). An Aerosol Generator of High Stability. *Am. Ind. Hyg. Assoc. J.* 36: 861-865.

Mathis, U., Ristimäki, R., Mohr, M., Keskinen, J., Ntziachristos, L., Samaras, Z. and Mikkanen, P. (2004). Sampling Conditions for the Measurement of Nucleation Mode Particles in the Exhaust of a Diesel Vehicle. *Aerosol Sci. Technol.* 38: 1149-1160.

Mohr, M., Lehmann, U. and Rütter, J. (2005). Comparison of Mass-Based and Non-Mass-Based Particle Measurement Systems for Ultra-Low Emission from Automotive Sources. *Environ. Sci. Technol.* 39: 2229-2238.

Niemelä, V., Janka, K., Isherwood, H., Keskinen, J. and Rostedt, A. (Ed.). Non-collective Electrical Aerosol Sensor. Proc. 5th Asian Aerosol Conference, Kaohsiung, Taiwan, 2007.

Ntziachristos, L., Giechaskiel, B., Ristimäki, J. and Keskinen, J. (2004). Use of a Corona Charger for the Characterisation of Automotive Exhaust Aerosol. *J. Aerosol Sci.* 35: 943-963.

Ntziachristos, L., Polidori, A., Phuleria, H., Geller, M.D. and Sioutas, C. (2007). Application of a Diffusion Charger for the Measurement of Particle Surface Concentration in Different Environments. *Aerosol Sci. Technol.* 41: 571-580

Petzold, A. and Niessner, R. (1996). Photoacoustic Soot Sensor for In-Situ Bblack Carbon Monitoring. *Appl. Phys. B.* 63: 191-197.

Quay, B., Lee, T.W., Ni, T. and Santoro, R.J. (1994). Spatially Resolved Measurements of Soot Volume Fraction Using Laser-Induced Incandescence. *Combust. Flame*. 97: 384-392.

Regulation (EC) No 692/2008 of the European Parliament and of the Council of 18 July 2008.

Tikkanen, J., Moisio, M., Janka, K., Pietarinen, K., Keskinen, J. and Rostedt, A. (2007). Method and a Sensor Device for Measuring Particle Emission from the Exhaust Gases of a Combustion Engine. Finnish Patent FI118278, US patent 7406855.

Virtanen, A., Ristimäki, J., Marjamäki, M., Vaaraslahti, K., Keskinen, J. and Lappi, M. (2002). Effective Density of Diesel Exhaust Particles as a Function of Size. SAE Paper No. 2002-01-0056.

Wang, S.C., Flagan, R.C. (1990). Scanning Electrical Mobility Spectrometer. *Aerosol Sci. Technol.* 13: 230-240.

Will, S., Schraml, S. and Leipertz, A. (1995) Two-Dimensional Soot-Particle Sizing by Time-Resolved Laser-Induced Incandescence. *Opt. Lett.* 20: 2342-2344.

Received for review, March 24, 2009
Accepted, July 7, 2009

Paper III

Rostedt, A., Arffman, A., Janka, K., Yli-Ojanperä, J. and Keskinen, J., 2014. *Characterization and Response Model of the PPS-M Aerosol Sensor*. Aerosol Sci. Technol., 48:10, 1022-1030, doi: 10.1080/02786826.2014.951023

Aerosol Science and Technology, 48:1022–1030, 2014

ISSN: 0278-6826 print / 1521-7388 online
DOI: 10.1080/02786826.2014.951023

Characterization and Response Model of the PPS-M Aerosol Sensor

Antti Rostedt,[1] Anssi Arffman,[1] Kauko Janka,[2] Jaakko Yli-Ojanperä,[1] and Jorma Keskinen[1]
[1]*Aerosol Physics Laboratory, Department of Physics, Tampere University of Technology, Tampere, Finland*
[2]*Pegasor Oy, Tampere, Finland*

The Pegasor PPS-M sensor is an electrical aerosol sensor based on diffusion charging and current measurement without particle collection. In this study, the role and effect of each component in the instrument is discussed shortly and the results from a thorough calibration measurements are presented. A comprehensive response model for the operation of the PPS-M sensor was developed based on the calibration results and computational fluid dynamics (CFD) modeling results. The obtained response model, covering the effects of the particle charger, the mobility analyzer, and both diffusion and inertial losses, was tested in the laboratory measurements with polydisperse test aerosols, where a good correlation between the model and the measured results was found.

INTRODUCTION

The concern about the health effects of the exposure to fine particles has led to an increasing request for aerosol measurement and monitoring. Aerosol concentration measurement may be realized for various particle properties, such as particle number, mass, surface area, and volume (Kulkarni et al. 2011). Real time aerosol concentration instruments are usually based on the electrical or optical detection techniques. The optical instruments typically utilize light scattering or absorption of particles, while the electrical instruments are most commonly based on charging of the particles and subsequent measurement of the charge carried by the particles as an electrical current.

Particle charging is usually accomplished by unipolar diffusion chargers based on corona discharge, as reviewed, e.g., by Marquard et al. (2006) and Intra and Tippayawong (2009). Because of the simplicity, one of the most straightforward ways to produce an electrical aerosol detector is to combine unipolar diffusion charger with a faraday cup electrometer. The measured quantity is electrical current, which is related to the particle number concentration and particle size. Ntziachristos et al. (2004) demonstrated such instrument for the real time monitoring of active surface area of particles emitted by a diesel engine. Fissan et al. (2007) introduced a similar instrument with a varying charging efficiency for the monitoring of the lung deposited particle surface area. Recent development of these diffusion charger-based instruments has focused on minimizing the size of the instruments to produce handheld instruments. The AeraSense Nanotracker (Marra et al. 2009) and Matter Aerosol DiSCmini (Fierz et al. 2011) are good examples of such instruments, the latter being even able to provide information on the average particle size of the measured aerosol. To make the instrument even smaller, micro-electromechanical (MEMS) techniques have been used by Lee et al. (2011).

All of the electrical instruments mentioned above are based on the collection of the particles after charging. Lehtimäki (1983) demonstrated electrical aerosol instrument without particle collection, based on measuring the charge escaping the charger with the charged particles. The idea has also been applied by Rostedt et al. (2009b). Recently, Fierz et al. (2014) described a non-collecting instrument based on induced current measurement.

The Pegasor PPS-M (Pegasor Oy, Tampere, Finland) sensor treated in this article is based on the escaping charge principle. The basic principle of the sensor has been presented by Lanki et al. (2011). Application of the sensor to engine exhaust measurements has been described by Ntziachristos et al. (2011, 2013). In this article, we present the first detailed calibration of the instrument, and a comprehensive model for the response of the instrument as a function of particle size together with laboratory test measurements.

SENSOR COMPONENTS AND OVERALL RESPONSE

The operation of the PPS-M sensor is based on electrical charging and detection of the charged aerosol particles. The design combines a sheath air-assisted corona charger with an

Received 17 April 2014; accepted 7 July 2014.
Address correspondence to Antti Rostedt, Aerosol Physics Laboratory, Department of Physics, Tampere University of Technology, P.O. Box 692, Tampere FI-33101, Finland. E-mail: antti.rostedt@tut.fi

ejector pump (Tikkanen 2009). A schematic view of the sensor (on the left side) and the actual sensor (on the right side) is shown in Figure 1. The instrument design consists of the following main components: a pre-cut cyclone to prevent the sensor from fouling, an ion source to provide charge to the particles, an ejector pump to provide the sample flow, an ion trap to remove the excess ions and to act as a mobility analyzer for the particles, and an electrometer to measure the charge on the particles.

Charging and Electrical System

The charger and ejector combination is designed so that the flow coming out from the ion production area is mixed with the sample and used as a pump flow in the ejector pump. In the charging region, the particles are charged by diffusion charging. The design of the flow-assisted ion source resembles the design presented already by Whitby (1961). This arrangement has the advantage of keeping the discharge electrode in a clean air flow. The volume of the charging region is rather small, resulting in a relatively low residence time for the charging process.

An ion trap is applied to prevent the charging ions from escaping the instrument and contributing to the charge measurement. In the present design, the trap geometry is annular and the applied electrical field can be varied directly from the user interface. By changing the electrical field, the cut point of the ion trap can be changed. The trap is dimensioned so that it is also able to collect a part of the particles, if the collection voltage is set high enough. This makes the trap to act as a simple zeroth-order mobility analyzer, which gives the possibility to estimate the average particle size of the measured aerosol. For this, the shape of the size distribution must be either known or assumed. This technique has earlier been used for particle density measurement by Rostedt et al. (2009a).

The electrical current measurement is realized without collecting the particles, by measuring the net current leaving the instrument. As a consequence, the response of the instrument depends on the initial charge state of the input aerosol and any ion leakage out from the instrument. Because of this escaping current measurement technique, the power sources for the corona charger and ion trap are isolated from the ground. Since the current is measured with a high sensitivity electrometer between the isolated virtual ground and the ground potential, both a low noise level and a high isolation resistance are required for the isolation. The electrometer is realized using an operational amplifier with a capacitive feedback circuit. Because of the electrometer design, the voltage difference between the two measurement points is well below 1 mV (Keithley Instruments Inc. 2004). For the practical use of the sensor, the sampling rate of the electrometer and the low pass filtering of the measured signal can be altered to suit the application in question.

Flow System

Computational fluid dynamics (CFD) simulation was used for optimizing the flow system of the sensor design. It was primarily used during the design process to estimate the ejector performance and the turbulent flow patterns inside the sensor. The CFD simulations also provided information on the diffusion losses within the whole sensor. The flow fields inside the sensor were modeled using Ansys Fluent 14.0. For the three-dimensional simulations, SST-k-ω turbulence transfer model was employed, and the computation grid consisted of 2.3 million cells. Boundary conditions at the flow boundaries were pressure inlets and pressure outlets.

The design of the ejector pump was optimized for minimizing the pressurized air consumption, while still providing enough pressure difference to provide an adequate sample

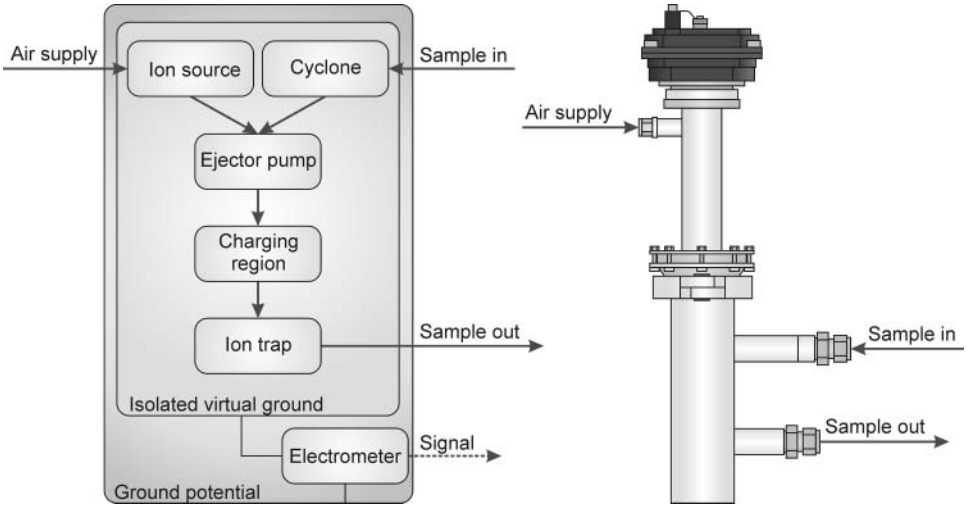

FIG. 1. Schematic view of the sensor components on the left and picture of the sensor on the right.

flow in a practical measurement setup. The needed pressure difference was minimized by returning the ejector outlet to the same pressure with the sample. Practically, this means that in the sensor there is two connections for the sample flow; one delivering the sample into the sensor and the other returning the sample, pump flow, and needed sheath air flows to the same pressure where the sample is taken.

The CFD modeling indicated the flow to be turbulent in the mobility analyzer region. The turbulence leads to less steep collection efficiency curves, which limits the size resolution of the analyzer. However, this is considered acceptable since the information from the mobility analyzer is only used for estimating the median size for the measured size distribution.

Sensor Response

All the sensor components contribute to the sensor response and from a calibration point of view the combined overall response would be enough. However, in the current design the operation of the sensor can be altered by the user by varying the mobility analyzer collection voltage. For this reason, more thorough understanding on the response is required. The charger charging efficiency E_{ch} and the mobility analyzer penetration P_{ma} are the main contributors to the overall response, while the effect of the non-electrical components, such as inertial and diffusion losses, plays a smaller role. The combined sensor response R is a function of the particle size d_p and the mobility analyzer voltage V_{ma}. It has the form of Equation (1), where the diffusion and inertial losses are expressed as penetrations P_d and P_i, respectively:

$$R\left(d_p, V_{\mathrm{ma}}\right) = E_{\mathrm{ch}}\left(d_p, V_{\mathrm{ma}}\right) P_{\mathrm{ma}}\left(d_p, V_{\mathrm{ma}}\right) P_d\left(d_p\right) P_i\left(d_p\right) \quad [1]$$

Because of the complicated flow path and the integrated nature of the sensor design, it was not possible to measure the effect of each component individually. The term P_d describing the diffusion losses was obtained from the CFD simulations, while the effects of the remaining components were calculated from the calibration results.

EXPERIMENTAL

The objective of the calibration measurements was to find out the sensor response to particle number concentration as a function of the particle mobility size together with the particle collection characteristics of the mobility analyzer. The calibration measurements were started by first verifying the operation of the integrated electrometer. For this, a reference electric current source, providing currents from 100 fA to 40 pA, was used. To ensure the correct current levels, the source was first calibrated using a Keithley 6430 Remote SourceMeter (Keithley Instruments Inc., Cleveland, OH, USA).

Sensor Response

In the response calibration, the Single Charged Aerosol Reference (SCAR; Yli-Ojanperä et al. 2010) was used as an aerosol generator. The main advantage of the SCAR is that it produces a nearly monodisperse aerosol sample with particles containing only one elemental charge each. The generated aerosol was then classified by a differential mobility analyzer (DMA model 3071A, TSI Inc., Shoreview, MN, USA). As a result a truly monodispersed aerosol was obtained for the calibration measurements. The DMA was used with recirculating sheath air flow with the flow rate range of 3 to 10 lpm, while the sample flow was varied from 1 to 2 lpm. With these flow rate values, the particle size range for the monodisperse calibration aerosol was 20–920 nm. Although the used sheath air to sample flow rate ratios were not optimal for the best size resolution of the DMA, the flow rates were chosen in order to cover a wide particle size range and to maximize the particle output after the classification. The flow rate of the recirculated DMA sheath flow was monitored and controlled by a custom made flow controller unit calibrated with an air flow calibrator (Gillian

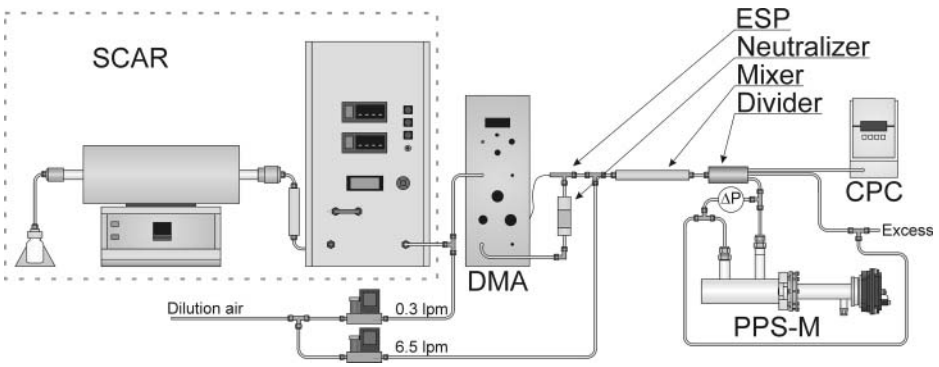

FIG. 2. The measurement setup used in the calibration. The SCAR was used as an aerosol source, the DMA for size classification and the CPC acted as the reference instrument.

Gilibrator-2, Sensidyne, LP, St. Petersburg, FL, USA). The whole measurement setup is shown in Figure 2.

In order to minimize the effect of the initial charge of the particles to the sensor response, the aerosol was neutralized using an ^{85}Kr aerosol neutralizer (Model 3077, TSI Inc., Shoreview, MN, USA). To ensure proper operation of the neutralizer, a small feed of pressurized air, 0.3 lpm, was introduced to the sample flow before the neutralizer. This was needed since the SCAR device produces the particles in a nitrogen atmosphere. After the neutralizer, the excess ions were removed by a small electrostatic precipitator (ESP). Because the total volumetric flow rate needed for the instruments was higher than the output of the classifying DMA, the sample was diluted by a second flow of pressurized air. Both dilution air flows were controlled with mass flow controllers (Alicat Scientific Inc., Tucson, AZ, USA) and the second dilution air flow was set to a level, which ensured a small excess flow from the sample line. After the dilution, a static mixer (Kenics 37-06-110, Chemineer, Dayton, OH, USA) was added to ensure proper mixing of the produced aerosol and dilution air. The sample was then divided with a flow divider (Model 3708, TSI Inc., Shoreview, MN, USA) into three parts: one for the sensor, one for a reference Condensation Particle Counter (CPC Model 3772, TSI Inc., Shoreview, MN, USA), and one for an excess flow. In order to ensure good accuracy in the number concentration measurement, the detection efficiency of the CPC used as a reference was calibrated with the method described in Yli-Ojanperä et al. (2012).

During the measurements, the pressure difference between the sensor inlet and outlet flows was monitored to ensure the correct sample flow into the sensor. During the measurements, the differential pressure was 165 Pa, sensor inlet being in a slightly lower pressure. This underpressure is low compared to the maximum pressure difference of 4.7 kPa, which the sensors ejector pump can supply with zero sample flow. The volumetric sample flow rate measured at the calibration conditions, i.e., with the same pressure difference, was 6.40 lpm and for the ejector pump flow a value of 3.63 lpm was measured after the calibration. For the measurements, the electronics was set up for 1 Hz sample rate with 3 s digital first-order low pass filter. With these settings, the short-term noise level of the measuring electronics was around ± 1 fA. The instrument and sample gas temperature was 296 ± 3 K.

Mobility Analyzer

The measurement setup also provided the possibility to calibrate the mobility analyzer of the sensor with the help of the singly charged particles. For the mobility analyzer calibration, the measurement setup was almost the same described above, only the aerosol neutralizer and the ESP were removed from the setup. Additionally, the charger inside the sensor was turned off. In this measurement, the singly charged particles were collected by the mobility analyzer inside the sensor, resulting in a current measured by the sensor electrometer. The polarity of the current was inverted compared to the normal operation, since instead of escaping out from the sensor the particles were collected inside the sensor. The desired quantity from the measurement was the fraction of particles collected by the mobility analyzer. The measured quantities were the current caused by the collected particles and the number concentration at the sensor inlet. This means that the current measured by the sensor needed to be converted to a particle number. For this, the charge state of the particles must be known. By using the SCAR as an aerosol source, all the particles are known to have a single elementary charge with the uncertainty of 0.16% (Högström et al. 2011).

RESULTS

To find out a model for the sensor response, the effect of each sensor component needs to be studied individually. For the diffusion losses, the results from the CFD simulations were used. For the effects of the other components, the parameters of the model were fitted to the calibration results. The flow system performance was also verified by measuring the sample flow rate and the maximum pressure the ejector can produce. These values were compared to the values obtained by CFD simulation. SI units were used for the parameters of the model, except for the charging efficiency and the overall response. Those are expressed in units of fAcm^3 for convenience.

Flow System Performance and Diffusion Losses

The nominal sample inlet flow was measured with minimal pressure difference between the sample inlet and outlet. To find out the maximum underpressure for the ejector with zero sample flow, a differential pressure meter was connected to the sample inlet. For the measurement, a nominal supply air pressure of 0.15 MPa was used. The measured result together with the corresponding results from the CFD simulations are collected to Table 1. Although there are some differences, the agreement between the measured values and the simulation results is good.

Diffusion losses inside the sensor were simulated in Eulerian fashion. Aerosol was fed to the sensor as a component of

TABLE 1
Parameters of the ejector flow system. CFD simulation results compared to the measured values

Parameter	CFD	Measured
Pump flow pressure (MPa)	0.15	0.15
Pump flow rate (lpm)	3.2	3.63
Ejector maximum underpressure (kPa)	4.3	4.7
Nominal sample flow rate (lpm)	6.9	6.70
Cyclone cut point (μm)	$\sim$2.0	—

the gas mixture. The boundary condition for aerosol concentration at the wall boundaries was zero in order to calculate the diffusion flux of particles to the sensor walls. Laminar diffusion coefficient was then adjusted to match the different size particles (Stokes–Einstein relation was used for the diffusion coefficient; Hinds 1999). Turbulence enhances the diffusion inside the sensor, and this was taken into account by using the effective diffusion coefficient for the aerosol mixture component. The effective diffusion coefficient is a sum of the laminar and turbulent diffusion coefficients, where the turbulent coefficient is computed from the turbulent transfer model (SST-k-ω) according to the Fluent standard formulation (ANSYS 2011). The computation grid was tetrahedral, and adapted several times until the results were unaffected by further improvements. The dimensionless wall coordinate y+ was in the range 0.1–3 in the final grid. Next, a functional form of diffusion losses was fitted to the CFD results. Despite the fact that the flow inside the sensor is mostly turbulent, it was found that the transport efficiency for laminar flow through a cylindrical tube gives the best fit for the modeled diffusion losses. According to Gormely and Kennedy (1949), the transport efficiency has the form of Equation (2), which is a function of the particle (laminar) diffusion coefficient D_p multiplied by a fitted parameter $\mu_0 = 1.79 \times 10^5$ s/m^2. The parameter μ_0 value corresponds to diffusion losses of a 6 m long tube in laminar flow conditions with the sample inlet flow rate. The unit for the diffusion coefficient is m^2/s.

$$P_d(D_p) = \begin{cases} 1 - 2.56(\mu_0 D_p)^{2/3} + 1.2\mu_0 D_p + 0.177(\mu_0 D_p)^{4/3} \\ \quad \mu_0 D_p < 0.03 \\ 0.819e^{-3.657\mu_0 D_p} + 0.097e^{-22.3\mu_0 D_p} + 0.032e^{-57\mu_0 D_p} \\ \quad \mu_0 D_p \geq 0.03 \end{cases} \quad [2]$$

Mobility Analyzer

The collection of charged particles in the cylindrical mobility analyzer in the case of turbulent plug flow is obtained using the equation derived by Deutsch in the 1920s. The penetration efficiency of the particles can consequently be written as

$$P_{\mathrm{ma}}(d_p, V_{\mathrm{ma}}) = e^{-\frac{neC_c}{3\pi\eta_g d_p Z_0(V_{\mathrm{ma}})}} \quad [3]$$

The term in the exponent is the collection efficiency of the same geometry in laminar flow conditions, which can be expressed as the ratio of the particle electrical mobility to the limiting electrical mobility Z_0. The electrical mobility is a function of the particle size d_p. The other terms needed are the number of charges per particle n, the elementary charge e, the slip correction factor C_c, and the gas viscosity η_g. The limiting electrical mobility is the minimum electrical mobility that would cause 100% collection efficiency for laminar flow conditions. It is a value specific to the geometry and can be obtained from the dimensions of the analyzer with the help of the Equation (4). The dimensions needed are the inner and outer diameters, $s_i = 0.022$ m and $s_o = 0.030$ m, length $l_e = 0.032$ m of the analyzer, the volumetric flow rate inside the analyzer Q_{tot}, and the applied voltage V_{ma}. The flow rate Q_{tot} is a sum of the volumetric flow rates of the sample flow Q_s and the ejector pump flow Q_p in the conditions of the mobility analyzer. As seen from Equation (4), the limiting electrical mobility in the laminar flow conditions is directly proportional to the total flow rate and inversely proportional to the applied voltage. All the remaining terms can be combined to a single constant K:

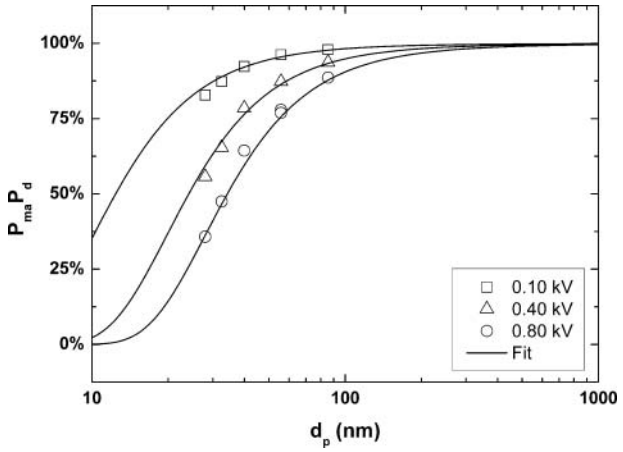

FIG. 3. Ion trap acting as a mobility analyzer: particle penetration efficiencies with different trap voltages. Open symbols are the penetration efficiencies measured with singly charged particles and the solid line is the penetration according to the fitted model.

$$Z_0(V_{\mathrm{ma}}) = \frac{Q_{tot}\ln\left(\frac{s_o}{s_i}\right)}{2\pi V_{\mathrm{ma}} l_e} \Rightarrow Z_0 = \frac{(Q_s + Q_p)K}{V_{\mathrm{ma}}} \quad [4]$$

The diffusion losses also contribute to the mobility analyzer penetration efficiency and the effect was taken into account. The fit for the $P_{\mathrm{ma}}P_d$ product, drawn in Figure 3, is obtained using Equations (2)–(4) with the value $K = 1.37$ m^{-1} for the constant. This value gives the best fit to the measured data, although it differs slightly from the value calculated from the mechanical dimensions $K_{\mathrm{teor}} = 1.54$ m^{-1}. As seen in Figure 3, the penetration efficiency is over 90% for particles larger than 100 nm with all mobility analyzer collection voltages.

Charging Efficiency and Average Number of Charges

The sensor response was obtained from the ratio of the current measured with the sensor to the number concentration measured by the CPC. The response decreases as the mobility analyzer voltage is increased, since increasing part of the small

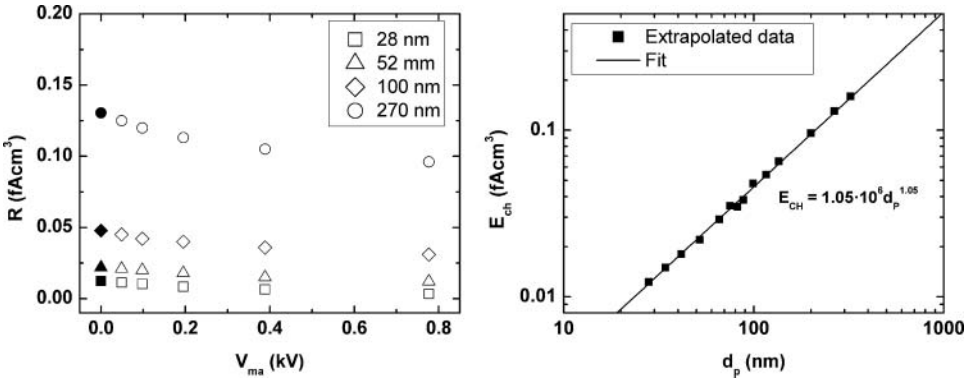

FIG. 4. Left: measured sensor responses (open symbols) as a function of the applied trap voltage together with the extrapolated responses (closed symbols). Right: the extrapolated sensor response points with zero trap voltage (closed symbols) with the power function fit (line) as a function of the particle size.

particles is collected by the mobility analyzer. For the sensor response, a model for the charging efficiency of the charger E_{ch} is needed. Typically, in unipolar diffusion chargers, the charging efficiency is approximated by a power function described by Equation (5), where the parameters a and b are obtained by fitting to calibration measurements (Kulkarni et al. 2011).

$$E_{\mathrm{ch}}(d_p) = a d_p^b \qquad [5]$$

Because of the ion leakage, it is not possible to have a calibration measurement for the charging efficiency without the effect of the mobility analyzer. This issue was solved by plotting the sensor responses measured for different mobility analyzer voltages as a function of the applied voltage for different particle sizes. Then the responses were extrapolated with a cubic Hermite spline to zero voltage, resulting in an estimate for the maximum charging efficiency without the effect of the mobility analyzer. The plot on the left-hand side of Figure 4 shows an example of the extrapolation. In the plot, the open markers show the measured sensor responses as a function of the mobility analyzer voltage for selected particle sizes and the closed markers show the extrapolated values for zero trap voltage. The extrapolated values for different particle sizes are collected to the plot on the right-hand side of Figure 4 as a function of the particle size. For the extrapolation, only calibration results from particle sizes below 350 nm were used in order to exclude the effect of the inertial losses. From the extrapolated data, the values for the parameters a and b in Equation (5) were obtained.

The main component in the charger efficiency is the product of the particle penetration through the charger and the average number of elementary charges the particles acquire during charging. Usually the value of the product is enough for the use of the diffusion charger (Marjamäki et al. 2000), but in this case the average number of charges per particle is separately needed in order to calculate the collection efficiency of the mobility analyzer. The number of charges could in principle be obtained by measuring separately the particle charge (via electrical mobility) after the charger or the particle penetration (of charged particles) through the charger. Since thorough measurement of either would be laborious, the following approximation is used instead. The results in Figure 3 presenting the penetration efficiencies measured with charger *off* for singly charged particles at different trap voltage settings indicate that a constant value of 100% could be used as a first approximation for the penetration with charger *off*. This is because the experimental penetration efficiencies are nearly 100% at large particle sizes. To check that the approximation applies also for the charger *on* case, the penetration was experimentally determined using 100 nm monodisperse particles for the charger *on* and charger *off* case. The penetration through the charger for *on* and *off* cases was found to be equal and high, over 95%. Based on this, it was assumed that the particle losses inside the charger are negligible, excluding the separately calculated effects of the electrical collection within the trap, the diffusion losses, and the inertial losses. The average number of elementary charges per particle was then estimated to be equal to the charging efficiency divided by the flow rate and the elementary charge. This somewhat underestimates the number of elementary charges of the charged particles, but is expected to be reasonable when limited to a minimum value of one. The resulting functional form is shown in Equation (6), where particle diameter is in meters:

$$n_{\mathrm{AVE}}(d_p) = \begin{cases} 1, & d_p < 1.63 \cdot 10^{-8}\,\mathrm{m} \\ 6.13 \cdot 10^7 d_p^{1.05}, & d_p \geq 1.63 \cdot 10^{-8}\,\mathrm{m} \end{cases} \qquad [6]$$

It turned out that the mobility analyzer collection voltage affects the sensor response more than can be explained by the mobility analyzer collection efficiency. The fact that the difference was seen throughout the measured size range suggests

that the applied collection voltage affects slightly the particle charging efficiency. It is possible that the ion losses in the charging region increase with increasing collection voltage. In order to take the effect into account, a functional form for the parameter a was fitted. In the fitting process, calibration results from particle sizes 200–400 nm were used in order to minimize the effect of the mobility analyzer and the inertial losses. The resulting final form for charger efficiency, Equation (7), was obtained. The unit for the charging efficiency is fAcm^3, the unit for the voltage is V, and the unit for the particle diameter is m:

$$E_{\mathrm{ch}}(d_p, V_{\mathrm{ma}}) = \left(1.05\cdot 10^6 - 7.23\cdot 10^4 \ln\left(1 + 1.12\cdot 10^{-2} V_{\mathrm{ma}}\right)\right) d_p^{1.05} \quad [7]$$

Inertial Losses

As a final step for the sensor response, a fit for the inertial losses in the flow system is needed. For simplicity, it is assumed that for particles larger than 400 nm, the difference between the measured response values and the values obtained using Equation (7) is caused by inertial losses. A simple equation was fitted to the results as

$$P_i(d_a) = 1 - \frac{1}{1 + \left(\frac{6.36\cdot 10^{-7} m}{d_a}\right)^{2.06}} \quad [8]$$

This form has been used to describe inertial impactors (Dzubay and Hasan 1990). Since the particle density affects the inertial losses, the term d_a in the equation is the aerodynamic particle diameter. The fitted parameters are the cut point (636 nm) and the slope of the penetration curve (2.06). Based on the fact that the flow field inside the sensor is turbulent, it is possible that there are turbulence-induced impaction losses inside the sensor. This would explain the rather low response for the large particles.

Sensor Response

The overall sensor response is a particle size-dependent function formed as the product of the charging efficiency E_{ch}, the ion trap penetration P_{ma}, and the particle penetration after inertial and diffusion losses, described by the two penetration terms P_i and P_d as shown in Equation (1). The overall response describes the relation between the inlet number concentration and the sensor output as a function of the particle size. The sensor response with different trap voltages is plotted in Figure 5, where also the measured calibration points and the maximum charging efficiency of the charger are plotted as reference. The inertial losses in the plotted response are calculated with a density value of 912 kg/m^3, which is the density of the particles used in the calibration measurements.

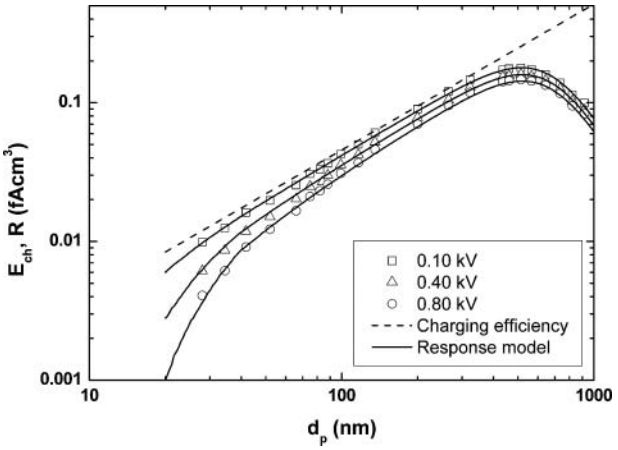

FIG. 5. Measured calibration points (open symbols) together with the fitted PPS-M sensor response as a function of the particle size with different trap voltages (solid line). The dashed line represents the maximum charging efficiency (E_{ch}) of the charger. For the inertial losses a density value of 912 kg/m^3 is used.

Tests with Polydisperse Aerosol

After the calibration, the sensor model was tested in laboratory conditions with polydisperse test aerosol. The measured sensor signals were compared to the simulated signals calculated from the measured size distributions according to Equation (9). The simulated sensor output is obtained by integrating the product of the sensor response $R(d_p,V_{\mathrm{ma}})$ of Equation (1) and the particle number concentration $N(d_p)$ over the particle size. The different components of the sensor response are given by Equations (2), (3), (7), and (8).

$$\begin{aligned} I_{\mathrm{simulated}} &= \int R(d_p, V_{\mathrm{ma}}) N(d_p) dd_p \\ &= \int E_{\mathrm{ch}}(d_p, V_{\mathrm{ma}}) P_{\mathrm{ma}}(d_p, V_{\mathrm{ma}}) P_d(d_p) \\ &\quad \times P_i(d_p) N(d_p) dd_p \end{aligned} \quad [9]$$

During the tests, the median size of the test aerosol was varied between 35 and 120 nm, while the geometric standard deviation (GSD) of the distribution varied from 1.4 to 1.5. Different mobility analyzer collection voltages were also used in the range of 100–800 V. A scanning mobility particle sizer (SMPS, TSI Inc., Shoreview, MN, USA) was used as the reference instrument. In the measurement setup, the pressure difference between the sensor inlet and outlet was monitored in order to avoid too high pressure difference and the actual sensor inlet flow rate was measured and compensated in the simulations. Additionally, good care was taken in order to ensure equal particle concentrations for both instruments. A correlation plot of the measured and the simulated sensor signals is shown in Figure 6. As seen from the figure, the measured signals correlate very well with the simulated signals, although the measured signal is systematically 13% higher. The

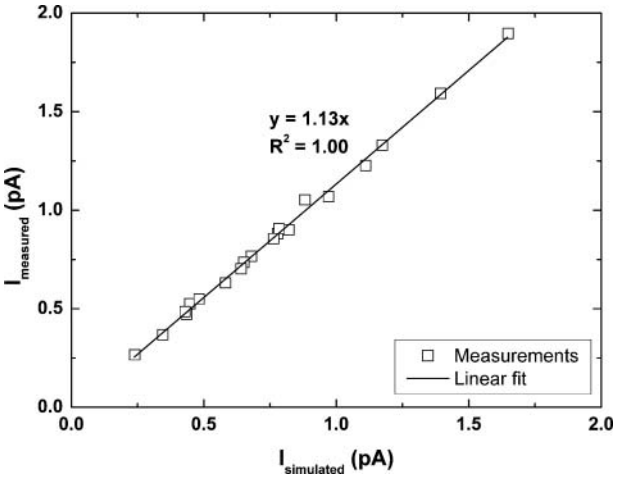

FIG. 6. Correlation plot of the measured and simulated sensor signals in the polydisperse test aerosol measurements.

difference between the measured and simulated values is most likely caused by the combined effect of the detection efficiency of the SMPS and the decreased concentration measurement accuracy caused by flow unbalance within the SMPS DMA. Instead of the sheath air recirculation used in the calibration measurements, the DMA flow rates were measured separately with the integrated mass flow meters that are calibrated on an annual basis. While this ensures good accuracy for the DMA total flow rate and consequently good accuracy on the particle size measurement, it does not ensure a good balance of the sample and monodisperse flows. This possible unbalance leads to a decreased accuracy for the particle concentration measurement.

CONCLUSIONS

In this article, calibration results together with a comprehensive model for the response of the PPS-M sensor were presented. The sensor was calibrated with monodisperse test aerosol, produced with the single charged aerosol reference (SCAR) by using calibrated condensation particle counter (CPC) as the reference instrument. The used calibration setup provided the possibility to have a calibration also for the sensors integrated mobility analyzer. CFD modeling results, used primarily to aid the sensor design, were used as a starting point for the sensor response model. The model covers the effects of the charging efficiency of the charger together with the average number of elementary charges it produces to the particles, the collection efficiency of the mobility analyzer, and both diffusion and inertial losses for the particles. The obtained model fits very well to the calibration data. Although the mobility analyzer is not ideal for mobility classification, the mobility analyzer part of the model is in good agreement with both the measured collection efficiencies and the expected collection efficiency based on the mechanical dimensions. The overall response model was also tested in the laboratory measurements with polydisperse test aerosols and the results were in good agreement with the model.

In applications, where the particle size distribution stays relatively stable and a good approximation can be made for the distribution, it is possible to calculate conversion factors with the help of the model. These factors can be used in converting the sensor output to number, surface area, or mass concentration. The accuracy of the conversion depends on the accuracy of the size distribution approximation. The model brings also more insight on the instrument performance for the data analysis.

FUNDING

This work was conducted within the Measurement, Monitoring and Environmental Assessment (MMEA) research program of CLEEN Ltd., supported by Tekes.

REFERENCES

ANSYS Inc. (2011). *ANSYS Fluent Theory Guide*, 14th release. ANSYS Inc., Canonsburg, PA.

Dzubay, T. G., and Hasan, H. (1990). Fitting Multimodal Lognormal Size Distributions to Cascade Impactor Data. *Aerosol Sci. Technol.*, 13(2): 144–150.

Fierz, M., Houle, C., Steigmeier, P., and Burtscher, H. (2011). Design, Calibration, and Field Performance of a Miniature Diffusion Size Classifier. *Aerosol Sci. Technol.*, 45(1):1–10.

Fierz, M., Meier, D., Steigmeier, P., and Burtscher, H. (2014). Aerosol Measurement by Induced Currents. *Aerosol Sci. Technol.*, 48:350–357.

Fissan, H., Neumann, S., Trampe, A., Pui, D., and Shin, W. (2007). Rationale and Principle of an Instrument Measuring Lung Deposited Nanoparticle Surface Area. *J. Nanopart. Res.,* 9:53–59.

Gormely, P. G., and Kennedy, M. (1949). Diffusion from a Steam Flowing through a Cylindrical Tube. *Proc. R. Irish Acad.,* 52:163–169.

Hinds, W. C. (1999). *Aerosol Technology. Properties, Behaviour and Measurement of Airborne Particles*. Wiley, New York.

Högström, R., Yli-Ojanperä, J., Rostedt, A., Iisakka, I., Mäkelä, J. M., Heinonen, M., et al. (2011). Validating the Single Charged Aerosol Reference (SCAR) as a Traceable Particle Number Concentration Standard for 10 nm to 500 nm Aerosol Particles. *Metrologia*, 48:426–435.

Intra, P., and Tippayawong, N. (2009). Progress in Unipolar Corona Discharger Designs for Airborne Particle Charging: A Literature Review. *J. Electrostat.,* 67(4):605–615.

Keithley Instruments Inc. (2004). *Low Level Measurement Handbook*, 6th ed., Keithley Instruments Inc., Cleveland, OH.

Kulkarni, P., Baron, P. A., and Willeke, K. (2011). Introduction to Aerosol Characterization, in *Aerosol Measurement: Principles, Techniques, and Applications*, P. A. Baron, P. Kulkarni, and K. Willeke, eds., John Wiley & Sons, Hoboken, NJ, pp. 3–13.

Lanki, T., Tikkanen, J., Janka, K., Taimisto, P., and Lehtimäki, M. (2011). An electrical sensor for long-term monitoring of ultrafine particles in workplaces. *J. Phys.: Conf. Ser.,* 304:012013. Available at http://iopscience.iop.org/1742-6596/304/1/012013

Lee, S. G., Hyun, J., Park, D., Hwang, J., and Kim, Y. J. (2011). Application and Performance Test of a Micro-Machined Unipolar Charger for Real-Time Measurements of Exhaust Particles from a Diesel Engine Vehicle. *J. Aerosol Sci.,* 42:747–758.

Lehtimäki, M. (1983). In Modified Electrical Aerosol Detector. in *Aerosols in the Mining and Industrial Work Environments*, Vol. 3, V. A. Marple, and B. Y. H. Liu, eds., Ann Arbor Science Publishers, Ann Arbor, pp. 1135–1143.

Marjamäki, M., Keskinen, J., Chen, -R., and Pui, D. Y. H. (2000). Performance Evaluation of Electrical Low Pressure Impactor (ELPI). *J. Aerosol Sci.*, 31:249–261.

Marquard, A., Meyer, J., and Kasper, G. (2006). Characterization of Unipolar Electrical Aerosol Chargers-Part II: Application of Comparison Criteria to Various Types of Nanoaerosol Charging Devices. *J. Aerosol Sci.*, 37 (9):1069–1080.

Marra, J., Den Brink, W., Goossens, H., and Kessels, S. (2009). Nanoparticle Monitoring for Exposure Assessment Nanotechnology Magazine. *IEEE* 3:6–13.

Ntziachristos, L., Amanatidis, S., Samaras, Z., Janka, K., and Tikkanen, J. (2013). Application of the Pegasor Particle Sensor for the Measurement of Mass and Particle Number Emissions. *SAE Int. J. Fuels Lubr.,* 6(2): 521–531.

Ntziachristos, L., Fragkiadoulakis, P., Samaras, Z, Janka, K., and Tikkanen, J. (2011). Exhaust Particle Sensor for OBD Application. *SAE Technical Paper 2011-01-0626*.

Ntziachristos, L., Giechaskiel, B., Ristimäki, J., and Keskinen, J. (2004). Use of a Corona Charger for the Characterisation of Automotive Exhaust Aerosol. *J. Aerosol Sci.*, 35(8):943–963.

Rostedt, A., Marjamäki, M., and Keskinen, J. (2009a). Modification of the ELPI to Measure Mean Particle Effective Density in Real-Time. *J. Aerosol Sci.,* 40:823–831.

Rostedt, A., Marjamäki, M., Yli-Ojanperä, J., Keskinen, J., Janka, K., Niemelä, V., et al. (2009b). Non-Collecting Electrical Sensor for Particle Concentration Measurement. *AAQR*, 9:470–477.

Tikkanen, J. (2009). Particle Measurement Process and Apparatus. Patent publication no WO 2009/109688.

Whitby, K. T. (1961). Generator for Producing High Concentrations of Small Ions. *Rev. Sci. Instrum.,* 32(12):1351–1355.

Yli-Ojanperä, J., Mäkelä, J. M., Marjamäki, M., Rostedt, A., and Keskinen, J. (2010). Towards Traceable Particle Number Concentration Standard: Single Charged Aerosol Reference (SCAR). *J. Aerosol Sci.*, 41: 719–728.

Yli-Ojanperä, J., Sakurai, H., Iida, K., Mäkelä, J. M., Ehara, K., and Keskinen, J. (2012). Comparison of Three Particle Number Concentration Calibration Standards Through Calibration of a Single CPC in a Wide Particle Size Range. *Aerosol Sci. Technol.*, 46:1163–1173.

Paper IV

Rostedt, A., Ntziachristos, L., Simonen, P., Rönkkö T., Samaras, Z., Hillamo, R., Janka, K., and Keskinen, J., 2017. *A new miniaturized sensor for ultra fast on-board soot concentration measurements*. SAE Int. J. Engines 10(4):2017, doi: 10.4271/2017-01-1008.

Published 03/28/2017

doi:10.4271/2017-01-1008
saeeng.saejournals.org

A New Miniaturized Sensor for Ultra-Fast On-Board Soot Concentration Measurements

Antti Rostedt, Leonidas D. Ntziachristos, Pauli Simonen, and Topi Rönkkö
Tampere University of Technology

Zissis C. Samaras
Aristotle University of Thessaloniki

Risto Hillamo
Finnish Meteorological Institute

Kauko Janka
Pegasor Oy

Jorma Keskinen
Tampere University of Technology

ABSTRACT

In this article we present a design of a new miniaturized sensor with the capacity to measure exhaust particle concentrations on board vehicles and engines. The sensor is characterized by ultra-fast response time, high sensitivity, and a wide dynamic range. In addition, the physical dimensions of the sensor enable its placement along the exhaust line. The concentration response and temporal performance of a prototype sensor are discussed and characterized with aerosol laboratory test measurements. The sensor performance was also tested with actual engine exhaust in both chassis and engine dynamometer measurements. These measurements demonstrate that the sensor has the potential to meet and even exceed any requirements around the world in terms of on-board diagnostic (OBD) sensitivity and frequency of monitoring. Further to potential OBD applications, this has the capacity to be used as an engine and combustion diagnostics sensor, for example to detect misfiring, cylinder combustion variability, exhaust gas recirculation flowrate, etc.

CITATION: Rostedt, A., Ntziachristos, L., Simonen, P., Rönkkö, T. et al., "A New Miniaturized Sensor for Ultra-Fast On-Board Soot Concentration Measurements," *SAE Int. J. Engines* 10(4):2017, doi:10.4271/2017-01-1008.

INTRODUCTION

Meeting stringent particulate matter (PM) and particle number (PN) emission limits for diesel light-duty and heavy-duty vehicles necessitates the use of a diesel particle filter (DPF) in the exhaust line. As a consequence, on board monitoring of the DPF performance is required first to make sure that the DPF operates correctly and, second, to confirm that emission limits are not violated under real-world operation. The latter is performed by on-board diagnostic (OBD) sensors which make sure that specific OBD threshold limits (OTL) are not exceeded.

Currently three different operation principles are implemented in commercial DPF performance monitoring sensors. The first technique relies on particle deposition and resistance measurement [1, 2]. The particles are deposited onto a collection surface, where electrodes are separated by an electrically insulating material. The deposited conductive particles gradually change the surface conductivity. By measuring the resistance between the electrodes it is possible to assess the amount of soot deposited to the surface, which is then linked to the soot concentration in the exhaust line. In principle, this method is based on an integral measurement of particle concentration over a period of time, and requires periodic regeneration of the deposition surface for a new deposition cycle to begin. The frequency of those regenerations is a measure of particle concentration. Therefore, the response time of these sensors is from several seconds to minutes, depending on the particle concentration.

The second family of sensors comprises those measuring the amount of deposited soot into the DPF filter. This can be estimated by either measuring the pressure difference over the filter or by measuring microwave transmittance through the DPF [3].

The third measurement technique involves electrical particle detection. For this, the charge of particles following combustion can be utilized, such as in the PMTrac sensor [4, 5], where the naturally

charged exhaust particles are collected inside the sensor by an electric field and an amplified electric current proportional to the particle concentration is measured.

The electrical methods described above rely on the conductivity of the emitted particles, hence on particle properties. Therefore, electrical detection methods appear to be in need of engine specific calibration to accurately detect PM or PN OTL exceedances. Moreover, the sensitivity of electrical resistance and DPF soot loading estimation sensors is not enough to enable reduction of current OTL levels, to bring them in line with corresponding emission limits.

On the other hand, many of the widely-used aerosol measurement instruments rely on the diffusion charging of particles by ions generated in a corona discharge. For the measurement of exhaust gas particle concentrations, a simplified electrical instrument based on the diffusion charging was first demonstrated by Ntziachristos et al. [6]. The instrument consisted of a particle charger and a Faraday cup aerosol electrometer. In the years since, that same concept has been used in several rather simple aerosol instruments such as NSAM [7] and DiSCmini [8].

In diffusion charging instruments, the charge acquired by the aerosol during the charging process is not only dependent on the particle number concentration but also on the particle size and this has an effect on the instrument response. However, in typical exhaust aerosol of either diesel or gasoline vehicles, the mean particle size typically remains within a narrow size range. While the particle morphology is known to have a small effect [9], the charging is relatively independent on the particle material [10]. Based on this weak material dependence, this detection method is equally suitable for both conductive soot particles and non-conductive ash particles. However, in order to overcome the morphology effect, the instrument response needs to be determined for exhaust-like aerosol. Diffusion charger based instruments typically offer good correlation and good signal repeatability for a stable size distribution, which also make them a promising approach as an OBD particle sensor.

In this study, a new miniaturized sensor based on particle diffusion charging is presented, with the potential to be used as an OBD sensor or as a general combustion diagnostics sensor. The design of the new sensor is based on the Pegasor PPS-M [11], which have been used for exhaust particle emission measurements [e.g. 12, 13].

OPERATING PRINCIPLE AND SENSOR DESIGN

The operating principle and sensor construction is similar to the Pegasor PPS-M sensor, but in a much more compact form. The unit is now designed so, that the sensor probe, measuring 16 mm in diameter and 40 mm in length, can be positioned directly into the exhaust line. The necessary electronics are integrated to the sensor head, and a CAN serial bus is provided for the data output. Both the sensor probe and the integrated electronics are placed inside a static shielding to avoid electromagnetic interference. The overall dimensions of the sensor are 190 mm length and 36 mm diameter at the largest point. M18×1.5 thread is provided for the connection to the exhaust line. The sample flow rate of the tested prototype sensor was 3.5 lpm, while the required pressurized air supply was 8 slpm with 1.5 bar overpressure compared to the exhaust line. The current measurement range of the electrometer is ±2.5 nA.

A schematic of the cross section of the prototype sensor is presented in Figure 1, showing the key components and operational parameters of the design. The operation is based on diffusion charging of the aerosol particles and subsequent charge detection. Like the PPS-M sensor, the new sensor utilizes the escaping current measurement method, where the particles need not be actually collected. The charge detection is realized by measuring the charge that the particles carry away from the electrically floating corona discharge. In order to avoid charger fouling, the corona discharge electrodes are protected by a clean sheath air flow and the ions produced are brought into contact with the sample by a high velocity air stream from the discharge region. The same air stream is used also as a pump flow providing the sample flow for the sensor.

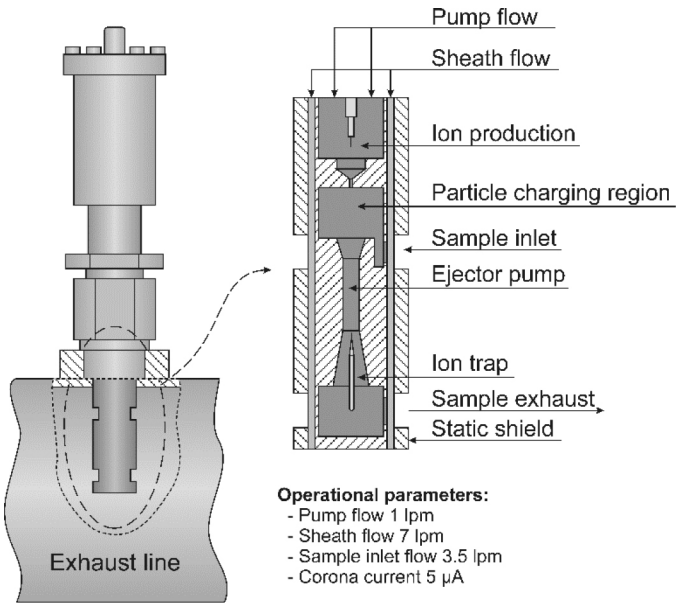

Figure 1. The sensor prototype pictured on the left together with the cross section on the right showing the main components and operational parameters of the sensor design.

Particle charging takes place in the charging region positioned right after the critical orifice separating the discharge region and the sample volume. The sample enters the charging region through the sampling port followed by a sharp bend in the flow channel. The purpose of the bend is to act as a pre-cut impactor preventing the large particles from entering the sensor and clogging the sample flow path. After the charging region the sample flows through the ejector pump. An ion trap is positioned downstream of the ejector pump to remove the excess ions before the sample exits the sensor through the

sample exhaust port. The ion trap is dimensioned so that the cut point is approximately 5 nm, in order to have minimal particle losses. As in the PPS-M sensor design, the sample inlet and exhaust ports are positioned on the same side of the sensor probe to minimize the pressure difference between the inlet and outlet ports. Although the inlet and exhaust ports are relatively close to each other, the sample recirculation is effectively prevented by the high flow velocity of the exhaust flow.

SENSOR RESPONSE AND SENSITIVITY

The sensor output signal is an electrical current produced by the charged particles as they exit the sensor. The sensor response relates this output to the number concentration of the aerosol particles in the sample flow. The operation is based on diffusion charging of the particles, and hence the response is proportional to the charging efficiency. Since the charging efficiency is dependent on particle size, the sensor response is also a function of it. The charging efficiency depends on the $N_i t$-magnitude, which is the product of the ion number concentration (N_i) and the particle residence time (t) in the charging region. While the charging efficiency could be approximated from the $N_i t$ -product, the ion properties, and the particle size, it is however often approximated to follow a power function of the particle size, shown in equation 1. The parameters a and b in equation 1 are typically determined by calibration, where the charger output signal is compared to the aerosol concentration when using monodisperse aerosol in the laboratory.

$$R_s(d_p) = a{d_p}^b \quad (1)$$

For the prototype sensor it was not possible to produce monodisperse calibration aerosol in sufficient concentrations for the high volumetric flow rate needed for the calibration. Instead, the sensor output was measured with different polydisperse aerosol size distributions as an input. Then, a fitting routine was used in order to find out the parameter values for the charging efficiency. The response measurement setup is shown in Figure 2. The measured test aerosols were produced by a modified diesel fuel burning heater [14]. The size distribution was controlled by varying the fuel feed and the air flow into the burner. The number-weighted geometric median of the size distribution was varied between 35 nm and 210 nm, while the geometric standard deviation range was 1.6 - 1.8. A scanning mobility particle sizer (SMPS, TSI Inc.), consisting of a model 3071 differential mobility analyzer (DMA, TSI Inc.) and a model 3775 condensation particle counter (CPC, TSI Inc.), was used to measure the size distribution. The total number concentration was measured with a model A20 CPC (Airmodus Oy). In total three ejector dilutors were used for dilution. Two in series, in front of the SMPS, and a third one in series upstream of the CPC. The total dilution ratio for the SMPS measurement was 90:1, and 900:1 for the CPC measurement. Since the particle size distribution was measured after dilution, the measured distributions were monitored not to contain nucleation mode particles.

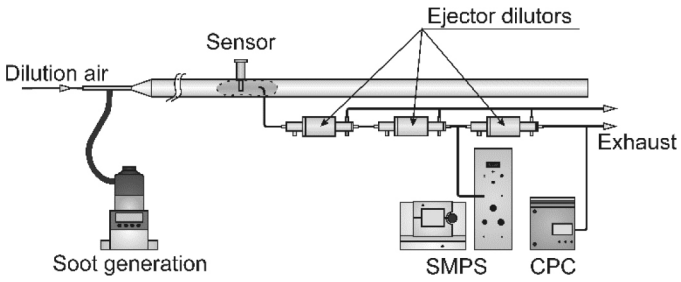

Figure 2. The setup used for the prototype sensor response measurement.

For data processing, the measured total number concentrations were first corrected with the dilution ratio to obtain the total number concentration in the sample line. The measured number size distributions were then normalized to the measured total number concentration of the test aerosol. In order to obtain the values for eq. 1 parameters, the measured sensor signal was compared to a simulated sensor output calculated from the corrected number size distributions using the response function shown in eq. 1. The best fitting values for parameters a and b in the response function were obtained by using a minimum square sum fitting routine. The resulting sensor response is shown in eq. 2 and plotted on Figure 3 together with a correlation plot between the measured and simulated sensor outputs. The measured sensor response points in Figure 3A are plotted as the function of the median diameter of the size distribution weighted with the sensor response.

$$R_s(d_p) = 0.16{d_p}^{1.03} \quad (2)$$

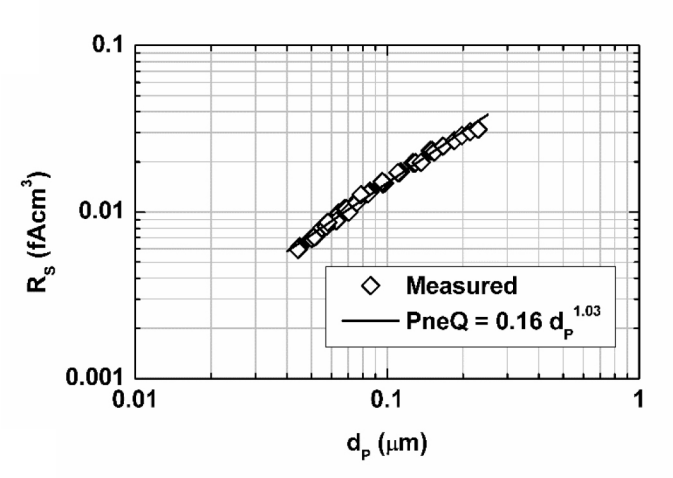

A.

Figure 3.

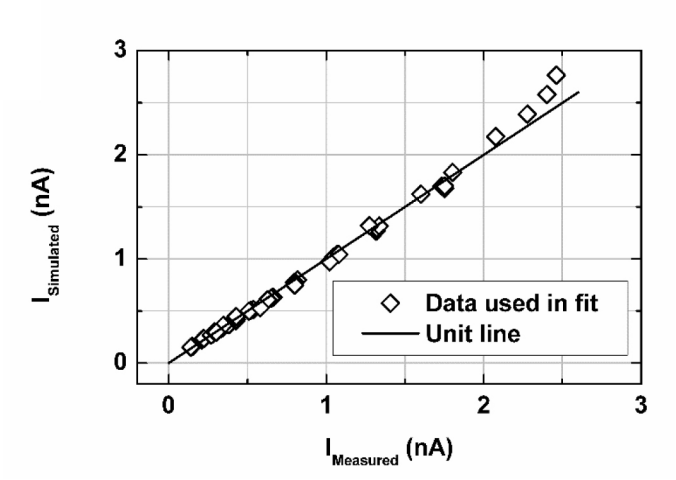

B.

Figure 3 (cont.). (A) Fitted sensor response as a function of the particle size. The measured response points are plotted as a function of the median size of the size distribution weighted with the fitted response function, and (B) correlation plot between the simulated and measured sensor responses.

The correlation plot in Figure 3B shows a good correlation between the measured and simulated responses, implying that the fitted response adequately describes the sensor behavior in the measured size range. While the overall fit between the response model and the measured data points is very good, it can however be seen that the model starts to slightly deviate from the measurement at large particle sizes. In particular, the simulated signal appears to be larger than the measured one. This could be caused for instance by inertial particle losses in the sensor. However, there is relatively high measurement uncertainty in these larger particle sizes, since these approach the SMPS upper size limit. The fitted response however fits rather well in the size range from 40 - 200 nm, which is relevant for typical exhaust particles. The fitted power of 1.03 is in line with corresponding values reported for other electrical aerosol instruments, where diffusion charging is the major charging mechanism [15].

If required by the application, the sensor output can be converted to mass or number emission with the help of the response fit. The needed conversion factors can be obtained in a similar way as presented earlier for the PPS-M sensor [9]. According to the response model for a size distribution, with a count median size of 50 nm and a geometric standard deviation 1.7, the PN measurement range of the prototype sensor is approximately from 10^4 to 10^9 1/cm^3, with a sampling interval of 1 s. In terms of raw exhaust conditions, for a passenger car producing exhaust volume in the order of 1 Nm^3/km, the sensor is able to detect concentrations down to 10^{10} part./km, i.e. more than one order of magnitude lower than current PN emission limits of 6×10^{11} part./km. In terms of mass, and assuming a typical lognormal size distribution as before and a particle density profile for diesel vehicles [16], this would correspond to a soot mass of less than 3 µg/km, i.e. several times lower than any PM limits around the world.

TEMPORAL RESOLUTION

As already mentioned, the diffusion charging process is dependent on the N_it-product. Unipolar diffusion chargers are typically designed so that the particles reach saturation charge level. According to Davison et al. [17] this is accomplished at N_it-product values above 10^7 s/cm^3. In the sensor design the ion current produced by the corona and entering the charging region is in the order of hundred nano-amperes, which would correspond to an ion production rate in the order of 10^{12} ion/s. If the ions lifetime is assumed to be 1 ms, and the charging region volume is approximately 0.5 cm^3, the ion concentration would be above 10^9 ion/cm^3. These numbers suggest, that the saturation charge level for the particles would be reached within 10 ms. Another factor affecting the temporal resolution is the gas exchange rate in the sensor. The total sample volume inside the prototype sensor is approximately 1.0 cm^3. The flow rate inside the sensor sample volume is a sum of the sample flow rate 3.5 lpm and pump flow rate 1 lpm, which equals 4.5 lpm in total. Combining the sample volume and the flow rate leads to a sample residence time of 13 ms inside the sensor, which sets a theoretical lower limit for the response time.

In practice, the electronic noise of the high sensitivity electrometer sets also limitations for the sensor time resolution. The higher the sampling rate and the shorter the integration time the more noise is present in the measured current signal and a higher signal is required for the measurement. To overcome this problem, the integration time of the sensor electrometer can be selected according to the measurement needs. With the highest sampling rate of 100 Hz, the noise level is approximately 1 pA, and a with 1 Hz sample rate the noise level drops down to 100 fA.

The temporal performance of the sensor was tested with laboratory measurements using the calibration measurement setup. A step response in the sample concentration was induced by directing a high velocity particle free air stream directly into the sampling port of the sensor. The airstream was controlled by a fast acting magnetic valve and the flow velocity was adjusted high enough in order to achieve a rapid change in the sample concentration. The first test was performed without particles in the sample to confirm that the fast high velocity air injection did not cause interferences to the sensor operation. The sensor output measured during particle concentration transients was then recorded with 100 Hz sampling frequency and the status information from the magnetic valve was recorded with 800 Hz sample rate. In the data processing the measured step responses were aligned together using the measured valve status signal. Approximately 100 repetitions were averaged to form an average step response, shown in Figure 4A together with a fitted step response. A time constant τ value of 18 ms, gave the best fit to the measured data, which corresponds to a value of 40 ms for a 10 - 90% rise time. The impulse response fit, shown in Figure 4B, was composed from the measured step response data and the fitted step response.

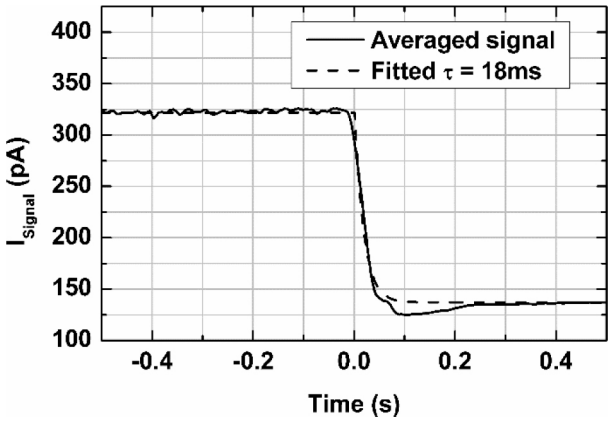

A.

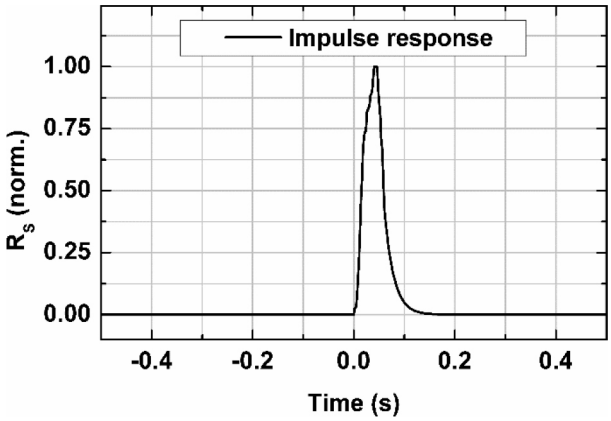

B.

Figure 4. (A) Step response of the prototype sensor as an average of 100 repetitions of rapid concentration drop; a fitted step response with a time constant of 18 ms shown for reference. (B) Fitted impulse response of the prototype sensor.

PERFORMANCE WITH REAL EXHAUST AEROSOL

In order to test its performance in real exhaust aerosol, the prototype sensor was fitted at the tailpipe of a light duty vehicle. This mounting point does not represent the targeted mounting point of the sensor in actual applications, but was chosen for practical reasons. The tailpipe was connected to a transfer line leading the exhaust to a Constant Volume Sampler. This guaranteed no backflow of ambient air in the tailpipe. Total particle number concentration measurement was realized with a CPC (Model 3776, TSI Inc., with 2.5 nm cut point) measuring diluted exhaust sample. The dilution system used consisted of a perforated tube diluter as the first stage dilution, with dilution ratio of approximately 12:1, and an ejector diluter as the secondary dilution stage. The CPC sample was further diluted with a dilution ratio of 42:1. The tested vehicle was Volkswagen Polo 1.2 TSI, equipped with a stoichiometric gasoline direct injection (GDI) engine. The test cycle was the NEDC (New European Driving Cycle), starting with a pre-warmed engine. In the measurement results, shown in Figure 5, the raw signal from the sensor measurement and the total number concentration of particles larger than 3 nm are plotted over the test cycle. In the measurement an averaging time of 1 s was used for the prototype sensor signal to match the CPC time resolution. A correlation plot of the signals is shown in Figure 6.

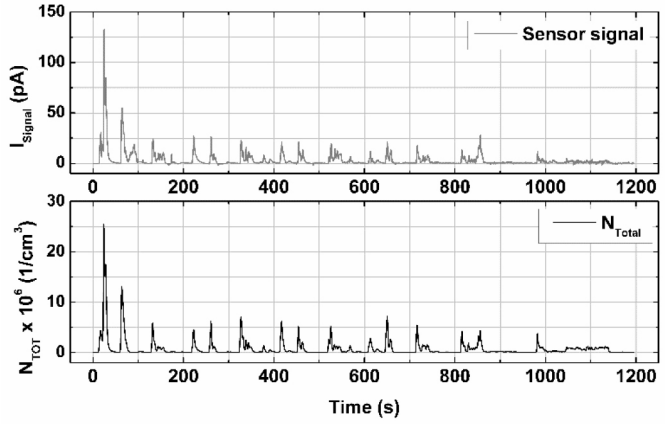

Figure 5. Sensor signal and particle total number concentration measured over the NEDC.

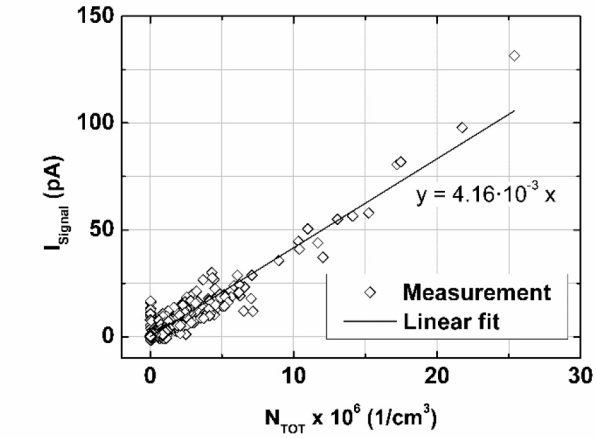

Figure 6. Second-by-second sensor signal and total particle number correlation over the NEDC.

Even though the sensor response is affected by the changes in the size distribution, the raw sensor signal correlates very well to the measured total particle number concentration as shown in Figures 5 and 6. The largest difference between the signals is seen at the beginning of the cycle during a period of 75 to 100 s. At this point there is a distinct signal seen from the sensor, while the measured total number concentration was essentially zero. The same difference was observed also in other repetitions; however, the sensor signal amplitude during this time frame varied between the runs. At this point in the NEDC test cycle there is a deceleration from 32 km/h. Since the sensor was mounted at the end of the tailpipe, where the exhaust gas temperature is much lower than for what the sensor is designed for, it is possible that this behavior is caused by water condensation on the electrical insulators, thus causing an artifact measurement, before it evaporates again.

APPLICATION TO COMBUSTION DIAGNOSTICS

The fast response characteristics of the sensor prototype were also tested in the engine dynamometer measurements with a six-cylinder, 1000 kW medium speed diesel engine used in locomotives. The sensor was fitted in the exhaust gas recirculation (EGR) line for practical reasons, and the EGR valve position was adjusted so that the concentration measured by the sensor was within the measurement range. Since the EGR line is positioned before the turbocharger the sensor was operating at an elevated exhaust line pressure, reaching 3 bar overpressure and over 500°C temperature at maximum load point. The sensor air supply pressure was kept 1.5 bar above the exhaust manifold pressure to ensure proper operation of the integrated ejector pump. The outer part of the sensor was cooled with pressurized air, to prevent excessive heating of the electronics.

The in-cylinder pressure was measured from one cylinder in order to have reference engine timing information for the data alignment. The pressure signal was measured at 800 Hz sample rate, while the sensor output was recorded at 100 Hz sample rate. During data processing several time frames containing data from 20 engine revolutions were aligned together with the help of the timing signal. The signals acquired in different frames were then averaged. An example of the measured signal from an engine load point of 750 RPM and 513 kW is shown in Figure 7. The same figure also shows the measured signal at the same load point with the sensor charger switched off. This was recorded in order to test whether the pressure pulses, the high temperature or the charge produced by combustion would disturb the measurement. As seen from the figure, the signal level in the charger-off measurement is close to zero, indicating that the impact of external disturbances to the measured values is low.

The signals are plotted as a function of engine crank angle, showing a time span of ten engine revolutions. While the time resolution of the sensor is not good enough to detect all temporal details caused by the individual power strokes, a clearly periodic waveform is seen with six distinct particle concentration peaks every two engine revolutions. The peak nearest to the 0° crank angle is significantly lower than the others, which may be resulting for instance from the distance between this particular cylinder and the sampling point or the pressure waves inside the EGR line. Unfortunately, there is no independent measurement to rule out all possible interferences or to compare the signal time-dependence or absolute values with. The result should be treated as a demonstration of the repeatability and resolution of the sensor in detecting individual combustion events and the related exhaust pulses.

In order to test the sensor's ability to distinguish particle emissions from different cylinders, the fuel injection was delayed in one of the cylinders when the engine was run at the lowest load point of 350 RPM/62 kW. The measurement results are shown in Figure 8. A clear change in the measured signal waveform can be seen indicating higher particle emissions from the delayed injection cylinder due to the poor burning of the fuel. Moreover, different particle exhaust levels for the subsequent combustion cylinders, compared to the reference levels, are observed as the engine is adjusted to match the same output power as in the reference case.

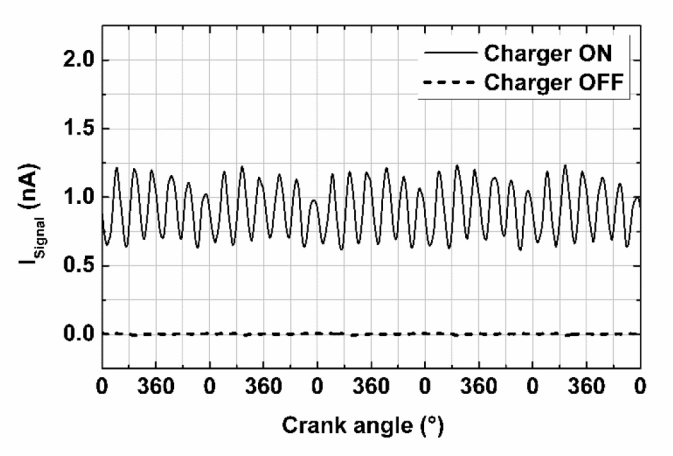

Figure 7. Measured prototype sensor signal (Charger on) from load point 750 RPM/513 kW. Shown also for reference the measured with the sensor charger off at the same load point.

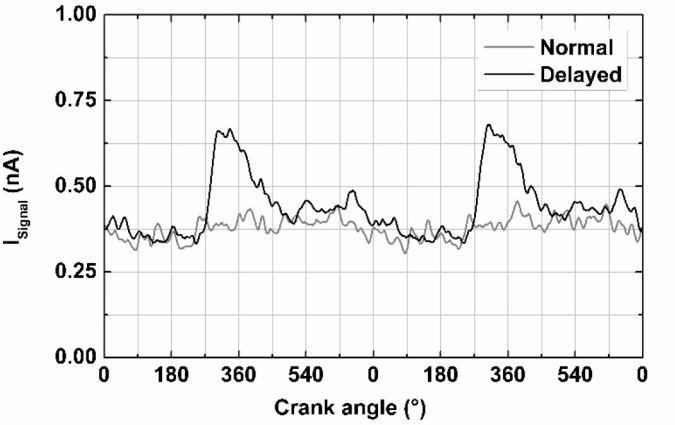

Figure 8. Measured signals from both normal engine operation and delayed fuel injection in one cylinder during load point 350 RPM/62 kW.

CONCLUSIONS

The design of a new particle sensor prototype was presented. The sensor is based on diffusion charging and electrical detection of exhaust particles and is intended for on board measurement of soot emissions from engines and vehicles. The study determined the sensor sensitivity and its response to exhaust particles and presented measurement results in real exhaust aerosol.

A fit for the sensor response was obtained from the laboratory tests. The obtained response with particle size roughly scales with a power of one and this brings it in good agreement with other diffusion charging based instruments. Using pulse signals, a response time of 18 ms was determined, which is in the same range of the theoretical value estimated from the sensor dimensions and operation principle. Moreover, its sensitivity in terms of PN and PM emissions of passenger cars is in the order of 10^{10} part./km and 3 µg/km, respectively. Such performance is by far better than the characteristics of currently used OBD sensors for DPF monitoring.

The sensor performance was validated with transient vehicle chassis tests and steady-state engine dynamometer measurements. A very good correlation between the sensor signal and the measured total number concentration was observed on the chassis dynamometer measurements. Tests on the engine operating at low speed demonstrated that the sensor was able to distinguish particle emission peaks originating from individual combustion events in the different engine cylinders. This demonstrates the potential of the sensor to even be used as a combustion diagnostic.

The prototype sensor still requires further development for practical OBD applications. For instance, the pressurized air line is a major concern for practical implementation, and one key issue is the minimization of both required pump and sheath air flows. Furthermore, the current prototype is dimensioned for 1.5 bar overpressure, which is quite high and needs to be decreased. Additionally, the sensor real world performance needs to be further studied, as do the long term operation capability and stability. However, the presented concept seems promising for an on board particle emission sensor.

REFERENCES

1. Hauser, G., "Smoke Particulate Sensors for OBD and High Precision Measuring," SAE Technical Paper 2006-01-3549, 2006, doi:10.4271/2006-01-3549.
2. Ochs, T., Schittenhelm, H., Genssle, A., and Kamp, B., "Particulate Matter Sensor for On Board Diagnostics (OBD) of Diesel Particulate Filters (DPF)," *SAE Int. J. Fuels Lubr.* 3(1):61-69, 2010, doi: 10.4271/2010-01-0307.
3. Fischerauer, G., Förster, M. and Moos, R. (2010) Sensing the soot load in automotive diesel particulate filters by microwave methods, Meas. Sci. Technol. 21 (2010) 035108.
4. Steppan, J., Henderson, B., Johnson, K., Yusuf Khan, M. et al., "Comparison of an On-Board, Real-Time Electronic PM Sensor with Laboratory Instruments Using a 2009 Heavy-Duty Diesel Vehicle," SAE Technical Paper 2011-01-0627, 2011, doi:10.4271/2011-01-0627.
5. Bilby, D, Kubinski, D, J., Maricq, M. M. (2016) Current amplification in an electrostatic trap by soot dendrite growth and fragmentation: Application to soot sensors. J. Aerosol Sci. 98:41-58, doi: 10.1016/j.jaerosci.2016.03.003.
6. Ntziachristos, L., Giechaskiel, B., Ristimäki, J. and Keskinen, J. (2004) Use of a corona charger for the characterisation of automotive exhaust aerosol, Journal of Aerosol Science, 35 (8), pp. 943-963, doi: 10.1016/j.jaerosci.2004.02.005.
7. Fissan, H., Neumann, S., Trampe, A., Pui, D., and Shin, W. (2007). Rationale and Principle of an Instrument Measuring Lung Deposited Nanoparticle Surface Area. J. Nanopart. Res., 9:53-59, doi: 10.1007/s11051-006-9156-8.
8. Fierz, M., Houle, C., Steigmeier, P., and Burtscher, H. (2011). Design, Calibration, and Field Performance of a Miniature Diffusion Size Classifier. Aerosol Sci. Technol., 45(1):1-10, doi: 10.1080/02786826.2010.516283
9. Shin, W. G., Wang, J., Mertler, M., Sachweh, B., Fissan, H. and Pui, D. Y. H. (2010). The effect of particle morphology on unipolar diffusion charging of nanoparticle agglomerates in the transition regime, Journal of Aerosol Science, 41, pp. 975-986, doi: 10.1016/j.jaerosci.2010.07.004
10. Shin, W. G., Qi, C., Wang, J., Fissan, H. and Pui, D. Y. H. (2009). The effect of dielectric constant of materials on unipolar diffusion charging of nanoparticles, Journal of Aerosol Science, 40, pp. 463 - 468, doi: 10.1016/j.jaerosci.2009.01.003.
11. Ntziachristos, L., Fragkiadoulakis, P., Samaras, Z., Janka, K. et al., "Exhaust Particle Sensor for OBD Application," SAE Technical Paper 2011-01-0626, 2011, doi:10.4271/2011-01-0626.
12. Ntziachristos, L., Amanatidis, S., Samaras, Z., Janka, K. et al., "Application of the Pegasor Particle Sensor for the Measurement of Mass and Particle Number Emissions," *SAE Int. J. Fuels Lubr.* 6(2):521-531, 2013, doi:10.4271/2013-01-1561.
13. Amanatidis, S., Maricq, M. M., Ntziachristos, L., Samaras, Z., (2015). Measuring number, mass, and size of exhaust particles with diffusion chargers: The dual Pegasor Particle Sensor, Journal of Aerosol Science, 92, pp. 1-15,doi: 10.1016/j.jaerosci.2015.10.005.
14. Högström, R., Karjalainen, P. Yli-Ojanperä J., Rostedt, A., Heinonen, M., Mäkelä, J. M., and Keskinen, J. (2012) Study of the PM Gas-Phase Filter Artifact Using a Setup for Mixing Diesel-Like Soot and Hydrocarbons, Aerosol Sci. Technol., 46:9, 1045-1052, doi: 10.1080/02786826.2012.689118
15. Kulkarni, P., Baron, P.A. and Willeke, K. (2011) Introduction to aerosol characterization, in Aerosol measurement: principles, techniques, and applications, edited by Baron, P.A., Kulkarni, P., and Willeke, K. John Wiley & Sons, Hoboken, N.J. 3-13, doi: 10.1002/9781118001684.
16. Maricq, M.M., & Xu, N. (2004). The effective density and fractal dimension of soot particles from premixed flames and motor vehicle exhaust. Journal of Aerosol Science, 35, 1251-1274.
17. Davison, S. W., Hwang, S. Y., Wang, J., and Gentry, J. W. (1985) Unipolar Charging of Ultrafine Particles by Diffusion of Ions: Theory and Experiment. Langmuir 1985:1, 150-158, doi: 10.1021/la00061a027.

CONTACT INFORMATION

Antti Rostedt
Aerosol Physics Laboratory
Department of Physics
Tampere University of Technology
P.O. Box 692
33101 Tampere, Finland
antti.rostedt@tut.fi

ACKNOWLEDGMENTS

This work was conducted within the Measurement, Monitoring and Environmental Assessment (MMEA) research program of CLEEN Ltd., supported by Tekes - the Finnish Funding Agency for Innovation.

DEFINITIONS/ABBREVIATIONS

CPC - Condensation particle counter

DPF - Diesel particulate filter

DMA - Differential mobility analyzer

EGR - Exhaust gas recirculation

NEDC - New European driving cycle

OBD - On-board diagnostics

OTL - On-board diagnostics threshold limit

PM - Particulate matter

PN - Particle number

SMPS - Scanning mobility particle sizer

Tampereen teknillinen yliopisto
PL 527
33101 Tampere

Tampere University of Technology
P.O.B. 527
FI-33101 Tampere, Finland

ISBN 978-952-15-4084-4
ISSN 1459-2045